Late Quaternary biogenic opal sedimentation and diatom assemblages in Congo Fan sediments

Dissertation
zur Erlangung des Doktorgrades

am Fachbereich Geowissenschaften
der Universität Bremen

vorgelegt von
Eleonora Uliana

Bremen 2001

Tag des Kolloquiums:

13.07.2001

Gutachter:

Prof. Dr. Gerold Wefer
Prof. Dr. Tom Wagner

Prüfer:

Prof. Dr. Volkhard Spieß
Prof. Dr. Ulrich Bleil

Acknowledgements

I would like to thank Prof. Gerold Wefer for giving me the opportunity to carry out this work, and as well as for his constant support and guidance during the three and a half years in Germany.

I am very grateful to my SUPERvisor Carina Lange who with her enthusiasm and devotion encouraged me and brought me into the scientific world of diatoms.

To my husband, Frank Schmieder, who has devoted his time to my personal and professional well-being since my arrival in Germany. Petra, Dirk and Sebastian Rahe gave me a family in the Lüneburger Heide.

To my office mate, Helge Arz with whom I have shared three very important years in my life, and who has showed me into the world of oxygen isotopes and paleoclimate. Helge's encouragement and endless support is appreciated.

To my friends in Bremen, Junghyn Kim, Adesina Agdegbie, Peer Helmke, Frank & Eileen Lamy, Flor Albertoni, and Niko Wolf, Janneth Pachon de Heller, Claudia Winter- Rivera, Holger Dierssen, André & Britta Janke, Thomas Felis, Jens Funk, Babette Böckel, Britta Jahn, and Carsten Rühlemann for their moral support.

Marco Klann and Volker Diekamp provided technical support and lively atmosphere in the laboratory.

To Ralph Schneider, Lydie Dupont, Ute Treppke, Stefan Mulitza, Barbara Donner, Jens Holtvoeth, Jolanda van Iperen, Fred Jansen, and Carl Richter who have helped with data, and whose positive criticisms improved this work.

I would like to express my sincere gratitude to the whole "Arbeitsgruppe Wefer" who have greeted me with kindness, and have supported and encouraged me over the years.

Adelheid Grimm-Geils, Britta Schilder, Gisela Boelen and Carmen Murken helped me to deal with all the administrative work, always with good humor.

A mi familia y amigos en la Argentina que desde las lejanas Pampas siguieron mis pasos, y me dieron el apoyo afectivo necesario cuando se está tan lejos.

Finally, I would like to thank to Prof. Dr. Helmut Willems and the Graduierten-Kolleg. This work was supported by the Sonderforschungsbereich 261 "Der Südatlantik im Spätquartär: Rekonstruktion von Stoffhaushalt und Stromsystem" at the Universität Bremen. .

Table of Contents

1- Summary

Fluctuations in the sedimentation of biogenic opal and diatoms in the Congo Fan area (Lower Congo Basin off west Africa) during the past 1 million years in the Late Quaternary are the central topics of this thesis. Sediments of ODP Site 1077 (5°10'S, 10°26'E; 2,382 m water depth) were analyzed.

The time interval studied, the last million year in the Late Quaternary, is a very interesting time in the global climate system when a change from a predominantly 41 kyr cyclicity in the early Pleistocene to the late Quaternary 100 kyr ice age cycles took place. This shift occurred around 800 to 900 ka, following the so-called Mid-Pleistocene Transition. The origin of the 100 kyr age cycle dominating the late Pleistocene is an issue not yet fully understood (Imbrie et al., 1993; In: *Paleoceanography*, **8**: 699-735) because the direct influence of eccentricity on insolation is by far too small to produce the corresponding climate style.

The study area is interesting because here one of the largest rivers in terms of freshwater discharge joins an oceanic high-fertility area. The regional environment is dominated by seasonal coastal upwelling and associated filaments and eddies moving offshore, by riverine input from the Congo River, and by incursions of open-ocean waters. Thus, the combination of pelagic and terrigenous information contained in these fan-margin deposits provides an excellent opportunity for studying simultaneous climatic changes on land and at sea.

For the Congo Fan area, biogenic opal concentrations, accumulation rates and relative abundances of marine siliceous microfossils (especially diatoms) turned out to be excellent proxies of changes in marine productivity and surface circulation. Marine diatoms and opal fluctuated in tune with glacial-interglacial cycles, showing highest concentrations during glacial stages and cooler substages of the last interglacial (**Manuscript 1**). The continental signal derived from freshwater diatoms, on the other hand, provided information about humid conditions on land and/or northward movements of the Congo River plume. Humid periods with increased rainfall and river discharge fostered by an intensified monsoon during times of maximum insolation in the Northern Hemisphere were inferred during Stages 10 and 11, and for the period 28-119 ka (**Manuscript 1**).

A long-term trend within the past 450,000 years and an abrupt change in the amplitude of the siliceous signal as well as in the diatom assemblages was evident at Termination II. The system seems to have changed from predominately marine to mixed marine/brackish/freshwater (**Manuscript 1**). High relative abundances of a marine diatom species tolerant to low salinity conditions and large concentrations of freshwater diatoms since Termination II were observed.

In **Manuscript 2,** we addressed the question of what caused this remarkable change in environmental conditions, and hypothesized that this change was the result of a freshening of the ambient water masses. To test this hypothesis we compared changes in the freshwater signal derived from freshwater diatoms at Site 1077 with concomitant changes in the oxygen isotope ratios of planktic foraminifers from the study area (Site 1077; and GeoB1008: 6°35´S 10°19´E) and from the eastern equatorial Atlantic (GeoB1041: 3°48'S 7°05'W). The $\delta^{18}O$ record of the planktic foraminifer *Globigerinoides ruber* (pink) revealed negative deviations from the global oxygen isotope signal during

warm stages 1, and sub-stages 3.2, 5.1, 5.3, and 5.5. Marked peaks were up to 0.6‰ lighter than the "normal" interglacial limit. To test for freshwater and temperature effects on the observed differences between Site 1077 and GeoB 1041, we evaluated in which way temperature and salinity control the present-day oxygen isotope ratio in the working area (**Manuscript 2**). Monthly equilibrium $\delta^{18}O_{calcite}$ values were calculated for an east-west transect along 5°S (10°W to 12°E) including the two core locations. We concluded that the freshwater effect on the isotopic signal is by far more important than the temperature effect for the deviations seen in $\delta^{18}O_{calcite}$ between both sites, and that the observed lighter values in the foraminiferal oxygen isotope record of Site 1077 were a consequence of freshwater pulses of the Congo River.

We were puzzled by the fact that such fresh pulses in the oxygen isotope record were not recorded prior to Termination II, especially because the Congo River has existed since the Pliocene and no substantial changes in the catchment area have been reported at least for the Late Quaternary. We then explored possible causes and consequences of this freshening of the past 120-130 kyr, including local enhancement of monsoonal precipitation, latitudinal migration of the Inter-Tropical Convergence Zone, and regional movements of oceanic fronts (**Manuscript 2**). We concluded that the changes observed since Termination II may not have been linked to environmental conditions on land, but may have been related to an equatorward movement of the Angola-Benguela Front, which in turn was responsible for a northward deflection of the river plume and therefore produced a major freshwater influence over Site 1077.

Fluctuations in opal concentration were examined in relation to orbital forcing and global climate change during the past one million years (**Manuscript 3**). Spectral analysis over the entire Site 1077 record (1,000 ka; Dt = 4.0 kyr) was performed to investigate for cyclicities that might drive opal variability in the Congo Fan area. The opal record is dominated by variance at the 100 kyr periodicity. The phase lock between opal and orbital eccentricity began at ca. 1 Myr, earlier than the establishment of large ice sheets in the Northern Hemisphere. Distinct peaks exactly at the eccentricity periods near 95 and 124 kyr indicated that the deposition of biogenic silica in the study area is largely controlled by the 100 kyr ice age cycle, and hence by high-latitude variations. We suggested that other factors in conjunction with (or in addition to) upwelling intensity may be regulating the deposition of biogenic opal in these sediments. We followed the conceptual model presented by Pollock (1997 in *Global and Planetary Change*, 14: 113-125) and proposed that enhanced opal concentrations in the Congo Fan area during glacial periods must have been the result of increased silica availability in the surface waters. A link to advection of silicate-enriched deep and intermediate waters from the Southern Ocean was suggested for glacial periods coinciding with enhanced Benguela Current circulation, and increased vertical mixing which in turn was induced by strengthening of the Trade winds.

Finally, we compared opal sedimentation in the Congo Fan area with other locations in the equatorial and tropical eastern Atlantic to the north (Site 663; 1°S 11°W) and south (Site 1084; 25°S 13°E) (**Manuscript 3**). Greater resemblance with the equatorial site was observed for the last 500 kyr, a similarity that seems to break down in the older part of the record, when opal fluctuations at Site 1077 were synchronized with those from off Namibia.

2- Introduction

Biogenic opal and the global silica cycle

Silicon is an important component of the lithosphere (Seibold and Berger, 1993). Dissolved silica (Si) in seawater occurs mostly as silicic acid $Si(OH)_4$. Its distribution in the different water masses (surface, deep and bottom) is governed by complex interactions among physical, chemical, geological and biological processes. Thus, marked regional differences characterize the distribution of $Si(OH)_4$ in the world ocean (i.e. much higher concentrations in Antarctic surface waters than in central gyres; $Si(OH)_4$-rich deep and bottom waters; Tréguer et al., 1995).

Figure 1 summarizes the biogeochemical cycle of Si in the world ocean (Tréguer et al., 1995), as follows: The surface ocean receives $Si(OH)_4$ inputs from the lithosphere both directly, via chemical wheathering of the continental crust and transfer to the ocean via rivers, and indirectly, through eolian transport. The third pathway of net transfer of dissolved Si from the lithosphere to the hydrosphere is wheathering of submarine basalt (Tréguer et al., 1995). On time scales of $< 10^4$ years, the biogeochemical cycle of Si and its budget are affected by inputs of $Si(OH)_4$ from rivers, atmospheric deposition, seafloor wheathering, and hydrothermal activity. The transfer of silicic acid from the marine hydrosphere to the biosphere initiates the biological cycle of Si. This is the link between the cycle of this element to that of carbon.

Planktonic organisms for which silica is an important component include diatoms, radiolarians and silicoflagellates. They build up their skeletons by taking up $Si(OH)_4$ from seawater. Thus, biogenic Si production occurs within the surface reservoir (Fig. 1). Although it is difficult to distinguish between specific contributions, evidence strongly supports the main role played by diatoms in the global production of biogenic Si (Lisitzin, 1972; Takahashi, 1991; Nelson et al., 1995; Tréguer et al., 1995). In equatorial areas radiolarians are major producers of biogenic silica, and they can be present in important quantities in the underlying sediments (Kling, 1998). But their flux is not linked to primary production in surface waters. Silicoflagellates, which were widespread during the Tertiary period, are less important in modern biogenic silica production (Haq, 1998).

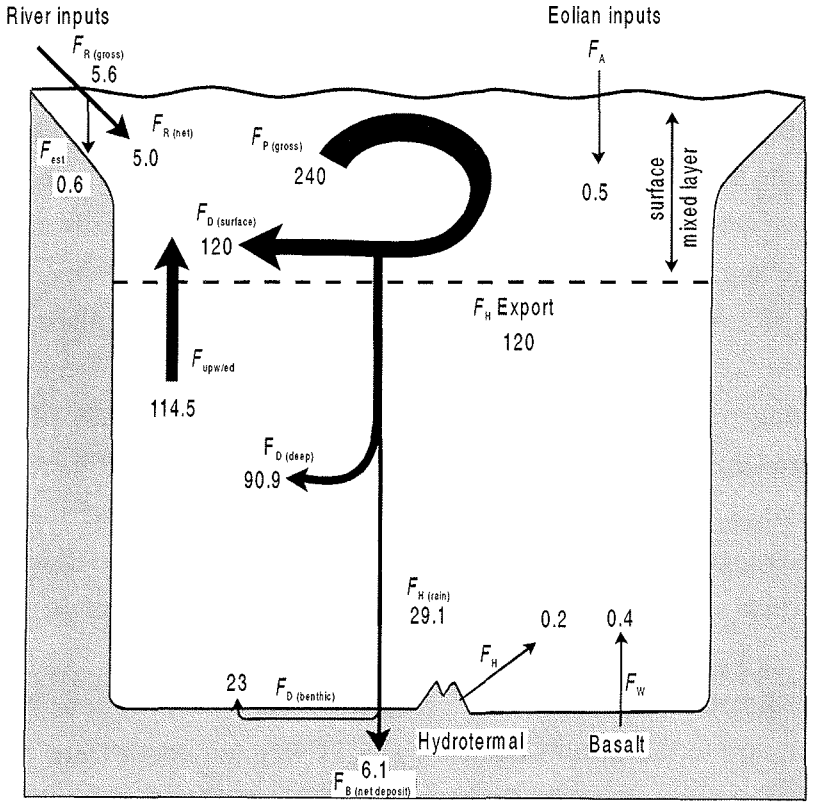

Fig. 1: Geochemical cycle of Si in the World Ocean at steady state; from Tréguer et al. (1995).

The fate of the biogenic Si produced in the euphotic layer is governed by the competition between dissolution in and export from the surface waters. Globally, more than 50% of the biogenic Si produced by the siliceous phytoplankton dissolves in the upper 100 m (Nelson et al., 1995), and 90% of the dissolution occurs in the water column above 1,000 m (Tréguer et al., 1995). Finally, the portion of opal that escapes dissolution sinks through the water column as phytoplankton particulate silicon or $Si(OH)_4$-rich fecal pellets (e.g. Dugdale et al., 1995), and reaches the seafloor where dissolution continues (Fig. 1). The net accumulation of opal constitutes the net output of Si from the biogeochemical cycle. The preservation ratio (opal accumulation in sediment/gross production in surface waters) averages 3 % (Tréguer et al., 1995), which is much higher than the preservation efficiency of organic carbon (Westbroeck et al., 1993).

Diatoms

Diatoms are unicellular, eukaryotic, photosynthetic organisms. They are distributed in almost all waters; they are abundant in the phytoplankton and phytobenthos of marine, brackish and fresh waters, at all latitudes (Round et al., 1990). Diatoms in the ocean tend to dominate in a number of oceanographic settings that offer both the high nutrient and turbulence conditions they require for growth (e.g. coastal upwelling areas, equatorial divergences, ice edges, river plumes; see summary in Ragueneau et al., 2001). In addition, some diatom species are able to grow under low light conditions and generate substantial production at depth (Kemp et al., 2000, and references therein). Others, are able to regulate their buoyancy through the formation of vertically migrating mats (e.g. Villarreal et al., 1999).

Diatoms have a highly differentiated cell wall which is impregnated with opaline silica (diatom frustule). The diatom frustule is basically composed of two valves, separated by a cingulum composed of intercalary bands (e.g. Round et al., 1990). New valves are constructed during cell division, followed by sequential deposition of the girdle bands (Round, 1972). Diatoms have an absolute requirement for $Si(OH)_4$ (Lewin, 1961) without which frustules are not formed and the cell cycle is not completed (Brzezinski, 1992).

The siliceous exoskeleton is variably resistant to decay. Heavily silicified diatom frustules are more likely to escape dissolution after cell death and during sinking to the seafloor. They are often overrepresented in the sedimentary record when compared to their abundance in the water column (e.g. Sancetta, 1992, 1995). This appears to be especially true for sediments underlying pelagic areas (e.g. Sancetta, 1992; Lange et al., 1994). Many diatoms can maintain division rates very close to the maximum specific cell-division rate at extracellular $Si(OH)_4$ that clearly limits Si uptake. Diatoms do this by producing thinner frustules thus decreasing their cellular Si content and Si:C ratio (Paasche, 1973; Brzezinski et al., 1990). This leads to thinner frustules which may make such cells more susceptible to destruction by dissolution and thus decrease the likelihood of their preservation in the sediments (Lewin, 1961; Lisitzin, 1966). An excellent review of the major steps in the silicification process of diatoms (Si uptake, intracellular processes, Si pool, mineralization, diatom cell cycle, etc.) is given in Ragueneau et al. (2000).

Diatoms and primary productivity

A substantial part of the ocean's primary productivity is provided by diatoms. Nelson et al. (1995) and Tréguer et al. (1995) proposed upper limits of 35% for the contribution of diatoms in oligotrophic areas, and 75% in coastal zones and other nutrient-rich systems. In general, the relative abundance of diatoms in the phytoplankton increases as primary productivity increases (e.g. Raymont, 1980). However, the increase of diatom productivity and silica production with increasing total primary productivity is non-linear (Ragueneau et al., 2000). Spatial variations in the Si:C production ratio exist. This ratio is affected by the relative contribution of diatoms to the total primary productivity, and several other factors (including temperature, light intensity, photoperiod, macronutrient limitation, and Fe availability) have been shown to influence the Si:C ratio within species (see summary in Ragueneau et al., 2000).

Export of biogenic Si from the photic layer

Physical, chemical and biological factors combine with intrinsic properties governing the dissolution of the biogenic opal formed in surface waters to control the competition between biogenic silica dissolution in surface waters and its export to the deep waters (see summary in Ragueneau et al., 2000). Among the physical factors, temperature plays a prevailing role in the dissolution of siliceous organisms in the photic zone. Silica dissolution is known to be strongly temperature dependent, with the specific dissolution rate increasing by an order of magnitude with each 15°C increase in temperature. Most of the biogenic silica produced in surface waters is dissolved in the first 100 m of the water column where the strongest changes in temperature take place (Nelson et al., 1995); deep waters are confined to a much narrower range of rather low temperatures. Additionally, other factors such as the physiological state of the diatom cells, bacterial activity, as well as grazing by microorganisms enhance the effect of dissolution by temperature (Jacobson and Anderson, 1986; Miller et al., 1995; Biddle and Azam, 1999). Lately, the importance of silicic acid availability in controlling the contribution of diatoms to the total production and hence, to export fluxes of biogenic matter out of the photic zone has emerged for both modern ocean (e.g. "silicate pump" model of Dugdale and Wilkerson, 1998) and for the glacial ocean (e.g. Herguera, 1992; Pollock, 1997; Berger and Lange, 2000).

Tréguer et al. (1995) estimated that 90% of the total silica produced in surface waters is dissolved in the euphotic zone, whereas only 10% occurs in the seabed. Sediment trap studies have shown that below the euphotic zone opal fluxes remain quite unaffected during settling through the water column (Ragueneau et al., 2000). Since organic matter is recycled more rapidly than biogenic Si this leads to a better preservation of biogenic Si compared to organic carbon during sedimentation, and a subsequent increase in the Si:C ratio with depth (i.e. the so-called decoupling between silicon and carbon) (Ragueneau et al., 2000). The extent of the Si:C decoupling in the water column depends largely upon the rapidity of the settling process. Higher Si:C ratios follow bloom periods due to the increasing contribution of diatoms to the total production during blooms and to their subsequent efficient export (i.e. diatom aggregation and mass settlement; Alldredge and Gotschalk, 1989).

The seabed preservation efficiency of biogenic opal depends upon several processes, including the sedimentation rate of a given area, the bioturbation intensity and the processes influencing the kinetic and thermodynamic properties of opal dissolution (Archer et al., 1993; van Capellen and Qiu, 1997a, 1997b; review in Ragueneau et al., 2000). Dissolution continues during burial until either the interstitial waters become saturated or altered chemical composition of the particle surfaces prevents further dissolution (e.g. Kamatani et al., 1988; Nelson et al., 1995). Dissolution properties of biogenic silica in the sediments have been suggested to depend not only on diagenetic reactions but also on water column processes such as the extent of surface water dissolution and quality of the particles as they arrive at the sediment-water interface (see review in Ragueneau et al., 2000).

In summary, any process that either lowers the rate of silica dissolution during sedimentation and burial (e.g. trace element chemistry of the surface layer in which that opal is formed: Lewin, 1961; Nelson, 1975; van Bennekom et al., 1991; low temperatures: Nelson and Gordon, 1982), or decreases the time the sedimenting particles are exposed to undersaturated conditions (e.g. shallow vs. deep water columns: DeMaster, 1981; Tréguer et al., 1995; rapid downward transport by mass flocculation of diatom spring blooms: Alldregde and Gotschalk, 1989; mass sedimentation after the breakdown of thermal stratification in autumn: Kemp et al., 2000; export via fecal pellets: Bathman et al., 1990) will increase the fraction of surface-produced opal that is preserved in the seabed (review in Nelson et al., 1995). In fact, Nelson et al. (1995) have argued that regional differences in silica preservation dominate over regional productivity differences. Furthermore, diatom cell size, silicification of the diatom frustule, and the species composition of the diatom assemblage play an important role in determining whether the siliceous material of a given species will reach the seafloor and preserve in the sedimentary record (Nelson et al., 1995).

Biogenic opal and diatoms in the sediments as proxies of paleoproductivity

Despite the complexity of the Si cycle, and due to the major role played by diatoms in the biological pump of CO_2, to the presence of silica-rich sediments in areas that play a major role in air-sea CO_2 exchange, and to the reasonably good overall preservation efficiency of biogenic opal, opal has a strong potential as a proxy for paleoproductivity reconstructions (Ragueneau et al., 2000). Opal is one of the three main constituents in deep-sea sediments (along with calcite and the products of terrestrial weathering). Opal-rich sediments are found at all depths (from the shelf to the abysses), all latitudes (Southern Ocean, North Pacific, equatorial divergences, and coastal margins) and all climate zones of the ocean that play a very important role in Earth climate (Lisitzin, 1972). Major biogenic Si deposit sites are the Southern Ocean, the North Pacific, the equatorial divergence, and coastal margins (Lisitzin, 1972). Among the latter, the coastal upwelling areas off Peru, NW Africa, and SW Africa are areas where the percentage of biogenic Si in the sediments often exceeds 20% by weight, and where diatom frustules and valves are a major component (Lisitzin, 1972) (Fig. 2).

Paleoceanographic studies often interpret the formation of opal-rich sediment as evidence of high diatom productivity. Indeed, abundances of marine diatom valves in surface and subsurface sediments have been extensively used by paleoceanographers as a measure of the diatom flux exported from the photic zone, and considered as a proxy for paleoproductivity. Data based on the taxonomic composition

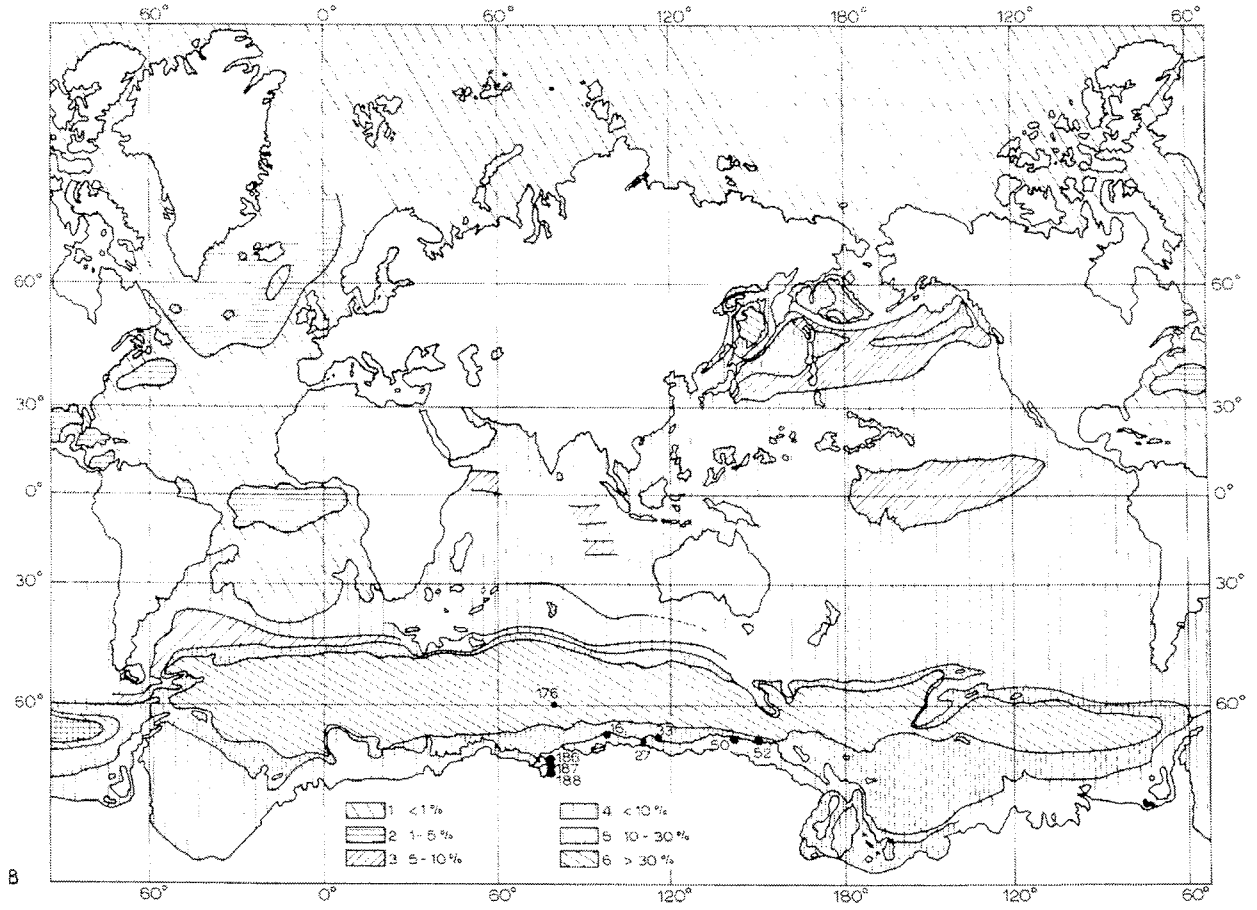

Fig. 2. Silica distribution in surface sediments, from Lisitzin (1971)

of microfossil assemblages are among the most useful methods for interpreting past environmental conditions (Sancetta, 1989). Changes in the rates of coastal and open-ocean upwelling, diatom production, and export and sequestration of organic carbon are considered to play a key role for the initiation of global cooling at the onset of the Pleistocene glacial periods (Pollock, 1997).

References Cited

Alldredge, A.L., and Gotschalk, C.C., 1989. Direct observations of the mass flocculation of diatoms blooms: characteristics, settling velocities and formation of diatom aggregates. *Deep-Sea Res.*, **36**(2): 159-171.

Archer, D., Lyle, M., Rodgers, K., and Froelich, P., 1993. What controls opal preservation in Tropical deep-sea sediments? *Paleoceanography,* **8**(1): 7-21.

Bathman, U.V., Noji, T.T., and von Bodungen, B., 1990. Copepod grazing potential in late winter in the Norwegian Sea – a factor in a control of spring bloom development? *Mar. Ecol. Prog. Ser.,* **60**: 225-233.

Berger, W.H., and Lange, C.B., 2000. Silica depletion in the thermocline of the glacial North Pacific: corollaries and implications. *Deep-Sea Res.*, **45**: 1885-1904.

Bidle, K. D. and Azam, F., 1999. Accelerated dissolution of diatom silica by marine bacterial assemblages. *Nature,* **197**: 508-512.

Brzezinski, M.A., 1992. The Si:C:N ratio of marine diatoms: interespecific variability and the effect of some environmental variables. *J. Phycol.*, **21**: 347-357.

Brzezinski, M.A., Olson, R.J., and Chisholm, S.W., 1990. Silicon availability and cell-cycle progression in marine waters. *Mar. Ecol.: Prog. Ser.*, **67**: 83-96.

DeMaster, D.J., 1981. The supply and accumulation of silica in the marine environment. *Geochim. Cosmochim. Acta*, **45**: 1715-1732.

Dugdale, R.C. and Wilkerson, F.P., 1998. Understanding the eastern equatorial Pacific as a continuous new production system regulating silicate. *Nature*, **391**: 270-273.

Dugdale, R. C., F. P. Wilkerson, and Minas, H.J., 1995. The role of a silicate pump in driving new production. *Deep-Sea Res. I,* **42**(5): 697-719.

Haq, B.U., 1998. 11- Silicofalgellates and ebridians. In: Haq, B.U., Boersma, A. (eds.). *Introduction to Mar. Microplaeontol.* Elsevier (Amsterdam), pp. 209-244.

Herguera, C., 1992. Deep-sea benthic foraminifera and biogenic opal: glacial to postglacial productivity changes in the western Equatorial Pacific. *Mar. Microplaeontol.*, **19**: 79-98.

Jacobson, D.M. and Anderson, D.M., 1986. Thecate heterotrophic dinoflagellates: feeding behavior and mechanism. *J. Phycol.*, **22**: 249-258.

Kamatani, A., Ejiri, N., and Tréguer, P., 1988. The dissolution kinetics of diatom ooze from the Antarctic area. *Deep-Sea Res.*, 35: 1195-1203.

Kemp, A., Pike, J., Pearce, R.B., and Lange, C.B., 2000. The "Fall dump" - a new perspective on the role of a "shade flora" in the annual cycle of diatom production and export flux. *Deep-Sea Res. II*, **47**: 2129-2154.

Kling, S.A., 1998. 9- Radiolaria. In: Haq, B.U., Boersma, A. (eds.). *Introduction to Marine Micropaleontology*. Elsevier (Amsterdam), pp. 209-244.

Lange, C. B., U. F. Treppke, and Fischer, G., 1994. Seasonal diatom fluxes in the Guinea Basin and their relationship to trade winds, hydrography and upwelling events. *Deep-Sea Res. I,* **41**(5/6): 859-878.

Lewin, J.C., 1961. The dissolution of silica from diatom walls. *Geochim. Cosmochim. Acta*, **21**: 182-195.

Lisitzin, A.P., 1966. Main distribution patterns of recent siliceous sediments and their correlation with climatic zonality. In: *Geokhimiya Kremnezema (Silica Geochemistry)*, Nauka, Moscow.

Lisitzin, A.P., 1971. Distribution of siliceous microfossils in suspension and in bottom sediments. In: Funnell, B.M. and Riedel, W.R. (eds.), *The Micropaleontology of Oceans*. Cambridge University Press (London), pp. 173-195.

Lisitzin, A.P., 1972. Sedimentation in the World Ocean, Banda Press, (Tulsa, Okla) 218 pp.

Miller, C.B., Nelson, D.M., Weiss, C., and Soeldner, A.H., 1995. Morphogenesis of opal teeth in calanoid copepods. *Mar. Biol.*, **106**: 91-101.

Nelson, D.M., 1975. *Uptake and regeneration of silicic acid by marine phytoplankton.* Ph.D. Dissertation, 157 pp., Univ. Alaska, Fairbanks.

Nelson, D.M. and Gordon, L.I., 1982. Production and pelagic dissolution of biogenic silica in the Southern Ocean. *Gecochim. Cosmochim Acta*, **46**: 491-501.

Nelson, D. M., Tréguer, P., Brzezinski, M. A., Leynaert, A., and Quéguiner, B., 1995. Production and dissolution of biogenic silica in the ocean: Revised global estimates, comparison with regional data and relationship to biogenic sedimentation. *Global Biogeochem. Cycles,* **9**: 359-372.

Paasche, E., 1973. Silicon and the ecology of marine plankton diatoms. I. *Thalassiosira pseudonana (Cyclotella nana)* growth in a chemostat with silicate as a limiting nutrient. *Mar. Biol.,* **19**: 117-126.

Pollock, D. E., 1997. The role of diatoms, dissolved silicate and Antarctic glaciation in glacial/interglacial climatic change: a hypothesis. *Global Planet. Change,* **14**: 113-125.

Ragueneau, O., Tréguer, P., Leynaert, A., Anderson, R.F., Brzezinski, M.A., DeMAster, D.J., Dugdale, R.C., Dymond, J., Fischer, G., François, R., Heinze, C., Maier-Reimer, E., Martin-Jézéquiel, V., Nelson, D.M., and Quéguiner, B., 2000. A review of the Si cycle in the modern ocean: recent progress and missing gaps in the application of biogenic opal as a paleoproductivity proxy. *Global and Planetary Change,* **26**: 317-365.

Raymont, J.E.G., 1980. Plankton and productivity in the oceans, 2nd ed., vol 1, *Phytoplankton.* Pergamon (New York), 489 pp.

Round , F. E., Crawford, R. M., Mann, D. G., 1990. *The Diatoms. Biology & Morphology of the Genera.* Cambridge University Press (Cambridge, U.K), 747 pp.

Sancetta, C., 1989. Processes controlling the accumulation of diatoms in sediments: a model derived from British Columbian Fjords. *Paleoceanography*, **7**: 183-194.

Sancetta, C., 1992. Comparison of phytoplankton in sediment trap time series and surface sediments along a productivity gradient. *Paleoceanography,* **7**(2): 183-194.

Sancetta, C., 1995. Diatoms in the Gulf of California: seasonal patterns and the sedimentary record for the last 15,000 years. *Paleoceanography,* **10**(1): 67-84.

Seibold, E. and Berger, W.H., 1993. The seafloor an introduction to marine Geology. Springer (Berlin), 356 pp.

Takahashi, K., 1991. Mineral flux and biogeochemical cycles of marine planktonic protozoa – Session summary. In: Reid, P.C. et al. (eds.), NATO ASI Series, Vol. 25, Protozoa and their role im marine processes, pp. 347-359.

Tréguer, P., Nelson, D.M., Van Bennekom, A.J., DeMaster, D.J., Leynaert, A., and Quéguiner, B., 1995. The silica balance in the World ocean: a reestimate. *Science,* **268**: 375-379.

van Bennekom, A.J., Buma, A.G.J., and Nolting, R.F., 1991. Dissolved aluminum in the Weddell-Scotia Confluence and the effect of Al on the dissolution kinetcs of biogenic silica. *Mar. Chem.*, **35**: 423-434.

van Cappellen, P. and Qiu, L., 1997. Biogenic silica dissolution in sediments of the Southern Ocean. I. Solubility. *Deep-Sea Res. II*, **44**(5): 1109-1128.

van Cappellen, P. and Qiu, L., 1997. Biogenic silica dissolution in sediments of the Southern Ocean. II. Kinetics. *Deep-Sea Res.*, **44**(5): 1129-1149.

Villarreal, T., Pilskaln, C., Brzezinski, M., Lipschultz, F., Dennett, M., and Gardner, G.B., 1999. Upward transport of oceanic nitrate by migrating diatom mats. *Nature,* **397**: 423-425.

Westbroeck, P., Brown, C.W., van Bleijswijk, J., Brownlee, C., Brummer, G.J., Conte, M., Egge, J., Fernandez, E., Jorrdan, R., Knapperstbusch, M., Stefels, J., Veldhuis, M., van der Wal, P., and Young, J., 1993. A model system approach to biological climate forcing. The example of *Emiliana huxleyi. Global Planet Change*, **8**: 27-46.

3- Objectives

The central topics of this thesis are the fluctuations in opal and diatom concentrations, and the changes in diatom assemblages in the Congo Fan area during the past one million years in the Late Quaternary.

The main objectives are:

1. To construct a biogenic opal record for the last one million years from the northern rim of the Congo River Fan (ODP Site 1077), an environment which is dominated by seasonal coastal upwelling and associated filaments and eddies moving offshore, by riverine input from the Congo River, and by incursions of open-ocean waters.

2. To examine fluctuations in opal concentration from the Congo Fan area in relation to orbital forcing and global climate change during the past million years.

3. To reconstruct temporal fluctuations in the Congo River freshwater outflow, and in marine productivity and their relationship to African climate (including local enhancement of monsoonal precipitation, latitudinal migration of the Inter-Tropical Convergence Zone, and regional movements of oceanic fronts), based on opal concentrations and siliceous microfossil assemblages.

4. To compare changes in the freshwater signal derived from freshwater diatoms with concomitant changes in the oxygen isotope ratios of planktonic foraminifers from the Congo Fan area, and from other sites in the eastern equatorial Atlantic.

5. To integrate our findings of the Congo area with those of other studies from nearby sites, from off Namibia, and the equatorial Atlantic.

4- Presentation of Results

This thesis comprises three manuscripts which are in press or have been submitted for publication. The studies were performed at the Fachbereich Geowissenschaften in the framework of the Graduierten-Kolleg, and were funded by the Sonderforschungsbereich 261 "Der Südatlantik im Spätquatär: Rekonstruktion von Stoffhaushalt und Stromsystem". The work has been supervised by Prof. Dr. Gerold Wefer.

In what follows the three manuscripts are briefly summarized. All data generated and used in this thesis are archived in the information system PANGAEA.

Manuscript 1 (published):

Siliceous phytoplankton productivity fluctuations in the Congo Basin over the past 460,000 years: marine vs. riverine influence, ODP Site 1077

Uliana, E., Lange, C.B., Donner, B., and Wefer, G., 2001

In: Wefer, G., Berger, W.H., and Richter, C. (Eds.), *Proc. ODP, Sci. Results*, **175**, 1-32 [Online]. Available from World Wide Web:

<http://www-odp.tamu.edu/publications/175_SR/chap_11chap_11.htlm>

Accumulation rates, concentration and relative abundance of siliceous microfossils from Site 1077 are used to reconstruct changes in marine productivity and climate history of the Congo Fan area. The major contributors to the siliceous productivity are marine diatoms showing highest concentrations during glacial stages and cooler substages of the last interglacial. Abrupt changes are observed during Termination II (boundary oxygen isotope stages 5/6):

1) The marine diatom signal varied in amplitude and in assemblage composition from predominately marine to marine/brackish.
2) The environmental setting on land obtained from freshwater diatoms and Chrysophycean cysts point to changes from more arid conditions accompanied by a large drainage area of the Congo River to more humid conditions and a decrease on the inland water content for the last 125 ky.

Manuscript 2 (submitted):

Evidence for Congo River freshwater load in Late Quaternary sediments of ODP Site 1077 (5°S, 10°E)

Uliana, E., Lange, C. B., and Wefer, G.

Submitted for publication in *Palaeogeogr., Palaeoclimat., Palaeoecol.* (March, 2001)

Fluctuations in the freshwater influence of the Congo river and their sedimentary imprint were reconstructed using different proxies in a core at the northern rim of the river fan for the late Quaternary. For these purposes three different parameters were assessed in ODP 1077 sediments: concen-

tration of freshwater diatoms, relative abundance of marine diatoms, and oxygen isotopes. High relative abundances of a marine diatom species tolerant to low salinity conditions (*Cyclotella litoralis*) and large concentrations of freshwater diatoms since Termination II are observed. The $\delta^{18}O$ record of the planktonic foraminifera *Globigerinoides ruber* (pink) revealed negative deviations from the global oxygen isotope signal which occurred during warm stages 1, and sub-stages 3.2, 5.1, 5.3, and 5.5. Comparison between the isotopic signal of ODP 1077 and the one from the pelagic core GeoB1041 confirm these results. The construction of an artificial $\delta^{18}O$ curve using the SST data from the nearby core GeoB 1008 allowed us to estimate the respective salinity and temperature effects on the ODP 1077 isotopic signal. Assuming salinity as the principal factor that has an effect on the $\delta^{18}O$ record of Site 1077, we used the oxygen isotope difference between both locations ($\Delta\delta^{18}O$) as a proxy for freshwater input. A general trend in the $\Delta\delta^{18}O$ calculated with more negative values since Termination II was observed. Conspicuous $\Delta\delta^{18}O$ pulses coincided with periods of maxima in Northern Hemisphere summer insolation over the African continent, suggesting an increase in the freshwater discharge from the Congo River due to enhanced precipitation on the hinterland. The abrupt change in surface water conditions recorded from isotopes and siliceous microfossils at Termination II is explained as an equatorward displacement of the Angola-Benguela Front which, in turn, caused a northward deflection of the Congo river plume and therefore produced a major freshwater influence over site 1077.

Manuscript 3 (to be submitted):

Opal sedimentation at the northern rim of the Congo Fan: A 1 Myr record from ODP Site 1077 (5°S, 10°E)

Uliana, E, Lange, C. B., and Wefer, G.

To be submitted to *Paleoceanography* (June, 2001)

We present Late Quaternary (1 Myr) biogenic opal and diatom records from the northern rim of the Congo River Fan (ODP Leg 175, Site 1077). Opal sedimentation in the area reflects surface ocean productivity, with marine microorganisms (especially diatoms) driving the biogenic opal signal. We find that opal has fluctuated in tune with eccentricity variations (100 kyr), with higher values during glacial stages reaching 25 wt % at the LGM. No evidence of forcing in the obliquity band and only a very slight response in the precessional band could be observed. A correlation with ODP Site 677 benthic oxygen isotope data (ice-volume proxy) indicates that the phase lock between opal and orbital eccentricity began at ca. 1 Myr, somewhat earlier than the establishment of large ice sheets in the Northern Hemisphere. Comparison of the Congo area with other opal records from the equatorial Atlantic (ODP Site 663) and the subtropical South Atlantic off Namibia (ODP Site 1084) suggests a greater resemblance with the equatorial site for the last 500 kyr. This similarity breaks down in the older part of the record, when opal fluctuations at Site 1077 were synchronized with those from off Namibia.

5- Material and Methods

Sediments were collected in the Lower Congo Basin off west Africa during the Ocean Drilling Program (ODP) Leg 175 (Shipboard Scientific Party, In: Wefer et al., 1998). The area was targeted for three drilling Sites, 1075, 1076, and 1077. We performed our studies on Site 1077 (5°10'S, 10°26'E), which is the intermediate-water drilled site located at 2,382 m water depth, at the northern rim of the Congo River Fan (Fig. 3). Our analyses focused on the last 1 Myr.

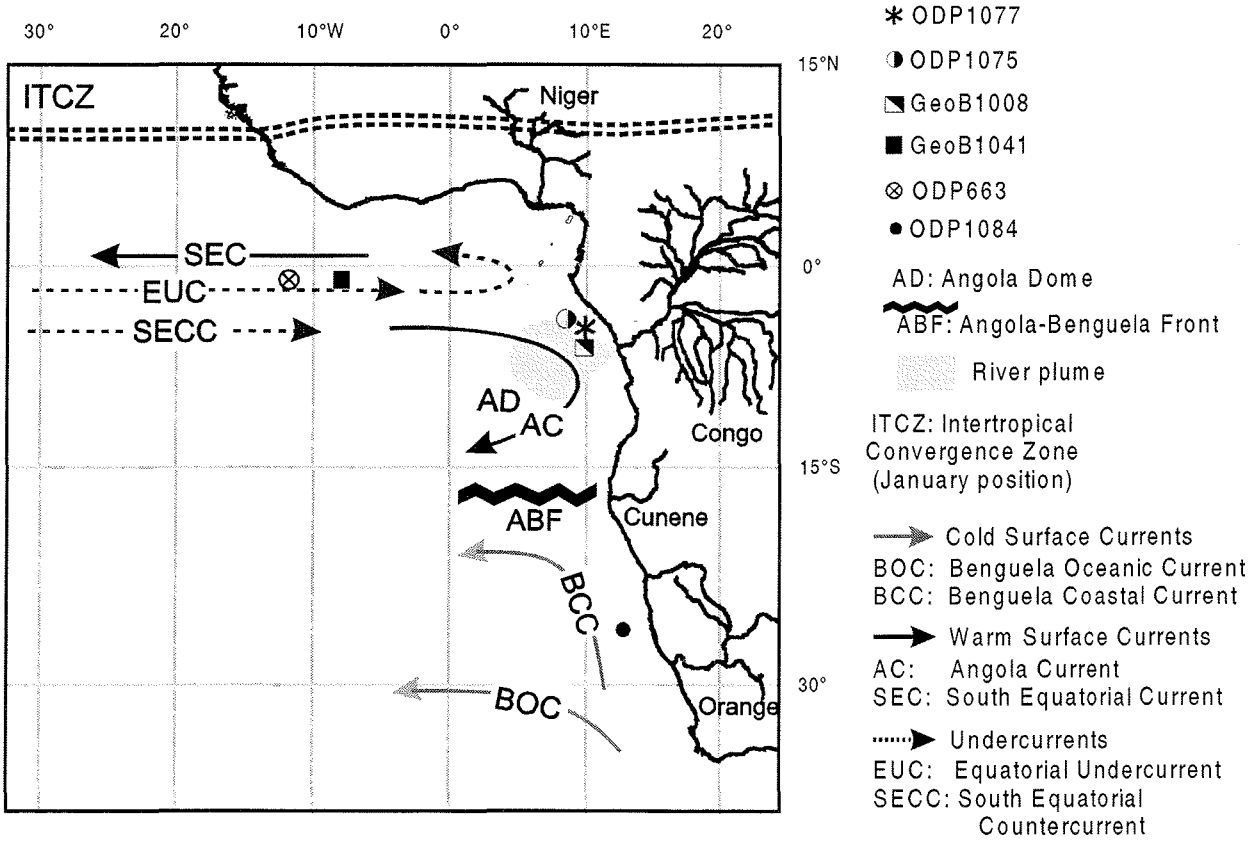

Fig. 3: Study area. Location of ODP and GeoB sites considered in this thesis; main surface and subsurface currents, and extension of the Congo River plume.

Sampling was mainly performed on Hole 1077A, although for some intervals additional samples were collected from Holes 1077B and 1077C. Meters below seafloor (mbsf) were transformed to meters composite depth (mcd) according to Shipboard Scientific Party, "Site 1077" (Wefer et al., 1998).

Stratigraphy

Stable oxygen isotope data measured on the planktonic foraminifer *Globigerinoides ruber* (pink) (size >150 μm) were used to generate the oxygen isotope stratigraphy for ODP Site 1077. Sampling resolution was 20 cm. A Finnigan MAT 251 micromass spectrometer equipped with a Kiel automated carbonate preparation device was used. Calibration to the PDB standard was via the VNBS19, and the internal standard SHK Bremen. Analytical precision during the measurements from working standards was ±

0.07 ‰ (M. Segl, pers. comm.). Stratigraphic pointers were obtained by tuning the $\delta^{18}O$ record of Site 1077 to the $\delta^{18}O$ record of Site 677 (Panama Basin, Shackleton et al., 1990). Detailed information about the age model is published in Dupont et al. (2001), and Uliana et al. (2001).

Siliceous microfossils

For the siliceous microfossils analyses 5 cm^3 sediment samples were collected. Sampling intervals varied from every 45 cm for the upper 44 mcd representing an average resolution of ~ 2000 yrs, to every 110-120 cm downcore to 70 mcd; resolution for the lower part ranges from ~ 5,000 to 10,000 years. Samples were freeze-dried, and 0.4 g of dry sediment for each sample was treated with hydrochloric acid and hydrogen peroxide to dissolve carbonates and organic matter following the method of Schrader and Gersonde (1978); sodium pyrophosphate was added to remove clay-size particles in suspension. Acid and salt remains were removed by repeated steps of rinsing with distilled water and settling. Preparation of slides for qualitative and quantitative analyses was performed according to Lange et al. (1994).

Identification and counting of taxa was done on permanent slides with a Zeiss-Axioscope (phase contrast illumination). Qualitative and quantitative analysis were done at 1000X magnification. Due to the overwhelming dominance of a few diatom taxa, and to maximize the information recorded for the less abundant groups the counting procedure was divided into two steps: (1) for the most abundant diatom species (e.g., *Thalassionema nitzschioides* var. *nitzschioides*, *Cyclotella litoralis, Chaetoceros* spp.) one transect across the slide was quantified; (2) for the rest of the diatom species, radiolarians, silicoflagellates, ebridians, phytoliths, chrysophycean cysts, and the siliceous skeleton of the dinoflagellate *Actiniscus pentasterias*, a fraction of the slide (1/3, 1/5, 1/10, depending on abundance) was counted. Sponge spicules were not included in our analysis. Definition of counting units followed that of Schrader and Gersonde (1978). Diatoms and silicoflagellates were identified to the lowest taxonomic level possible, whereas all other siliceous microfossils were counted as groups.

Abundances of taxa and/or microfossil groups were calculated as concentrations per gram and as accumulation rates. Relative abundances of individual species or groups of species were calculated as percent of total assemblage. Accumulation rates for the different microfossils studied was calculated according to van Andel et al. (1975), as follows:

$$AR = \delta\ (g/cm^3) * a\ (\text{valves or skeletons}/g_{\text{dry sed.}}) * SR\ (cm/k.y.)$$

where δ is the GRAPE density data obtained on board; a is the estimated concentration for each group of siliceous microfossil per gram of sediment; and SR refers to sedimentation rates obtained by linear interpolation between isotopic tie-points.

Opal measurements

Samples (n = 240) were taken at an average resolution of 4,000 years and analyzed for biogenic opal. Biogenic opal was determined using a sequential leaching technique (DeMaster, 1981) modified by Müller

and Schneider (1993). Opal content from the samples was extracted with 1 M NaOH at 85°C during one hour. Concentration of silica was simultaneously measured by continuous flow analysis with molibdate-blue spectrophotometry. This method has a precision of ± 0.5 %. We neglected the problem of the method not being able to discriminate between biogenic opal and volcanic glass, because no volcanic ash layers have been reported in earlier extensive sedimentological investigations (e.g. Jansen et al., 1984; van der Gaast and Jansen, 1984). Data are given as weight percentages (wt %) of biogenic silica.

Estimation of salinity

The oxygen isotopic composition recorded in the tests of planktonic foraminifers is determined by the temperature and isotopic composition of the water mass in which they calcified (e.g. Emiliani, 1954; for a review see Wefer and Berger, 1991); thus, $\delta^{18}O$ values of their carbonate tests are useful tools for reconstructing hydrological conditions of the upper water column. The $\delta^{18}O$ value of oceanic waters is mainly related to global ice volume and salinity.

To estimate the effects of freshwater and temperature on the oxygen isotope signal, we evaluated in which way temperature and salinity control the present-day oxygen isotope ratio in the working area. Calculations were based on temperature and salinity data from Conkright et al. (1998) and the empirical, lineal relationship for $\delta^{18}O_{calcite}$ from Epstein et al. (1953):

$$T(°C) = 16.5 - 4.3\ (\delta^{18}O_{calcite} - d^{18}O_{w}) + 0.14\ (d^{18}O_{calcite} - d^{18}O_{w})^2$$

where T is the temperature in °C, $\delta^{18}O_{calcite}$ is the isotopic composition of the calcite test in ‰ relative to the PDB standard, and $\delta^{18}O_{w}$ is the isotopic composition of the ambient sea water in ‰ (PDB). The relationship between $\delta^{18}O_{w}$ and salinity depends on the water mass, and on the regional evaporation and precipitation balance for the different oceanic basins (Fairbanks et al., 1992). Thus, there are different $\delta^{18}O_{w}$ and salinity relationships in each of the oceanic basins. Our study is based on the one for the eastern equatorial Atlantic, which is expressed as follows:

$$\delta^{18}O_{w} = 0.08\ S - 1.86$$

where S is the surface salinity in PSU. We used salinity values from Conkright et al. (1998).

We also estimated the $\delta^{18}O_{calcite}$ at our location for the last 200,000 years. The calculations were based on the alkenone-derived sea surface temperature (SST) data of Schneider et al. (1995) generated for nearby core GeoB1008.

Another effect that has to be taken into account is the so-called ice-effect. During the lowering of sea-level at glacial times, oceanic waters are stripped of the lighter isotope ^{16}O which is deposited in the polar ice-sheets. Thus, an enrichment in the heavier oxygen isotope (^{18}O) produces an increment in the global $\delta^{18}O_{w}$ values. To correct for this ice-effect, we used the correction curve of Imbrie et al. (1984), where an increment of 0.3 ‰ in $\delta^{18}O$ represents a change in sea-level of 120 m.

Spectral analyses and filters

To inspect for responses of the opal signal to orbital forcing, spectral analyses were performed using the program Spectrum (Schulz and Stattegger, 1997). We used the Lomb-Scargle method (window type: Welch-overlapped-segment averaging, three segments, level of significance = 0.05, lineal detrend, 6 dB Bandwidth = 0.003 kyr^{-1}).

On the basis of the results obtained in the frequency domain and to examine the timing and evolution of the opal response with respect to eccentricity, a bandpass filtering was carried out with the MatLab program version 5.1. The eccentricity-related component was extracted in the frequency band 85-135 kyr for opal, and 90-120 kyr for oxygen isotopes, applying a Butterworth bandpass filter.

Cross-spectral analysis between opal concentration and the eccentricity orbital parameter (Laskar, 1990) was conducted (Welch-overlapped-segment averaging, three segments, level of significance = 0.05, lineal detrend, 6 dB Bandwidth = 0.002 kyr^{-1}). The coherency (κ) estimated is a measure of the degree to which the analyzed signals (opal and eccentricity) are linearly related at a given periodicity. Positive phase values indicate that the opal signal lags eccentricity; conversely, negative values denote opal leading eccentricity.

References Cited

Conkright, M., Levitus, S., O'Brien, T., Boyer, T., Antonov, J., and Stephens, C., 1998. *World Ocean Atlas.* Available online and on CD-ROM Data Set Documentation.. Tech. Rep. 15, NODC Internal Report, Silver Spring, MD. 16 pp.

DeMaster, D.J., 1981. The supply and accumulation of silica in the marine environment. *Geochim. Cosmochim. Acta*, **45**: 1715-1732.

Dupont L.M., Donner B., and Schneider R., Wefer G., 2001. Mid-Pleistocene environmental change in tropical Africa began as early as 1.05 Ma. *Geology*, **29**: 195-198.

Emiliani, C., 1954. Depth habitat of some species of pelagic foraminifera as indicated by oxygen isotopic ratio. *Amer. Jour. of Sci.* **252**: 149-158.

Epstein, S., Buchsbaum, R., Lowenstam, H.A., and Urey, H.C., 1953. Revised carbonate-water isotopic temperature scale. Bull. *Geol. Soc. Amer.* **64**: 1315-1325.

Fairbanks, R.G., Charles, C.D., Wright, J.D., 1992. Origin of global meltwater pulses. In: Taylor, R.E., Long, A., and Kra, R. (eds.), *Radiocarbon after four decades; an interdisciplinary perspective*. Springer-Verlag, (New York), pp. 473-500.

Jansen, J.H.F., 1984. Structural and sedimentary geology of the Congo and southern Gabon continental shelf; a seismic and acoustic reflection survey. *Neth. J. Sea Res.*, **17**: 164-384.

Imbrie, J., J.D. Hays, D.G. Martinson, A. McIntyre, A.C. Mix, J.J Morley, N.G. Pisias, W.L. Prell, and N.J. Shackleton, 1984. The orbital theory of Pleistocene climate: support from a revised chronology of the marine $\delta^{18}O$ record. In: Berger, A., Imbrie, J., Hays, J., Kukla, G., and Saltzman, B. (eds.), *Milankovitch and climate*, D. Reidel Publishing Company (New York), USA, p. 269-305.

Lange, C.B., Treppke, U.F., and Fischer, G., 1994. Seasonal diatom fluxes in the Guinea Basin and their relationship to trade winds, hydrography and upwelling events. *Deep-Sea Res.I* **41**: 859-878.

Laskar, J., 1990. The chaotic motion of the solar system: A numerical estimate of the chaotic zones. *Icarus*, **88**: 266-291.

Müller, P.J. and R. Schneider, 1993. An automated leaching mehtod for the determination of opal in sediments and particulate matter. *Deep-Sea Res. I* **40**: 425-444.

Shackleton, N.J., Berger, A., and Peltier, W.R., 1990. An alternative astronomical calibration of the lower Pleistocene timescale based on ODP Site 677. *Trans. Royal Soc. Edinburgh: Earth Sciences* **81**: 251-261.

Shipboard Scientific Party, 1998. Chapter 1: Introduction: background, scientific objectives, and principal results for Leg 175 (Benguela Current and Angola-Benguela upwelling systems). In: G. Wefer, Berger, W.H., Richter, C., et al. (eds.), *Proc. Ocean Drilling Program, Initial Reports* **175**, College Station, TX (Ocean Drilling Program), p. 7-25.

Schneider, R.R., Müller, P.J., and Ruhland, G., 1995. Late Quaternary surface circulation in the east equatorial South Atlantic: evidence from alkenone sea surface temperatures. *Paleoceanography* **10**: 197-219.

Schrader, H.J., and Gersonde, R., 1978. Diatoms and sillicoflagellates. *Ultrecht Micropal. Bull.* **17**: 129-176.

Schulz, M., and Stattegger, K., 1997. Spectrum: spectral analysis of unevenly spaced paleoclimatic time series. *Computers & Geosciences* **23**: 929-945.

van Andel, T.H., Heath, G.R., and Moore, T.C., Jr., 1975. Cenozoic history and paleoceanography of the central equatorial Pacific Ocean: a regional synthesis of Deep Sea Drilling Project data. Mem.—*Geol. Soc. Am. Mem.* **143**: 1-134.

van der Gaast, S.J., and Jansen, J.H.F., 1984. Mineralogy, opal and manganese of Middle and Late Quaternary sediments of the Zaire (Congo) deep-sea fan: origin and climatic variation. *Neth. J. Sea Res.* **14**: 313-341.

Wefer, G., and Berger, W.H., 1991. Isotope paleontology: growth and composition of extant calcareous species. *Marine Geology*, **100**, p. 207-248.

Uliana, E., Lange, C. B., Donner, B., Wefer, G., 2001. Siliceous phytoplankton productivity fluctuations in the Congo Basin over the past 460,000 years: marine vs. riverine influence, ODP Site 1077. In: G. Wefer, W. H. Berger and C. Richter (eds.), *Proc. ODP, Sci. Res.*, 175, College Station, TX (Ocean Drilling Program).

6- Study Area

Our study area is the Lower Congo Basin off west Africa (Fig. 3). Here one of the largest rivers in terms of freshwater discharge joins an oceanic high-fertility area. The regional environment is dominated by seasonal coastal upwelling and associated filaments and eddies moving offshore, by riverine input from the Congo River, and by incursions of open-ocean waters.

Climatology

African tropical climate is governed by the seasonal migration of the Inter-tropical Convergence Zone (ITCZ) in response to changes in the location of maxima solar heating. This results in northern and southern belts of monsoonal climates with summer rains and winter drought, bracketing a humid equatorial zone characterized by a double rainfall maximum. Summer insolation maxima heat the continent and cause rising motion, resulting in increased monsoonal inflow of air from the Atlantic and wetter conditions in the Sahel and southern Sahara. Summer insolation minima suppress these tendencies and cause aridity.

On a geological timescale, strong monsoonal winds and enhanced precipitation over the African continent are induced by maximal Northern Hemisphere insolation when boreal summer coincides with minima in the Earth-sun distance (Pokras and Mix, 1985; deMenocal et al., 1993). This setting leads to a decrease in the strength of zonal Trade winds along the eastern tropical Atlantic and consequently reduces upwelling intensity (McIntyre, 1989; deMenocal et al., 1993). On the other hand, when boreal summers coincide with maximal Earth-sun distance, solar insolation over North and Central Africa and hence African monsoon intensity is reduced. The responsible orbital mechanism behind this insolation-driven scenery is precession of the Earth's rotational axis with periodicities of 19 and 23 kyr (Berger, 1978; Berger and Loutre, 1992).

Modern Hydrography

Detailed studies of modern hydrography in the eastern Angola Basin and the Congo Fan area are given by Eisma and van Bennekom (1978), van Bennekom and Berger (1984), and Schneider et al. (1995). The complex hydrography of the area involves different water masses with characteristic physical and biological properties. Basically, surface and shallow subsurface circulation is dominated by the Angola Current (AC) and the Benguela Coastal Current (BCC) (Fig.3). The AC flows southward along the African coast and is fed by the eastward-flowing, shallow-subsurface warm South Equatorial Countercurrent (SECC). The BCC transports cold and nutrient-rich waters northward across the Walvis Ridge. The two currents converge and form a strong temperature and productivity gradient, the Angola Benguela Front (ABF; Fig. 3). The position of the ABF depends on the intensity of both currents (Meeuwis and Lutjeharms, 1990), which in turn is strongly associated with the latitudinal movements of the ITCZ. Satellite images of SST reveal that the ABF moves from its northernmost location at 14°S in July-August to 16°S during January-February (Meeuwis and Lutjeharms, 1990). The ABF delineates the northern boundary

of the zonally directed tradewind field. North of the ABF, winds weaken and change to a meridional direction (Schneider et al., 1995).

In a zone between 10° and 16°S, the interaction between SECC, AC, and BCC creates a complicated pattern of fronts, gyres, and a thermal dome (Angola Dome), bringing nutrient-rich shallow subsurface waters into the euphotic zone (oceanic upwelling). North of the ABF, the BCC can be traced as a shallow subsurface current to 5°S (van Bennekom and Berger, 1984).

Superimposed on the system described above is the influence of the Congo River and Fan area which supplies freshwater, nutrients (including large amounts of dissolved SiO_2), and terrigenous particles to the ocean. The Congo River is the second most important river in the world in terms of mean annual flow (1300 km^3); its waters are characterized by high contents of dissolved silica (185 mmol L^{-1}) (Giresse et al., 1990). This silica is biologically available and part of it (38 mmol L^{-1}; Giresse et al., 1990) is already utilized within the river by freshwater organisms like diatoms. The siliceous material is then exported to the ocean where a large quantity of it is deposited and buried in the sediments (van der Gaast and Jansen, 1984). The rest is recycled in surface waters and enters the marine biological silica cycle. Especially, it is the input of silica that determines the dominant group within the primary producers of the region. Diatoms are the dominant group within the river plume, small flagellates dominate the area north of the plume (Cadée, 1978; 1984) and coccolithophores and dinoflagellates play an important role further south in the oceanic upwelling area off Angola (Shannon and Pillar, 1986).

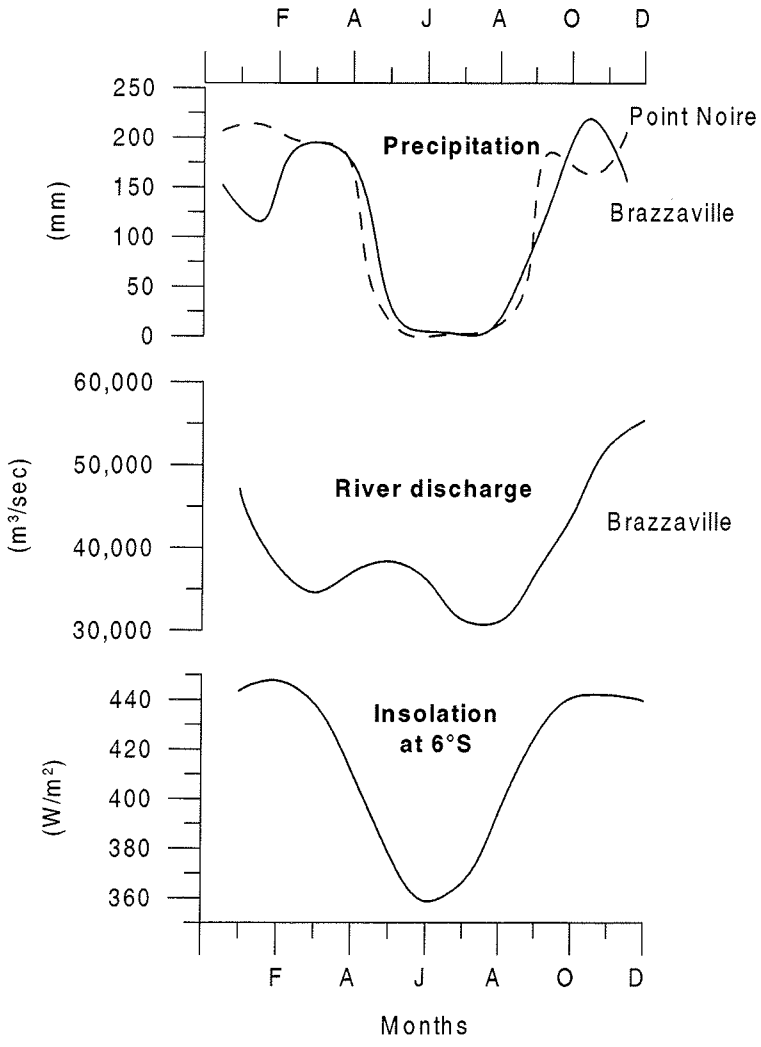

Fig. 4: Monthly precipitation data: at Brazzaville (4°S, 15° E), and at Point Noire (5°S, 12° E); monthly averages from IRI/LDEO Climate Data Library (Baker et al., 1994). River discharge at Brazzaville (Vorosmarty et al., 1998), and 10-year average of monthly insolation at 6°S (from Laskar, 1990). From Uliana et al. (submitted).

The Congo River discharge regime is associated with monsoonal circulation and precipitation (Eisma and van Bennekom, 1978; van Bennekom and Berger, 1984; Gasse, 2000); maximum river discharge is in December (Fig. 4).

A major feature is the river plume which has its maximum extension in February-March (van Bennekom and Berger, 1984). Salinity is usually below 27 ‰ in the inner plume area. Farther offshore (150-200 km from the river

mouth) the plume broadens and salinity rises to about 30 ‰ (van Bennekom and Berger, 1984). The main direction of the plume is always WNW near the river mouth. Offshore the direction of the plume axis changes to SW or SSW in February and March, to W or WSW from April to August, while in October and November the plume spreads in a NW direction (van Bennekom and Berger, 1984).

Modern primary productivity

Modern primary productivity in the surface waters off the Congo is high. Berger et al. (1989) give values of 90-125 $gC/m^2/yr$. High rates of primary productivity are assumed to be the result of 1) nutrient input from the river, and 2) upwelling of subsurface oceanic waters rich in nitrate and phosphate within the estuary and the inner plume area. High coastal productivity is restricted to two narrow areas north and south of the Congo estuary and is considered to be the result of upwelling of colder waters of the Equatorial Undercurrent.

Satellite pictures show high chlorophyll values all year round (Fig. 5). Surface water data from Conkright et al. (1998) indicate that a maximum in chlorophyll takes place at the Site 1077 location during August, when high nutrients and low SSTs are observed (Fig. 6). It is during boreal summer (August) when the ITCZ reaches its northernmost position, and the intensity of the southeast Trade winds increases producing strengthening of the upwelling along the southwest coast of Africa (Philander and Pacanowski, 1986). Atmospheric circulation reverses during boreal winter (February-March), the ITCZ moves to its southward position and the wind system is relaxed, then a minimum in productivity is observed.

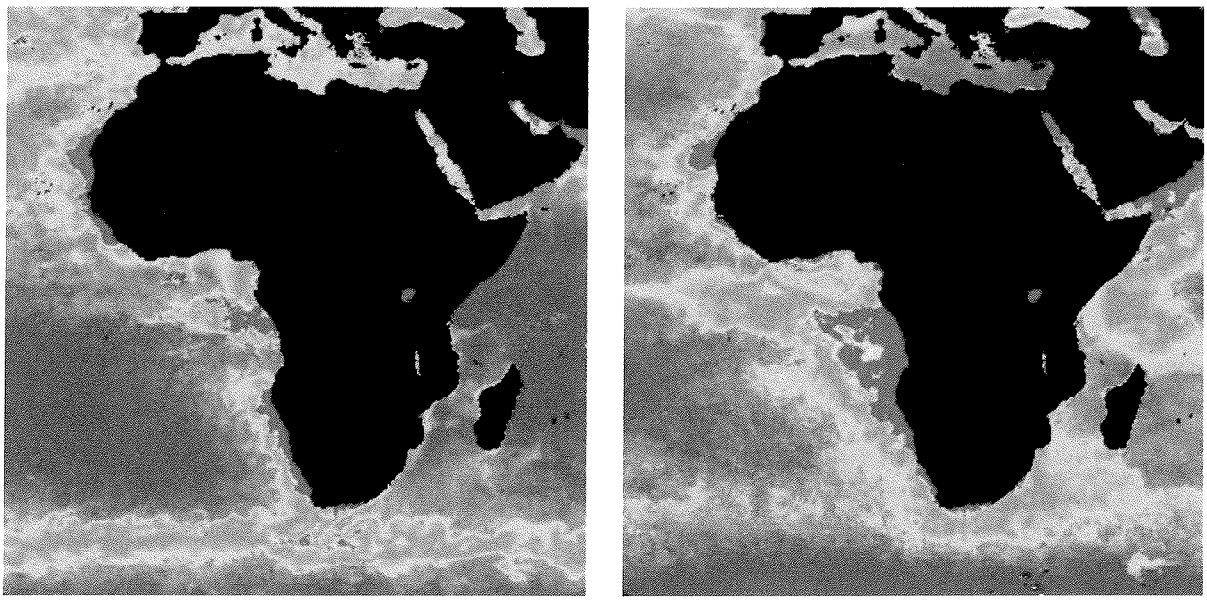

Fig. 5: Chlorophyll concentration from space for March (left) and August (right), from SeaWiFS (http://seawifs.gsfc.nasa.gov/SEAWIFS.html). Red color indicates high chlorophyll concentrations.

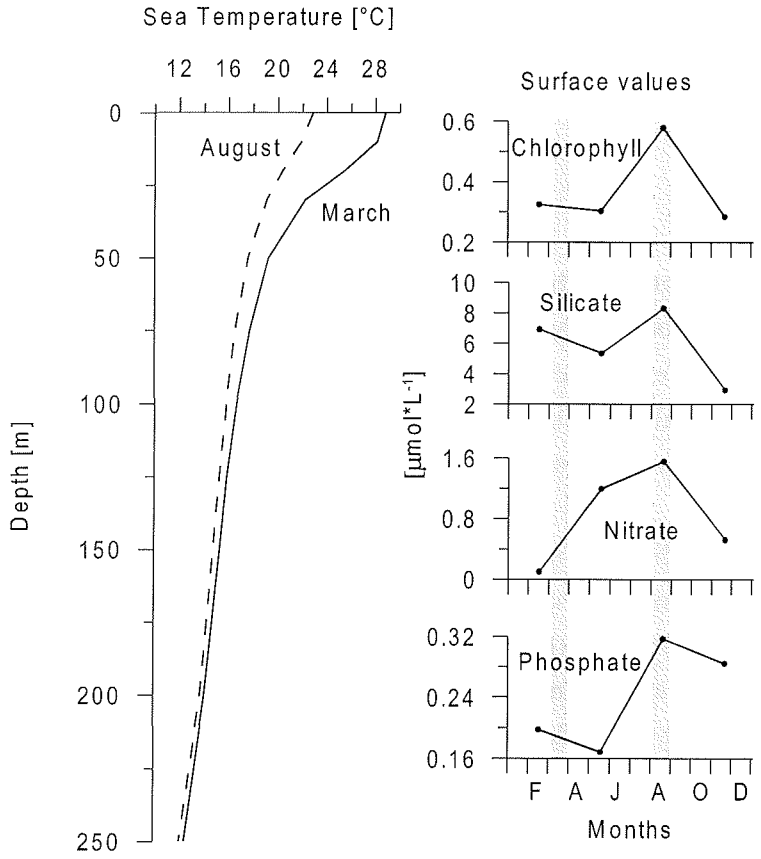

Fig. 6: Water column data: Vertical profile (0-250 m) of sea temperatures for March and August. Surface water data: Seasonal fluctuations in Chlorophyll, silicate, nitrate and phosphate. Data from Conkright et al. (1998).

Sediments

Sedimentation within the Lower Congo Basin is dominated by rain out of suspended clay derived from the Congo River and by pelagic settling of biogenic debris. Since the Congo River drops most of its coarse load before reaching the ocean (unlike other river-influenced hemipelagic systems), sediments in the area lack a significant river borne sand and silt fraction (Jansen et al., 1984). Wind-derived silt is minimal in relation to the amount of river-deposited clay (Jansen et al., 1984; van der Gaast and Jansen, 1984). Kaolinite and smectite are the most important clay minerals in the surface sediments of the Congo Fan (van der Gaast and Jansen, 1984; Gingele, et al., 1998). Other important terrigenous components include fresh- and brackish-water diatoms, plant remains, and phytoliths. The marine biogenic components include marine diatoms (dominating), coccoliths, planktic and benthic foraminifers, silicoflagellates, radiolarians, dinoflagellate cysts, ebridians, and sponge spicules (e.g., Jansen et al., 1984; Mikkelsen, 1977; van Iperen et al., 1987; Jansen and van Iperen, 1991).

Preliminary studies carried out on sediments of Site 1077 have shown that calcium carbonate is a minor component (varying between 0.8 and 13.2 % in the last 1 Myr), while total organic carbon content (TOC) is rather high for an ocean margin area (range: 1.29 to 4.7 %; Shipboard Scientific Party, 1998, "Site 1077"). Schneider et al. (1997) have shown that variations of TOC in the nearby Congo Fan core GeoB1008 are mainly a result of changes in marine organic carbon.

References Cited

Baker, C.B., Eischeid, J.K., Karl, T.R., and Diaz, H.F., 1994. The quality control of long-term climatological data using objective data analysis. Preprints of AMS Ninth Conference on Applied Climatology, Dallas, TX., January, 15-20.

Berger, A.L., 1978. Long term variations of daily insolation and Quaternary climatic change. *J. Atmosph. Sci.*, **35**: 2362-2367.

Berger, A. and Loutre, M. F., 1992. Astronomical solution for paleoclimate studies over the last 3 million years. *Earth Planet. Sci. Lett.* **111**: 369-382.

Berger, W.H., Smetacek, V.S., and Wefer, G., 1989. Ocean productivity and paleoproductivity -an overview. In: Berger, W.H., Smetacek, V.S., and Wefer, G. (eds.), *Productivity of the oceans: present and past*: New York (John Willey & Sons), pp. 1-34.

Cadée, G. C., 1978. Primary production and Chlorophyll in the Zaire River, estuary and plume. *Neth. J. Sea Res.* **12**: 368-381.

Cadée, G. C., 1984. Particulate and dissolved organic carbon and Chlorophyll a in the Zaire River, estuary and plume. *Neth. J. Sea Res.* **17**: 426-440.

Conkright, M., Levitus, S., O'Brien, T., Boyer, T., Antonov, J. and Stephens, C., 1998. *World Ocean Atlas.* Available online and on CD-ROM Data Set Documentation. Tech. Rep. 15, NODC Internal Report, Silver Spring, MD. 16 pp.

deMenocal, P. B., Ruddiman, W.F., and Pokras, E.M., 1993. Influences of high- and low latitude processes on African terrestrial climate: Pleistocene eolian records from Equatorial Atlantic Ocean Drilling Program Site 663. *Paleoceanography* **8**: 209-242.

Eisma, D. and van Bennekom, A. J., 1978. The Zaire river and estuary and the Zaire outflow in the Atlantic Ocean. *Neth. J. Sea Res.* **12**: 255-272.

Gasse, F., 2000. Hydrological changes in the African tropics since the Last Glacial Maximum. *Quat. Sci. Rev.* **19**: 189-211.

Gingele, F.X., Müller, P.M., and Schneider, R.R., 1998. Orbital forcing of freshwater input in the Zaire Fan area- clay mineral evidence from the last 200 kyr. *Palaeoceanogr., Palaeoclimat., Palaeoecol.* **138**: 17-26.

Giresse, P., Ouetiningue, R., and Barusseau, J.-P., 1990. Minéralogie et microgranulométrie des suspensions et des alluvions du Congo et de L'Oubangui. *Sci. Gèol. Bull.*, **43**: 151-173.

Jansen, J. H. F. and van Iperen, J. M., 1991. A 220,000-year climatic record for the East Equatorial Atlantic Ocean and Equatorial Africa: evidence from diatoms and opal phytolits in the Zaire (Congo) deep-sea fan. *Paleoceanography* **6**: 573-591.

Laskar, J., 1990. The chaotic motion of the solar system: A numerical estimate of the chaotic zones. *Icarus* **88**: 266-291.

McIntyre, A., Ruddiman, W.F., Karlin, K., and Mix, A., 1989. Surface water response of the Equatorial Atlantic Ocean to orbital forcing. *Paleoceanography* **4**: 19-55.

Meeuwis, J. M., and Lutjeharms, J. R. E., 1990. Surface thermal characteristics of the Angola-Benguela Front. *S. Afr. J. Mar. Sci.* **9**: 261-279.

Mikkelsen, N., 1977. On the origin of Ethmodiscus Ooze. *Marine Micropaleontology,* **2**: 35-46.

Philander, S.G. and Pacanowski, R.C., 1986. A model of the seasonal cycle in the tropical Atlantic Ocean. *J. Geophys. Res.*, **91**: 14192-14206.

Pokras, E. M., and Mix, A. C., 1985. Eolian evidence for spatial variability of Late Quaternary climates in Tropical Africa. *Quat. Res.* **24**: 137-149.

Schneider, R.R., Müller, P.J., and Ruhland, G., 1995. Late Quaternary surface circulation in the east equatorial South Atlantic: evidence from alkenone sea surface temperatures. *Paleoceanography* **10**: 197-219.

Schneider, R.R., Price, B., Müller, P.J., Kroon , D., and Alexander, I., 1997. Monsoon related variations in Zaire (Congo) sediment load and influence of fluvial silicate supply on marine productivity in the east equatorial Atlantic during the last 200,000 years. *Paleoceanography* **12**: 463-481.

Shannon, L.V., and Pillar, S.C., 1986. The Benguela Ecosystem Part III. Plankton. *Oceanogr. Mar. Biol. Ann. Rev.* **24**: 65-170.

Shipboard Scientific Party, 1998. Chapter 5: Site 1077. In: G. Wefer, Berger, W.H., Richter, C., et al. (eds.), *Proc. Ocean Drilling Program, Initial Reports* **175**, College Station, TX (Ocean Drilling Program), p. 115-141.

Uliana, E., Lange, C.B., and Wefer, G.. Evidence for Congo River freshwater load in Late Quaternary sediments of ODP Site 1077 (5°S, 10°E). Submitted for publication in *Palaeogeogr., Palaeoclimat., Palaeoecol.*

van Bennekom, A. J., and Berger, G. W. , 1984. Hydrography and silica budget of the Angola Basin. *Neth. J. Res.* **17**: 149-200.

van der Gaast, S. J., and Jansen, J. H. F., 1984. Mineralogy, opal and manganese of Middle and Late Quaternary sediments of the Zaire (Congo) deep-sea fan: origin and climatic variation. *Neth. J. Res* **14**: 313-341.

van Iperen, J.M., van Weering, T.C.E., Jansen , J.H.F., and van Bennekom, A.J., 1987. Diatoms in surface sediments of the Zaire deep-sea fan (SE Atlantic Ocean) and their relation to overlying water masses. *Neth. J. Res* **21**: 203-217.

Vorosmarty, C.J., Fekete, B.M., Tucker, B.A., 1998. Global River Discharge Database (RivDIS) V. 1.1. Available online [http://www-eosdis.ornl.gov] and on CD-ROM from the ORNL Distributed Active Archive Center, Oak Ridge National Laboratory, Oak Ridge, TN, USA.

7- Manuscripts

Manuscripts published, submitted or in preparation

7.1

Siliceous phytoplankton productivity fluctuations in the Congo Basin over the past 460,000 years: marine vs. riverine influence, ODP Site 1077

Uliana, E., Lange, C.B., Donner, B., and Wefer, G.

In: Wefer, G., Berger, W.H., and Richter, C. (Eds.), *Proc. ODP, Sci. Results*, **175**, 1-32, 2001
[Online]. Available from World Wide Web:
<http://www-odp.tamu.edu/publications/175_SR/chap_11chap_11.htlm>

ODP Scientific Results volume

SILICEOUS PHYTOPLANKTON PRODUCTIVITY FLUCTUATIONS IN THE CONGO BASIN OVER THE PAST 460,000 YEARS: MARINE VS. RIVERINE INFLUENCE, ODP SITE 1077

Uliana, E.[1], C. B. Lange[2], B. Donner[1], and G. Wefer[1]

[1]Fachbereich Geowissenschaften, Klagenfurter Strasse, Universität Bremen, 28359 Bremen, Germany.
[2]Scripps Institution of Oceanography, University of California at San Diego, Geosciences Research Division, La Jolla, CA 92093-0244, U.S.A.

Abstract: Accumulation rates, concentration and relative abundance of siliceous microfossils from Site 1077 are used to reconstruct changes in marine productivity and climate history of the Congo Fan area. The major contributors to the siliceous productivity are marine diatoms showing highest concentrations during glacial stages and cooler substages of the last interglacial. Abrupt changes are observed during Termination II (boundary oxygen isotope stages 5/6): 1) The marine diatom signal varied in amplitude and in assemblage composition from predominately marine to marine/brackish. 2)The environmental setting on land obtained from freshwater diatoms and Chrysophycean cysts point to changes from more arid conditions accompanied by a large drainage area of the Congo River to more humid conditions and a decrease on the inland water content for the last 125 ky.

Introduction

During Ocean Drilling Program (ODP) Leg 175, the Lower Congo Basin (LCB) off west Africa was the target for three drilling Sites, 1075, 1076 and 1077, along a transect on the northern rim of the Congo Fan (Shipboard Scientific Party, 1998, "Introduction"). Here one of the largest rivers in terms of freshwater discharge joins an oceanic high-fertility area. The regional environment is dominated by seasonal coastal upwelling and associated filaments and eddies moving offshore, by riverine input from the Congo River, and by incursions of open-ocean waters, especially from the South Equatorial Countercurrent (Fig. 1). Thus, the combination of pelagic and terrigenous information contained in these fan-margin deposits provides an excellent opportunity for studying simultaneous climatic changes on land and at sea.

One of the goals of Leg 175 included the reconstruction of the history of productivity off Angola and Namibia and the influence of the Congo River, thereby extending available information about the late Quaternary (e.g., Schneider et al., 1994, 1996, 1997; Jansen et al., 1996, and references therein) to earlier periods (Shipboard Scientific Party, 1998, "Introduction"). According to Jansen (1985), river-induced phytoplankton activity extends about 160 km beyond the shelf edge and would affect all three sites drilled. However, it is also evident from these earlier studies that major productivity changes off the Congo are determined by wind-forcing and oceanic subsurface nutrient supply rather than merely reflecting fertility changes induced by river discharge of nutrients. In an elegant work using oxygen and carbon isotope data of two planktonic foraminifers, Schneider et al. (1994) showed that off the Congo, ocean dynamics have overwhelmed the influence of one of the world's largest rivers on marine coastal productivity over the past 190,000 yr. This is contrary to other areas off major rivers where a strong freshwater signal was described (Pastouret et al., 1978; Showers and Bevis, 1988).

High opal content characterizes the Congo Fan sediments (Müller and Schneider, 1993) where diatoms are dominating. Schneider et al. (1997) suggested that enhanced opal production in this region was the result of additional fluvial supply of dissolved silica during humid climates characterized by more intense chemical weathering on the continent, while total paleoproductivity created by oceanic upwelling was high in periods of increased zonal trade wind intensity at precessional insolation minima and during cold, more arid glacial climate conditions.

Here we present a record of siliceous microfossil paleoproductivity spanning the last 460,000 yr from late Pleistocene sediments of ODP Site 1077. By using accumulation rates and the relative contribution of siliceous components of both continental origin (freshwater diatoms, phytoliths, chrysophycean cysts) and marine origin (marine diatoms, silicoflagellates, radiolarians) in combination with organic matter and opal data from nearby sites, ODP Site 1075 and GeoB1008, we aim to reconstruct temporal fluctuations in the Congo River freshwater outflow, coastal upwelling, and open-ocean contributions to the dynamics of the region. Our findings are integrated with and compared to those of previous studies from near by sites in the Congo Fan and off Angola (e.g., Mikkelsen, 1984; Jansen et al., 1984; van Iperen et al., 1987; Jansen and van Iperen, 1991; Schneider et al., 1994, 1995, 1997; Gingele et al., 1998).

Regional Setting

Hydrography

Detailed studies of modern hydrography in the eastern Angola Basin and the Congo Fan area are given by Eisma and van Bennekom (1978), van Bennekom and Berger (1984), and Schneider et al. (1995). The complex hydrography of the area involves different water masses with characteristic physical and biological properties.

In the eastern Angola Basin (0° to 20°S), the surface and shallow subsurface circulation is dominated by the Angola Current (AC) and the Benguela Coastal Current (BCC). The AC flows southward along the African coast, and is fed by the eastward-flowing, shallow-subsurface warm South Equatorial Countercurrent (SECC). The BCC transports cold and nutrient-rich waters northward across the Walvis

Ridge. The two currents converge between 14° and 16°S depending on the season, and form the Angola Benguela Front (ABF; Fig. 1). In a zone between 10° and 16°S, the interaction between SECC, AC, and BCC creates a complicated pattern of fronts, gyres, and thermal domes (e.g., Angola Dome), bringing nutrient-rich shallow subsurface waters into the euphotic zone (oceanic upwelling). North of the ABF, the BCC can be traced as a shallow subsurface current to 5°S (van Bennekom and Berger, 1984). The ABF delineates the northern boundary of the zonally directed tradewind field. North of the ABF, winds weaken and change to a meridional direction (summary in Schneider et al., 1995). Coastal upwelling is restricted to two narrow areas north and south of the Congo estuary and is considered to be the result of upwelling of colder waters of the Equatorial Undercurrent.

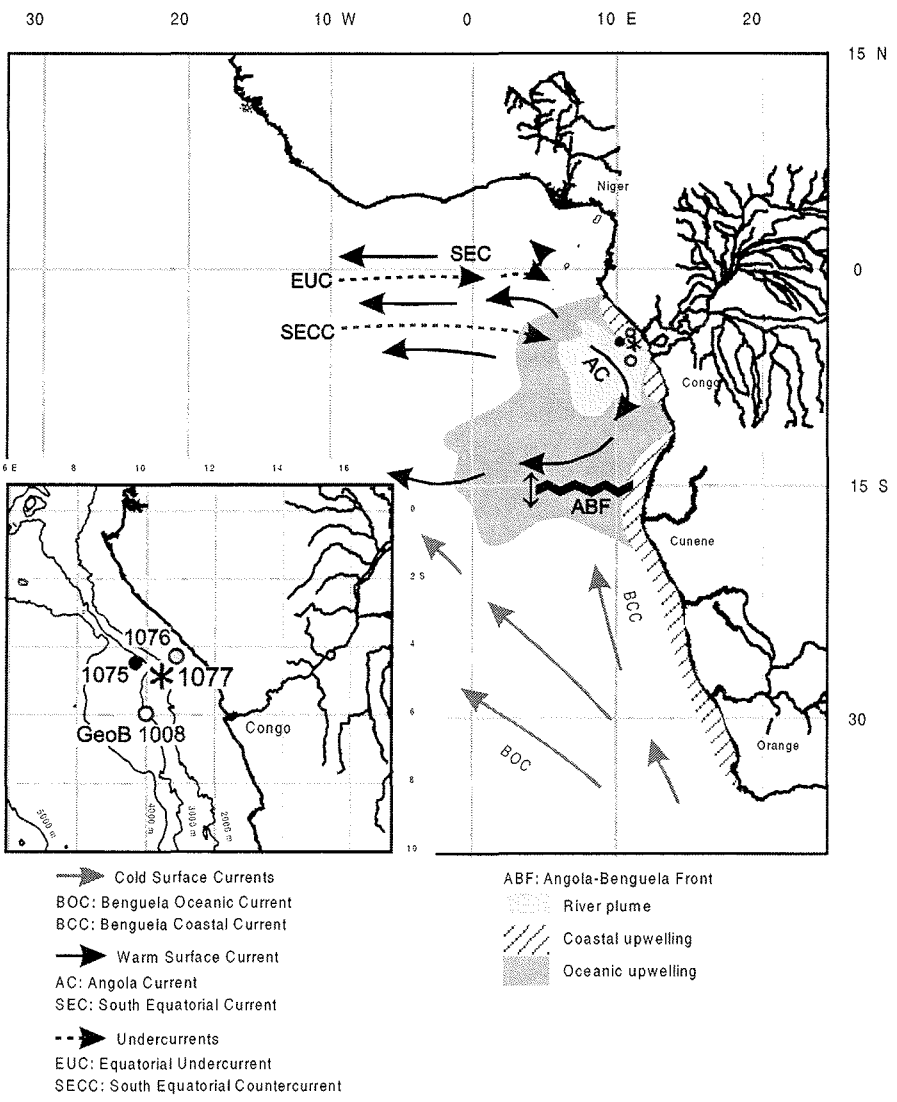

Figure 1. Location of Sites 1077, 1075 and GeoB1008. Main surface and subsurface currents and areas with high primary productivity in the eastern Angola Basin. Modified from Schneider et al. (1994).

Superimposed on the system described above is the influence of the Congo River and fan area which supplies freshwater, nutrients (including large amounts of dissolved SiO_2), and sediments to the ocean. The Congo River is the second largest river in the world. It has a peculiar estuarine hydrography caused by the small river mouth which includes the canyon head (Jansen, 1984). This forces a rapid outflow of river water toward the ocean in a sharply bounded turbid surface layer 5-15 m thick, which also entrains subsurface oceanic waters rich in phosphate and nitrate (Eisma and van Bennekom, 1978). The plume of Congo water, characterized by reduced surface-water salinity, can be detected as far as 800 km offshore during austral summer, when monsoonal circulation and precipitation reach their maximum seasonal intensity (Eisma and van Bennekom, 1978; van Bennekom and Berger, 1984). Salinity is below 30‰ in the inner plume area. Farther offshore (150-200 km from the river mouth) the plume broadens, salinity rises to about 30‰, and maxima in primary production (river-induced upwelling; van Bennekom and Berger,

1984), in diatom cell numbers (Cadée, 1978, 1984), and in diatom accumulation rates in the sediments (van Iperen et al., 1987) are found.

As a result of coastal, oceanic and river-induced upwelling, modern primary productivity is very high in the surface waters off the Congo; Berger et al. (1989) gives values of 90-125 $gC/m^2/yr$. Data on biogenic silica production indicate high diatom productivity in the surface waters surrounding the central Congo plume, accounting for 40-60% of the total carbon productivity (van Bennekom and Berger, 1984).

Sediments

Sedimentation within the LCB is dominated by rain out of suspended clay derived from the Congo River and by pelagic settling of biogenic debris. Since the Congo River drops most of its coarse load before reaching the ocean (unlike other river-influenced hemipelagic systems), LCB sediments lack a significant river borne sand and silt fraction (Jansen et al., 1984). Wind-derived silt is minimal in relation to the amount of river-deposited clay (Jansen et al., 1984; van der Gaast and Jansen, 1984). Kaolinite and smectite are the most important clay minerals in the surface sediments of the Congo Fan (van der Gaast and Jansen, 1984; Gingele et al., 1998). Other important terrigenous components include fresh- and brackish-water diatoms, plant remains, and phytoliths. The marine biogenic components include marine diatoms (dominating), coccoliths, planktic and benthic foraminifers, silicoflagellates, radiolarians, dinoflagellate cysts, ebridians, and sponge spicules (e.g., Jansen et al., 1984; Mikkelsen, 1984; van Iperen et al., 1987; Jansen and van Iperen, 1991).

Site 1077 (5°10S, 10°26E) is the intermediate-water drill site on a depth transect in the LCB, located at 2382 m water depth, at the northern edge of the Congo River plume (Fig. 1). Three holes (1077A, 1077B, and 1077C) were cored with the advanced hydraulic piston corer to a maximum depth of 205.1 m below seafloor, which recovered a continuous hemipelagic sedimentary section spanning the entire Pleistocene. Sediments are dominated by diatomaceous, partially carbonate-bearing clays (Shipboard Scientific Party, 1998, "Site 1077"). Sedimentological evidence suggests that Site 1077 is not affected by turbidity currents (Pufahl et al., 1998). The sediment composition of ODP Site 1075 does not differ significantly from Site 1077, and consists entirely of greenish gray diatomaceous clay and nannofossil-bearing diatomaceous clay (Shipboard Scientific Party, 1998, "Site 1075").

Material and Methods

Siliceous Microfossils

We investigated samples of Site 1077. Sampling was mainly performed on Hole 1077A, although for some intervals additional samples were collected from Holes 1077B and 1077C. Meters below seafloor (mbsf) were transformed to meters composite depth (mcd) according to Shipboard Scientific Party, "Site 1077" (1998).

High-resolution (20 cm sampling intervals) stable isotope analysis was performed on handpicked samples of the planktic foraminifer *Globigerinoides ruber* (size >150 ìm). A Finnigan MAT 251 micromass spectrometer equipped with a Kiel automated carbonate preparation device was used.

Samples (5 cm^3) were also collected for siliceous microfossil analysis. Sampling intervals varied from every 45 cm for the upper 44 mcd and representing an average resolution of ~ 2000 yrs, to every 110-120 cm downcore to 70 mcd; resolution for the lower part ranges from ~ 5,000 to 10,000 years. Samples were freeze-dried, and 0.4 g of dry sediment for each sample was treated with hydrochloric acid and hydrogen peroxide to dissolve carbonates and organic matter following the method of Schrader and Gersonde (1978); sodium pyrophosphate was added to remove clay-size particles in suspension. Acid and salt remains were removed by repeated steps of rising with distilled water and settling. Preparation of slides for qualitative and quantitative analyses was performed according to Lange et al. (1994).

Identification and counting of taxa was done with a Zeiss-Axioscope with phase contrast illumination at 1000X magnification. Due to the overwhelming dominance of a few diatom taxa, the counting procedure was divided into two steps: (1) for the most abundant diatom species (e.g., *Thalassionema nitzschioides* var. *nitzschioides*, *Cyclotella litoralis, Chaetoceros* spp.) just one transect across the slide was quantified; (2) for the rest of the diatom species, radiolarians, silicoflagellates, ebridians, phytoliths, chrysophycean cysts, and the siliceous skeleton of the dinoflagellate *Actiniscus pentasterias*, a fraction of the slide (1/3, 1/5, 1/10, depending on abundance) was counted. Sponge spicules were not included in our analysis. Definition of counting units followed that of Schrader and Gersonde (1978). Diatoms and silicoflagellates were identified to the lowest taxonomic level possible, whereas all other siliceous microfossils were counted as groups.

Abundances of taxa and/or microfossil groups were calculated as concentrations per gram and as accumulation rates. Relative abundances of individual species or group of species were calculated as percent of total assemblage. Accumulation rates for the different microfossils studied was calculated according to van Andel et al. (1975), as follows:

$$AR = \delta\ (g/cm^3) * a\ (\text{valves or skeletons}/g_{\text{dry sed.}}) * SR\ (cm/k.y.)$$

where: δ is the dry bulk density data obtained from http://www-odp.tamu.edu/publications/ GRAPE.dat; a is the estimated concentration for each group of siliceous microfossil per gram of sediment; and SR refers to sedimentation rates obtained by linear interpolation between isotopic tie-points.

All data are made available through the PANGAEA server (http://www.pangaea.de/Projects/SFB261/ EUliana_et_al_2000/).

We used the PhFD Index introduced by Jansen et al. (1989) as an index of paleoaridity over equatorial Africa. This index is a ratio between the concentration of phytoliths and freshwater diatoms (Ph/Ph+FD). High values are related to arid conditions over the continent (more abundance of Phytoliths) while low values (high freshwater diatom concentration) may reflect stronger river influence in the Congo area.

3.2 Biogenic components

Biogenic opal content was measured on Site 1075 samples by Hui-Ling at the National Sun Yat-Sen University of Taiwan. Opal contents were determined by the basic leaching method of Mortlock and Froelich (1989), modified by using different acid and base reagents (Lange et al., 1999; Lin et al., in press). Values reported here as opal contents are calculated as: %Opal = 2.4 x $\%Si_{opal}$ based on Mortlock and Froelich (1989).

Total carbon and organic carbon (TOC) concentrations were measured on Site 1075 using a LECO CS-244 carbon/sulfur analyzer. Analytical details are given in Lin et al. (in press).

Results

Oxygen isotopes and age model

The $\delta^{18}O$ record of the planktic foraminifer *G. ruber* (pink) from Site 1077 exhibit the shape typical for Quaternary records (Fig. 2), resulting from changes in seawater $\delta^{18}O$ due to the buildup and retreat of glacial polar ice caps and from changes in water temperature (e.g., Shackleton and Opdyke, 1973; Schneider et al., 1996). The Holocene peak at 1.25 mcd was fixed as age control point 7 ka. It corresponds to the Climatic Optimum, and also reflects increased discharge of isotopically light Congo River water. Already Pastouret et al. (1978) and Schneider et al. (1994) observed this variation superimposed on the classical $\delta^{18}O$ record of planktonic foraminifers in this area. All age-control points used are listed in Table 1, and the age model is plotted in Figure 3. Features in the $\delta^{18}O$ dataset of ODP Site 1077 were aligned with the record from Site 677 (Panama Basin, Shackleton et al., 1990). For depth intervals with low carbonate content (between 60 to 95 mcd), the record of magnetic susceptibility was successfully used to (1) align the isotope record, and (2) assign age-depth intervals (Dupont et al., in press). The magnetostratigraphy corresponds well with the isotope record (Matuyama/Brunhes boundary, Stage 19).

Sedimentation rates

Sedimentation rates were calculated by linear interpolation between age control points (Fig. 3). Lowest values (8-11 cm/k.y.) correspond to glacial stages 6, 10, and 12; highest values ranged between 17 and 22 cm/k.y. within stages 11, 9, 8, and during the past 120,000 yrs. In Figure 2 we compare sedimentation rates of the last 200,000 yrs of Site 1077 with those from a well-studied core (GeoB1008, Schneider, 1991) retrieved from 3124 m water depth, just south of our site and located within the Congo River plume (GeoB1008; 6°35´S, 10°19´E; water depth 3124 m). The shallower water depth at Site 1077 (2382 m) probably accounts for overall higher sedimentation rates. Discrepancies in the curve shapes (e.g., within Stages 5 and 6) may be attributed to local differences in sedimentation patterns, and/or errors in age-depth alignment by correlation of individual $\delta^{18}O$ records to the SPECMAP standard stack (Imbrie et al., 1984).

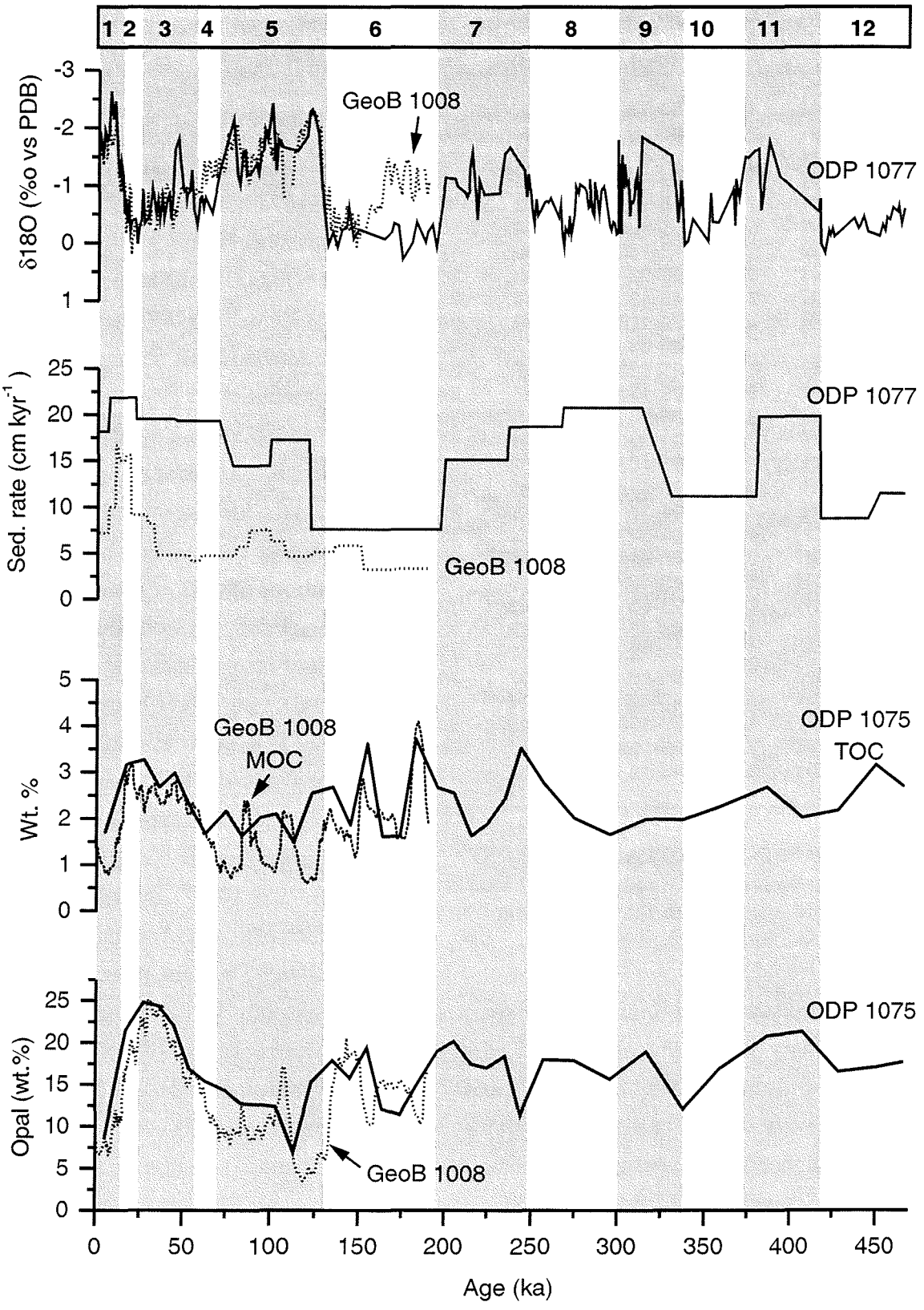

Figure 2. Comparison of Sites 1077 (this work) and 1075 (Lin et al., in press) with core GeoB1008 (Schneider, 1991): $\delta^{18}O$, sedimentation rates, organic carbon, and opal records . Head bars and gray/white columns denote SPECMAP oxygen isotope stages.

Hole	Core	Section	Interval (cm)	Depth (mcd)	Age (ka)
1077B	1H	1	85-88	0.85	6
	1H	2	25-28	1.75	8
	1H	4	5-8	4.55	22
	2H	3	65-68	9.25	46
1077A	3H	1	48-50	15.42	78
	3H	3	65-68	18.59	100
	3H	5	145-148	22.39	122
	4H	3	85-88	28.29	200
	4H	7	45-48	33.89	237
	5H	4	125-128	39.69	268
	6H	5	45-48	52.77	331
	6H	5	125-128	53.57	339
	6H	6	125-128	55.07	343
	7H	2	25-28	58.45	382
	7H	7	24-26	65.98	420
	8H	2	105-107	68.75	453
	8H	4	125-128	71.95	481
	9H	4	25-28	81.63	550
	10H	4	65-68	92.13	617
	10H	5	65-68	93.43	626
	11H	5	45-48	103.13	690
	11H	6	25-28	104.43	722
	12H	1	43-45	107.15	750
	12H	2	25-28	108.47	771
	12H	4	85-88	112.07	784
	12H	5	45-48	113.17	798
	13H	1	125-128	117.47	846
	13H	2	125-128	118.77	857
	13H	3	45-48	119.67	872

Table 1. Age model for Site 1077 based on the $\delta^{18}O$ record of the planktonic foraminifer *G. ruber* (pink) based on tie points which were aligned with the record from Site 677 (Panama Basin; Shackleton et al., 1990).

Records of biogenic constituents

Organic Carbon

Only shipboard data are available for Site 1077 (Shipboard Scientific Party, 1998, "Site 1077"). Total organic carbon (TOC) values range from 1.9 to 4.7 wt% over the past 500,000 yrs (Shipboard Scientific Party, 1998, "Site 1077"). Higher resolution data do exist for core GeoB1008 (Schneider et al., 1997) and for the near by Site 1075 (4°47´S, 10°4.5´E; 2995 m water depth) (Lin et al., in press). Both data sets are presented in Figure 2. Schneider et al. (1997) has shown that variations of total organic carbon in the Congo Fan core GeoB1008 are mainly a result of changes in marine organic carbon (MOC) with values between 0.5 and 4 wt.%. TOC concentrations at Site 1075 range from ~1.5 to 3.6 wt%. Also here, the organic matter appears to be mostly of marine origin (Shipboard Scientific Party, 1998, "Site 1075"), and the relative contribution of terrestrial organic carbon is low (~0.5 wt%; B. Jahn, pers. comm.). It is evident that discrepancies in the timing of some peaks and valleys, especially during Stage 5, are due to (1) the very preliminary stratigraphy of Site 1075 which is based on shipboard nannofossil datum events (Shipboard Scientific Party, 1998, "Site 1075"), and (2) differences in sampling strategy (every 5 cm for GeoB1008 and every ~1.5 m for Site 1075). However, the patterns are possibly comparable between both sites, and higher percentages of MOC correspond to Stages 2 and 3, substages 5.2, 5.4, 6.2, 6.4, and 6.6 (Fig. 2; Schneider et al., 1994).

Biogenic Opal

Late Quaternary Congo Fan sediments have high contents of biogenic silica (van der Gaast and Jansen, 1984; Schneider et al., 1997). In Figure 2 we plot two comparable records of biogenic silica, for core GeoB1008 (Schneider, 1991) and Site 1075 (Lin et al., in press), both measured with automated wet leaching methods (Müller and Schneider, 1993, for GeoB1008; Mortlock and Froelich, 1989, for Site

1075). Values range from ~5 to 25 wt%. Although discrepancies in the timing of events over the last 200,000 yrs are due to differences in sampling strategy and age model (see above), strong minima are observed in the Holocene and during the warmest period of the last interglacial (substage 5.5 for core GeoB1008), and higher contents correspond to late Stage 3-early Stage 2, substages 5.4, and within Stage 6.

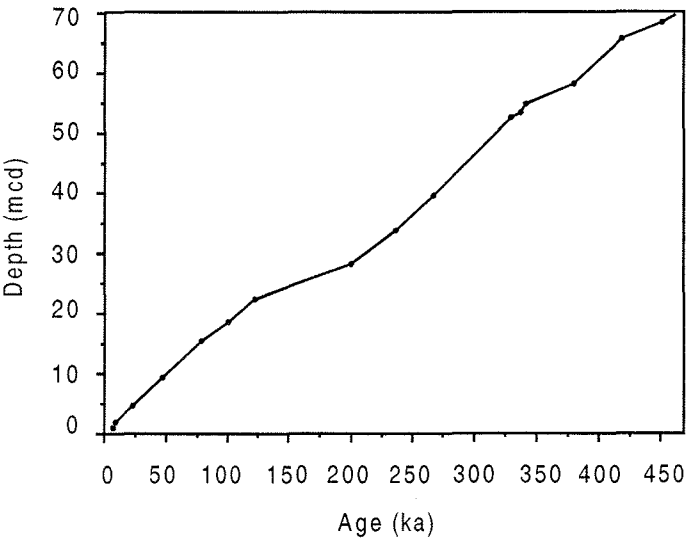

Figure 3. Age model used at Site 1077, based on $\delta^{18}O$ data of the planktonic foraminifera *Globigerinoides ruber* pink.

For the older record (beyond the last 200,000 yrs), the sample density of Site 1075 is too low and the age model is too preliminary to deduce accurate timing of changes in productivity based on TOC and opal fluctuations downcore. These preliminary data point to higher TOC values in late Stage 8-early Stage 7, Stage 11, and Stage 12. Obvious minima in opal wt% correspond to Terminations 7/8 and 9/10.

Siliceous Organisms

Sediments of the Congo Fan area contain large amounts of siliceous microfossils. Only the dominant siliceous components are discussed below (in terms of accumulation rates, concentration and species composition). Concentrations (per gram of dry sediment) of the most abundant microfossil groups counted are represented in Figure 4, Table 2, and their accumulation rates in Figure 5. The marine signal dominates at Site 1077, in agreement with previous studies (van Iperen et al., 1987; Jansen and van Iperen, 1991; Schneider et al., 1997). Abundances of marine diatoms are overwhelming (average of 5 x 10^7 valves/g); they compose 97% of the diatom assemblage (Table 3). The preservation state of the valves is moderate to good; lightly silicified species (e.g., vegetative cells and setae of *Chaetoceros*, *Bacteriastrum elongatum/furcatum,* and *Skeletonema costatum*) are present throughout. However, corroded valve edges were also observed (see also van Iperen et al., 1987). Silicoflagellates and radiolarians follow in second place, with abundances of 10^4-10^6 individuals/g of dry sediment. For the three marine siliceous groups, concentrations tend to be higher (although highly variable) between 10-70 ka (especially for marine diatoms and silicoflagellates), during cooler conditions (Schneider et al., 1995) of substages 5.2 and 5.4, and during glacial Stages 6 (especially for R), 8/9 (marine diatoms), and 10 and 12 (marine diatoms and silicoflagellates) (Fig. 4).

The continental signal is driven by freshwater diatoms with absolute abundances of the order of 10^6 valves/g (Fig. 4), an order of magnitude lower than marine diatoms. They originate from the drainage area of the Congo River. Chrysophycean cysts and phytoliths are present in almost all samples. Chrysophycean cysts are siliceous resting stages of Chrysophyceaen algae, which are commonly found in lakes (Smol, 1988); phytoliths are discrete, solid bodies of opaline silica in epidermal cells of grasses (Alexander et al.,

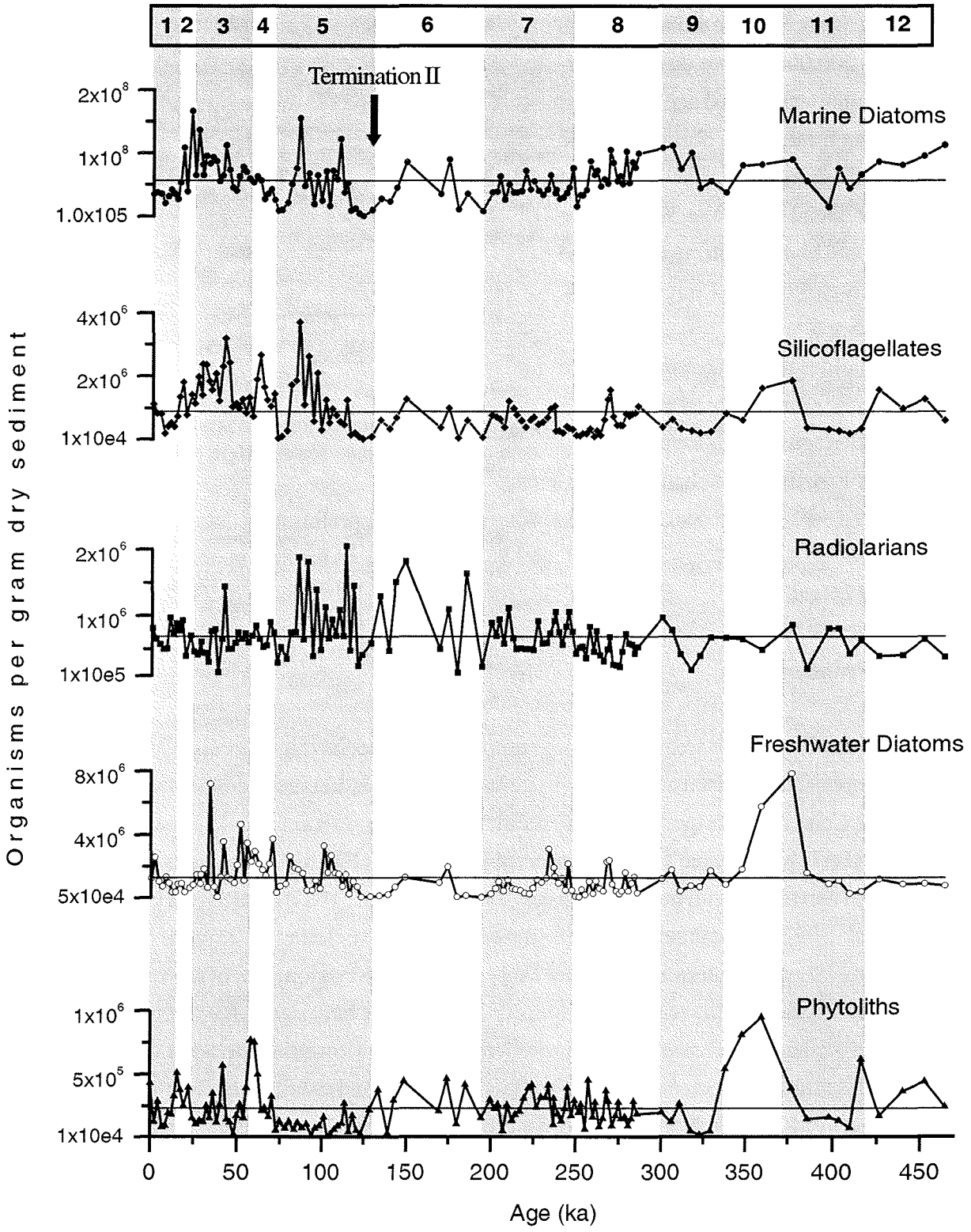

Figure 4. Abundances per gram of dry sediment of the most abundant siliceous microfossils counted. Horizontal lines refer to average value of each group and are for guidance.

1997; Runge, 1999). Phytolith concentrations average 10^5 bodies/g of dry sediment, and accumulation rates are ~10^7 bodies/cm/k.y.. The ratio of phytoliths to marine diatoms (x100) is low, 0.59, in agreement with the geographical distribution published by van Iperen et al. (1987). Phytolith maxima tend to coincide with glacial periods while higher contributions of Freshwater diatoms fall within interglacial stages (Fig. 4) and tend to occur during maxima in boreal summer insolation over Africa (Fig. 6). Both groups showed a significant difference in average concentration between glacial and interglacial times (Student's t test (Sokal, 1973): T freshwater diatoms = 26.7, and T phytoliths= 4.8; with $t_{(0.05;\,128)}$= 2.626). Values for the PhFD index (Jansen and van Iperen, 1991) average 0.2, and range between ~0 (almost no phytoliths) and 0.8 (reduced influx of freshwater diatoms to the sediments); they are comparable to Jansen and van Iperen's (1991) PhFD indices for nearby cores T78-3 (5°11S, 7°58E) and T78-46 (6°50S, 10°45E).

Accumulation rates (AR) were also calculated for each siliceous group. Although accumulation records are highly dependent on sedimentation rates (see discussion in Schneider et al., 1996), absolute abundances of each siliceous group are so high that they drive the AR pattern (compare Figs. 4 and 5). AR of marine diatoms range from 3.9 x 10^6 to 3.7 x 10^9 valves/cm/k.y., and are highest during Stage 2 and late Stage 3, substages 5.2 and 5.4, and stages 8 and late Stage 9. Between 460 and 125 ka, silicoflagellate values oscillate around the mean (1.8 x 10^7 skeletons/cm/k.y.), and show an abrupt increase at ~100 ka with maxima at ~40, 60 and 85 ka (Fig. 5). Radiolarian AR values fluctuate between 1.6 x 10^6 and 4.2 x 10^7 tests/cm/k.y..

An interesting feature is that all siliceous organism show both very low absolute abundances and accumulation rates at the Stage 5/6 boundary, a time of very low diatom diversity. This may point to a dissolution level also observed by Jansen and van Iperen (1991) in the Congo fan area.

Discussion. Temporal fluctuations in the composition of siliceous microfossils assemblages

The marine signal

A total of 154 diatom taxa were identified and counted. The most common taxa (28, with an overall average contribution of >1%) are summarized in Table 3. Marine diatoms dominate the assemblage in terms of relative contribution (~97% marine vs. ~3% freshwater) as well as concentrations per gram and accumulation rates (see Sedimentation rates, Siliceous Organisms).

In the sediments of the Congo fan, van Iperen et al. (1987) defined six marine diatom groups in surface sediments that reflect properties of the overlying water masses. Essentially, we keep their groupings with slight modifications based on our own experience with temporal and spatial distribution of diatom species in sediment traps and surface sediments in the equatorial and tropical Atlantic (summary in Romero et al., 1999a), including additional observations of Pokras and Molfino (1986). The composition of the resulting seven groups and their preferred environmental conditions is given in Table 3, their distribution downcore is illustrated in Figure 7, and their concentration per gram dry sediment is summarized in Table 4.

In accordance with the results of van Iperen et al. (1987), the marine diatom assemblage is dominated by two neritic, high-nutrient indicators, *Thalassionema nitzschioides* var. *nitzschioides* and resting spores of the genus *Chaetoceros*, and by *Cyclotella litoralis*. The latter can be considered a plume-

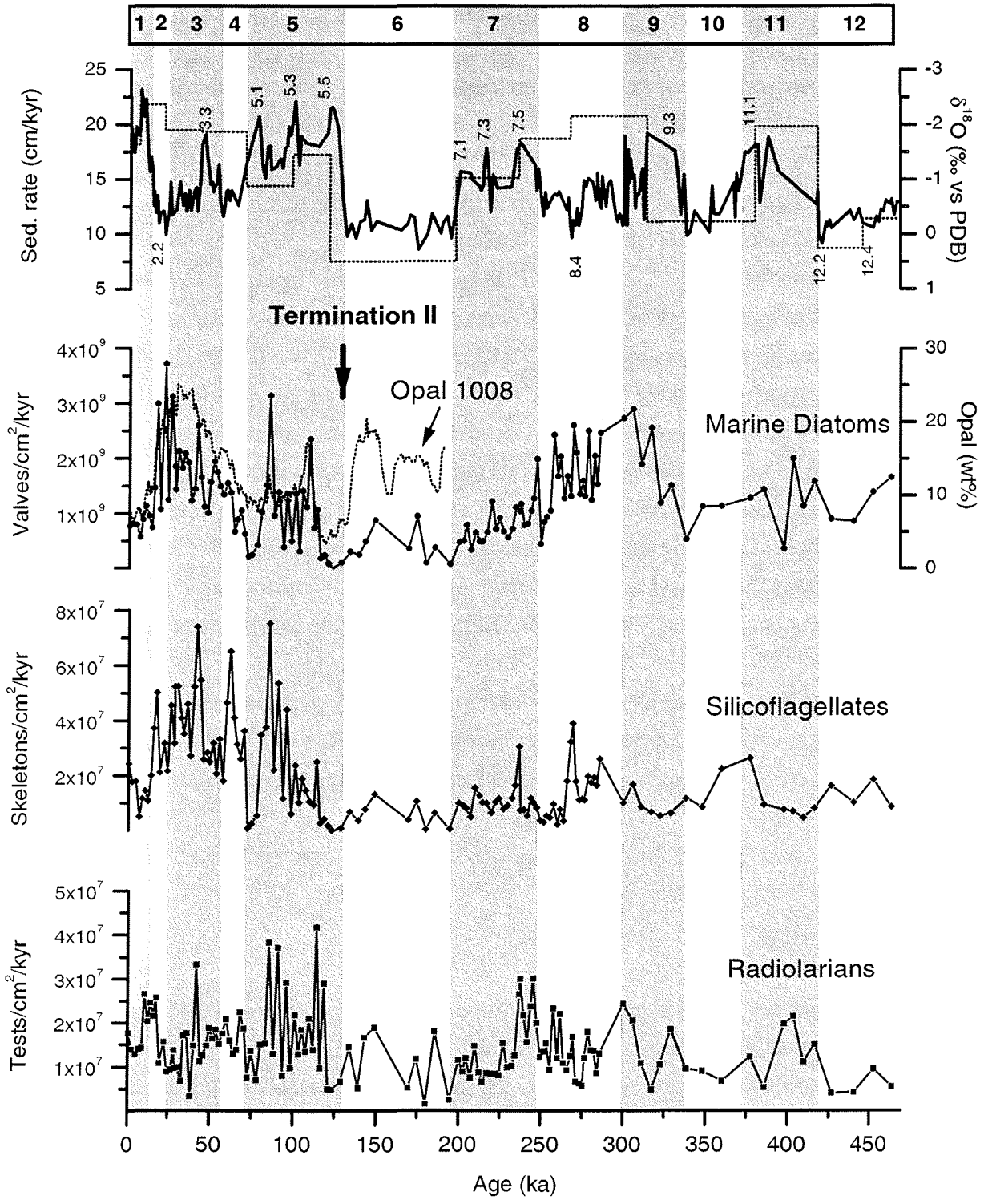

Figure 5. Marine signal. Accumulation rates of marine diatoms, silicoflagellates and radiolarians, sedimentation rates, the $\delta^{18}O$ record for Site 1077, and opal for GeoB1008.

related species in the Congo and the Niger area (van Iperen et al., 1987; Pokras, 1991). It is possible that in these previous studies, *C. litoralis* was misidentified as *C. striata* (van Iperen, pers. comm). Although little is known about the ecological preferences of *C. litoralis*, the species has been recurrently found in neritic environments with highly variable salinities (C. Lange, unpubl. obs.). Fluctuations in relative abundance and accumulation rates of this species at Site 1077 suggest two long term periods of lowered salinity

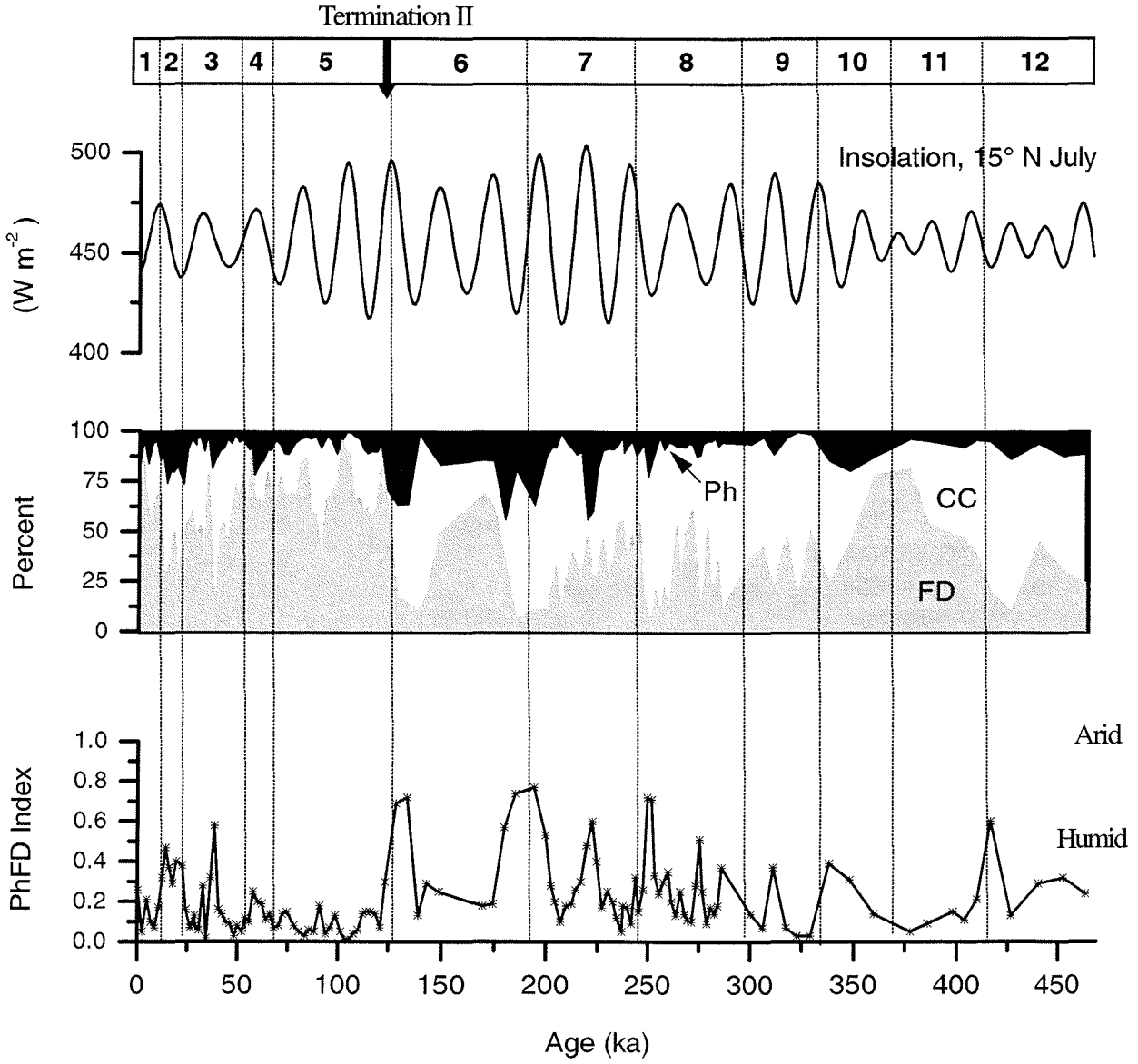

Figure 6. Continental signal. Relative contributions of freshwater diatoms (FD), chrysophycean cysts (CC), and phytoliths (Ph) based on the assumption that 100% continental signal is equal to the sum of individual percentages; and PhFD index of Jansen and van Iperen (1991), vs. precessional oscillation of boreal summer insolation (July) at 15°N (data from Berger and Loutre, 1991).

and enhanced river discharge, between 220-325 ka (moderate) and in the last 125 ka including two strong pulses at 10-50 ka and 75-125 ka.

The occurrence of *Chaetoceros* spp. resting spores and remains of vegetative cells in the Congo area can be attributed to seasonal variability of coastal upwelling and nutrient input from the river outflow (the Congo effect), and probably also reflects advection from the shelf (see discussion in Jansen and van Iperen, 1991). They are common members of the diatom assemblage (~ 20%) and their abundance pattern shows high variability especially during the past 250 k.y.. Maxima in the relative abundance are seen during interglacial Stages (Fig. 7).

We consider the record of *T. nitzschioides* var. *nitzschioides* as indicative of increased nutrient supply by the coastal upwelling process, in agreement with Jansen and van Iperen (1991), rather than of river influence (Pokras and Molfino, 1986). At Site 1077, a long term trend is evident with a clear

Site 1077 Diatom Group	Percentage (avg.)	Environmental conditions
Freshwater	2.7	Related to the Congo River discharge
Aulacoseira spp.	64.0	
Marine	97.3	
Nearshore		
Low Salinity	18.8	Related to the Congo River plume
Cyclotella litoralis		
High nutrients	64.0	
Chaetoceros spp	24.2	Highly productive waters where river-induced upwelling is inferred
Thalassionema nitzschioides var. *nitzschioides*	39.8	Highly productive nearshore waters to the north of the river plume
Neritic	11.0	nearshore
Actinocyclus aff. *curvatulus*		
Actinocyclus octonarius		
Coscinodiscus radiatus		
Rhizosolenia setigera/pungens		
Skeletonema costatum		
Thalassiosira angulata		
Thalassiosira eccentrica		
Littoral	0.7	Transported from the shelf
Actinoptychus senarius		
Actinoptychus vulgaris		
Offshore		
Warm	1.7	Related to the warm, high saline waters of the SECC with low nutrient levels
Alveus marinus		
Asteromphalus flabellatus		
Azpeitia nodulifera		
Nitzschia interruptestriata		
Planktoniella sol		
Pseudosolenia calcar-avis		
Rhizosolenia bergonii		
Thalassionema nitzschioides var. *parva*		
Thalassionema nitzschioides var. *inflatula*		
Thalassiosira ferelineata		
Thalassiosira lineata		
Thalassiosira simonsenii		
Oceanic temperate	3.2	Related to cold, nutrient-rich waters of the BCC, probably reflecting northward movement of the ABF
Bacteriastrum elongongatum/furcatum		
Fragilariopsis doliolus		
Thalassiosira oestrupii var. *oestrupii*		

Table 3. Species composition of the seven diatom groups in the sediments of Site 1077 and related environmental preferences based on observations of van Iperen et al. (1987), Pokras and Molfino (1986), and Romero et al. (1999a).

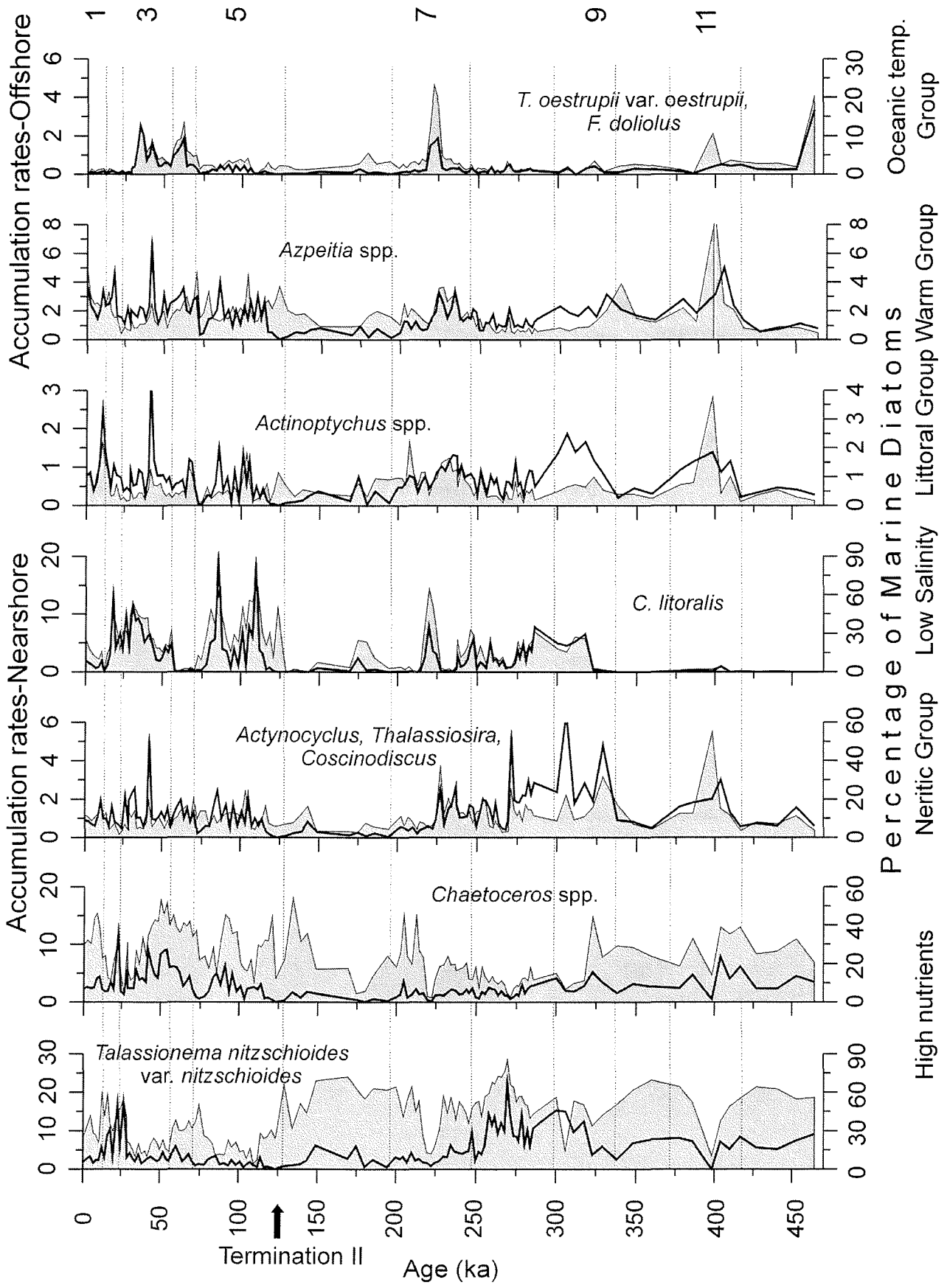

Figure 7. Accumulation rates (black curve upper axes) and relative abundances (percentage of total marine diatoms; gray area, lower axes) of the marine diatom groups present at Site 1077. Diatom groupings follow van Iperen et al. (1987) and Romero et al. (1999a). The scale for accumulation rates is valves x 10^7 cm^{-2} kyr^{-1} for the littoral and the warm group; all other scales are valves x 10^8 cm^{-2} kyr^{-1}.

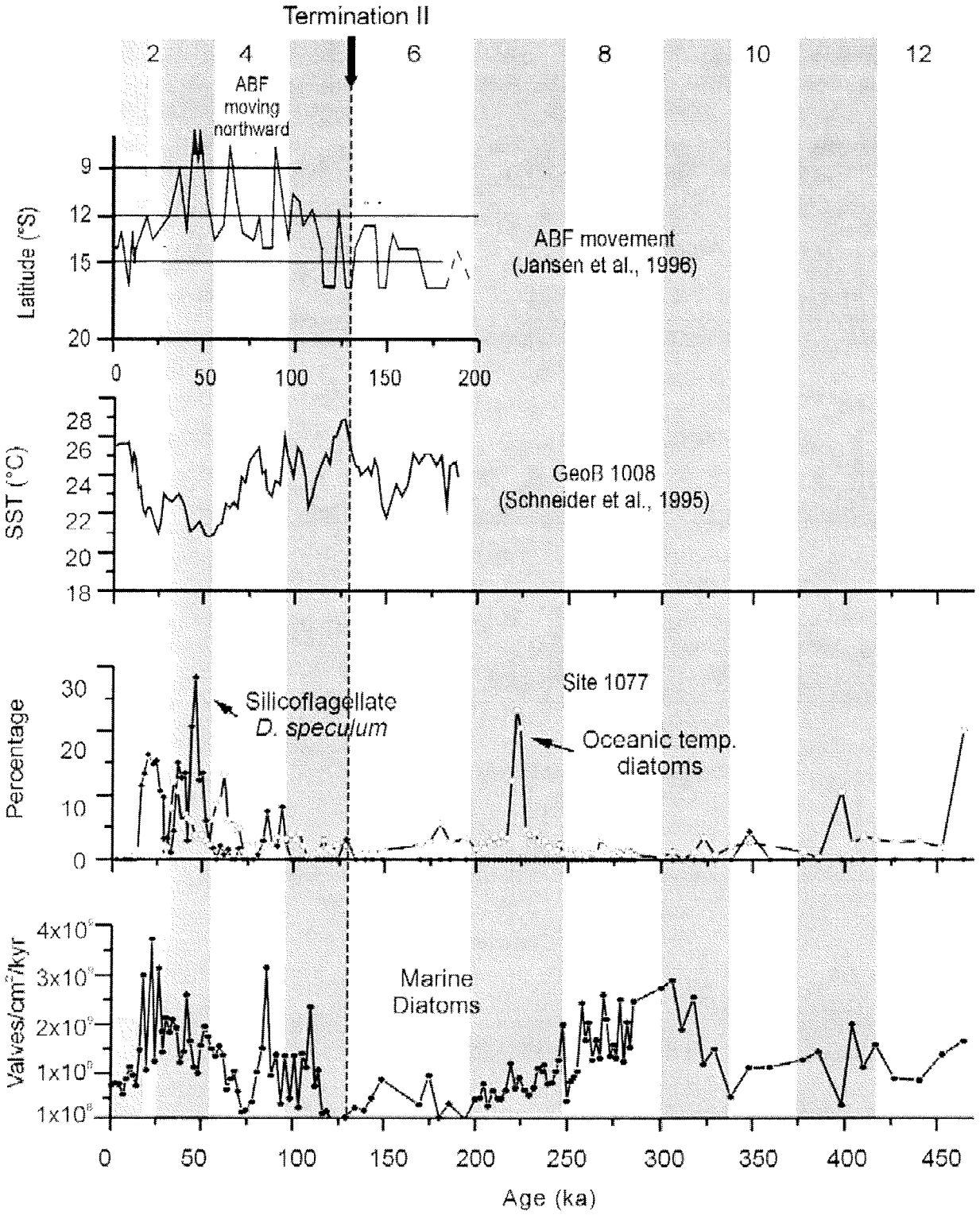

Figure 8. Marine diatom accumulation rates and relative contribution of cold-temperate water taxa compared to SST estimates from a nearby core, GeoB 1008 (from Schneider et al., 1995), and the reconstruction of the average position of the Angola-Benguela Front (modified from Jansen et al., 1996).

dominance (>50%) during 460 to 125 ka, dropping to low levels at Termination II (Fig. 7). On shorter time scales, abundance peaks are generally associated with glacial periods.

The presence of the littoral group (composed of benthic, tycopelagic, epiphytic species, etc.) is constant but rare (~ 1%); moderate peaks occurred during interglacials A significant (5% confidence

level) difference in average concentration between glacial and interglacial times was found (Student's t test, Sokal, 1973): T T = 4.669, , theoretic t-value = 2.626. The warm-water group was always present in low numbers (highest peak in Stage 11) as an indication that our study area has always been under the influence of warm and saline waters of the SECC. Episodic maxima of the oceanic temperate assemblage may be associated with cold water intrusions of the BC.

It is interesting to note two time intervals with prominent peaks in the relative abundance of a cold water silicoflagellate, *Dictyocha speculum* (at ~25 and 40-50 ky), and of the oceanic temperate diatom assemblage (at 40-70 ka, and 225 ka) (Fig. 8). In particular, the period 15-65 ka, and to a lesser extent 80-100 ka, coincides with high diatom accumulation rates and lower SSTs (Schneider et al., 1995) in the Congo Fan area (Fig. 8). These observations correlate well with inferences made by Jansen et al. (1996) of northward movements of the ABF. Although the peaks may not represent BCC waters *per se* (Jansen et al., 1996) we suggest that these times are characterized by enhanced production caused by frontal mixing of cold, nutrient-rich waters from the south (Fig. 8) and river-induced upwelling from the coast (high abundances of *Chaetoceros* spp. and *C. litoralis*; Fig. 7). We do not know if the 225-ka peak can also be related to an earlier northerly position of the ABF.

The continental signal

The presence of freshwater diatoms and phytoliths in marine sediments from the Atlantic Ocean is attributed to three different transport mechanisms: eolian, fluvial, and transport by turbidity currents (Pokras, 1991; Pokras and Mix, 1985; van Iperen et al., 1987; Gasse et al., 1989; Stabell, 1986; Treppke, 1996). The interpretation of these siliceous remains in the water column and sediments raises the problem of identifying their source area and transporting agents. In the equatorial and tropical regions between 20°N and 10°S, and west of 2°E, eolian transport with direct settling over the open ocean is assumed to be the main transport mechanisms of freshwater diatoms and Phytoliths (Pokras, 1991; Pokras and Mix, 1985; Stabell, 1986; Gasse et al., 1989; Romero et al., 1999b). In contrast, in nearshore areas influenced by river discharge (e.g. Niger, Congo, Amazonas) fluvial transport is responsible for the deposition of freshwater diatoms, phytoliths, and other continental remains (Melia, 1984; Gasse et al., 1989; van Iperen et al., 1987; Jansen and van Iperen, 1991).

Site 1077 is strongly influenced by Congo River discharge (Fig. 1); it lies outside of the turbidite fan area (van Weering and van Iperen, 1984; van Iperen et al., 1987; Pufahl et al., 1998). Although eolian influence at our study site cannot be completely ruled out as a possible mechanism of deposition of continental remains, wind contribution is probably minor when compared to the riverine input.

The continental signal recorded by freshwater diatoms is dominated by the genus *Aulacoseira* (mostly *A. granulata* and *A. islandica*), which represents an average of 64% of the freshwater assemblage (Table 3). Other freshwater species in sediments of Site 1077 include *Cyclotella meneghiniana, Luticola mutica,* and *Stephanodiscus astrea.* Their abundances may be underrepresented, since *Aulacoseira*-rich sediments from Site 1077 may also be a consequence of differential dissolution during transport within the river waters and discharge into the ocean where dissolution increases due to low dissolved silica contents and high ionic concentration (van Bennekom and Berger, 1984; Hurd, 1983). However,

Aulacoseira species are commonly found in African water bodies, especially in the Congo river where the genus makes up 80% of the total diatom population (Gasse et al., 1989). We believe that *Aulacoseira* values (and total freshwater loads) at Site 1077 are useful for reconstructing temporal fluctuations in the intensity of Congo River discharge. They reflect humid periods with increased rainfall and river discharge fostered by an intensified monsoon during times of maximum insolation in the Northern Hemisphere (Fig. 6; Schneider et al., 1997; Gingele et al., 1998).

The continental signal derived from Chrysophycean cysts is probably related to both humidity on land and changes in the Congo drainage area and inland water bodies. An interesting long-term, contrasting trend is evident when comparing freshwater diatoms and chrysophycean cysts records, with chrysophycean cysts being more abundant between 460 and 125 ka (except for two freshwater diatoms maxima at ~170 ka and ~370 ka), and freshwater diatoms dominating during the last 122,000 yr (Fig. 6). Because chrysophycean cysts are of limnic origin, we speculate that their higher values prior to Termination II may be attributed to a larger number of lakes drained by the Congo. Apparently, pre-Pleistocene times were characterized by lakes and swamps covering a large area around the Congo River (Beadle, 1974). Changes in vegetation were also recorded. A drop in the proportion of plants of the family Cyperaceae at and around Termination II was reported by Dupont et al. (1999). This family includes aquatic plants, adapted to a life in marshy and freshwater environments.

Our third continental proxy, the contribution of phytoliths, does not show marked long-term changes. Phytoliths were almost always present in much lower numbers than freshwater diatoms and chrysophycean cysts; highest relative abundances were observed during Stages 6 and 7 (Fig. 6). On the other hand, the PhFD index shows a spiky pattern with a moderate long-term trend pointing to more arid conditions on land prior to ca. 122 ka, and more humid conditions thereafter.

Conclusions

1-. Sediments of Site 1077 contain large amounts of siliceous microfossils. The marine signal dominates and marine diatoms are the most abundant siliceous microfossils group, followed by silicoflagellates and radiolarians.

2-. High abundances of diatoms, silicoflagellates, and radiolarians point to increase productivity during glacial stages and cooler conditions of substages 5.2 and 5.4.

3-. An abrupt change in the amplitude of the siliceous signal as well as in the diatom assemblages is evident at Termination II. The system seems to change from predominately marine to marine/brackish.

4-. The continental signal derived from freshwater diatoms shows two periods which can be correlated with humid conditions on land and/or northward movements of the Congo River plume during Stages 10 and 11, and during 28-119 ka.

5-. Fluctuations in the abundances of Chrysophycean cysts may be used as indicative of changes in the extension of inland waters. Theypoint to an abrupt reduction of the limnetic system particularly during the last 125 k.y.

6-. Sedimentation rates showed highest values at Stage 11, between Stages 9 and 7 and between Stages 5 and 1 in correspondence with the northward movements of the ABF detected by the oceanic temperate diatom assemblage in combination with D. speculum (cold water silicoflagellate).

7-. The opal signal recorded at Site 1075 correlates well with concentration of marine diatoms at the Site 1077 from ca 120 kyr to the present; differences in timing can be attributed to differences on the age model. Both parameters showed higher values during the last 125 k.y.

8-. Total organic carbon in sediments from Site 1075 is of marine origin, in agreement with the overwhelming dominance of marine siliceous microfossils.

Acknowledgments:

This study was supported by the Deutsche Forschungsgemeinschaft (Sonderforschungs-bereich 261 at the Bremen University). We thank the ODP technicians and the drilling crew for their effort in sediment recovery. We acknowledge fruitful discussions with Lydie Dupont, Britta Jahn, Fred Jansen and Jolanda van Iperen during Leg 175 and postcruise. We would like to thank U. Zielinski, J. Whitehead and an anonymous reviewer for their suggestions which helped improve the final version.

References

Alexander, A., Meunier, J.D., Lézime, A.M., Vicens, A., and Schwartz, D., 1997. Phytolits: indicators of grassland dynamics during the late Holocene in intertropical Africa. *Palaeoceanography, Palaeoclimatology, Palaeoecology*, 136: 213-229.

Beadle, L.C., 1974. *The inland waters of tropical Africa : an introduction to tropical limnology*: London (Longman), 346 pp.

Berger, A., and Loutre, M.F., 1991. Insolation values for the climate of the last 10 million years. *Quaternary Sci. Rev.*, 10: 297-317.

Berger, W.H., Smetacek, V.S., and Wefer, G., 1989. Ocean productivity and paleoproductivity -an overview. *In* Berger, W.H., Smetacek, V.S., and Wefer, G. (Eds.), *Productivity of the oceans: present and past*: New York (John Willey & Sons), pp. 1-34.

Cadée, G.C., 1978. Primary production and chlorophyll in the Zaire river, estuary and plume. *Netherlands Journal of Sea Research*, 12: 368-381.

Cadée, G.C., 1984. Particulate and dissolved organic carbon and chlorophyll a in the Zaire river, estuary and plume. *Netherlands Journal of Sea Research*, 17: 426-440.

Dupont, L., Schneider, R., Schmüser, A., and Jahns, S., 1999. Marine-terrestrial interaction of climate changes in West Equatorial Africa of the last 190,000 years. *Paleocanography of Africa*, 26: 61-84.

Dupont, L.M., Jahns, S., Marret, F., and Ning, S., 2000. Vegetation change in equatorial West Africa: time-slices for the last 150 ka. *Palaeoceanography, Palaeoclimatology, Palaeoecology*, 155: 95-122.

Dupont L.M., Donner, B., Schneider R., Wefer R., in press. Mid-Pleistocene environmental change in tropical Africa began as early as 1.05 Ma. *Geology*.

Eisma, D., and van Bennekom, A.J., 1978. The Zaire river and estuary and the Zaire outflow in the Atlantic Ocean. *Netherlands Journal of Sea Research*, 12(3/4): 255-272.

Gasse, F., Stabell, B., Fourtanier, E., and van Iperen, J., 1989. Freshwater diatom influx in intertropical Atlantic: Relationships with continental records from Africa. *Quaternary Research*, 32: 229-243.

Gingele, F.X., Müller, P.M., and Schneider, R.R., 1998. Orbital forcing of freshwater input in the Zaire Fan area- clay mineral evidence from the last 200 kyr. *Palaeoceanography, Palaeoclimatology, Palaeoecology*, 138: 17-26.

Hurd, D.C., 1983. Physical and chemical properties of siliceous skeletons. *In* Aston, S.R. (ed.), *Silicon geochemistry and biogeochemistry*: London (Academic Press), 187-244.

Imbrie, J., J.D. Hays, D.G. Martinson, A. McIntyre, A.C. Mix, J.J Morley, N.G. Pisias, W.L. Prell, and N.J. Shackleton, 1984. The orbital theory of Pleistocene climate: support from a revised chronology of the marine d18O record. *In* Berger, A., J. Imbrie, J. Hays, G. Kukla, and B. Saltzman (eds.), *Milankovitch and climate*: Palisades, NY, USA (D. Reidel Publishing Company), 269-305.

Jansen, J.H.F., 1984. Structural and sedimentary geology of the Congo and southern Gabon continental shelf; a seismic and acoustic reflection survey. *Netherlands Journal of Sea Research*, 17(2-4): 164-384.

Jansen, J.H.F., 1985. Middle and Quaternary carbonate production and dissolution, and paleoceanography of the eastern Angola Basin, South Atlantic Ocean. *In* Hsü, K.J., and Weissert, H.J. (Eds.), *South Atlantic Paleoceanography:* New York (Cambridge Univ. Press), 25-46.

Jansen, J.H.F., Alderliesten, C., Houston, C.M., de Jong, A.F.M., van der Borg, K., and van Iperen, J., 1989. Aridity in equatorial Africa during the last 225,000 years: a record of opal phytoliths/freshwater diatoms from the Zaire (Congo) deep-sea fan (northeast Angola Basin). *Radiocarbon*, 31: 557-569.

Jansen, J.H.F., van Weering, T.C.E., Gieles, R., and van Iperen, J., 1984. Middle and Late Quaternary oceanography and climatology of the Zaire-Congo fan and adjacent eastern Angola Basin. *Netherlands Journal of Sea Research*, 17: 201-249.

Jansen, J.H.F., and van Iperen, J.M., 1991. A 220,000-year climatic record for the East Equatorial Atlantic Ocean and Equatorial Africa: evidence from diatoms and opal phytolits in the Zaire (Congo) deep-sea fan. *Paleoceanography*, 6(5): 573-591.

Jansen, J.H.F., Ufkes , E., and Schneider, R.R., 1996. Late Quaternary Movements of the Angola-Benguela front, SE Atlantic, and implications for advection in the Equatorial Ocean. *In* Wefer, G., Berger, W.H., Siedler, G., and Webb, D.J. (Eds.), *The South Atlantic: Present and past circulation*: Berlin, Heidelberg (Springer-Verlag), pp. 553-575.

Lange, C.B., Treppke, U.F., and Fischer, G., 1994. Seasonal diatom fluxes in the Guinea Basin and their relationship to trade winds, hydrography and upwelling events. *Deep-Sea Research I*, 41(5/6): 859-878.

Lange, C. B., Berger, W. H., Lin, H.-L., Wefer, G., and Shipboard Scientific Party Leg 175, 1999. The early Matuyama Diatom Maximum off SW Africa, Benguela Current System (ODP Leg 175). *Marine Geology*, 161: 93-114.

Lin, H.-L, Lin, C.Y:, Meyers, P., and Adams, D, in press. Biogenic opal and organic carbon isotope evidence of late Quaternary variations in marine productivity along the southwest African margin. *Marine Geology*.

Melia, M.B., 1984. The distribution and relationship between palynomorphs in aerosols and deep-sea sediments off the coast of Northwest Africa. *Marine Geology*, 58: 345-371.

Mikkelsen, N., 1984. Diatoms in the Zaire deep-sea fan and Pleistocene palaeoclimatic trends in the Angola Basin and west equatorial Africa. *Netherlands Journal of Sea Research*, 14(2-4): 280-292.

Mortlock, R.A., and Froelich P.N., 1989. A simple method for the rapid determination of biogenic opal in pelagic marine sediments. *Deep-Sea Research*, 36: 1415-1426.

Müller, P.J., and Schneider, R., 1993. An automated leaching method for determination of opal in sediments and particulate matter. *Deep-Sea Research*, 40: 425-444.

Pastouret, L., Chamley, H., Delibrias, G., Duplessy, J.C., and Thiede, J., 1978. Late Quaternary climatic changes in Western Tropical Africa deduced from deep-sea sedimantation off the Niger delta. *Oceanologica Acta*, 1(2): 217-232.

Pokras, E.M., 1991. Source areas and transport mechanisms for freshwater and brackish-water diatoms deposited in pelagic sediments of the Equatorial Atlantic. *Quaternary Research*, 35: 144-156.

Pokras, E.M., and Mix, A.C., 1985. Eolian evidence for spatial variability of Late Quaternary climates in Tropical Africa. *Quaternay Research*, 24: 137-149.

Pokras, E.M., and Molfino, B., 1986. Oceanographic control of diatom abundances and species distributions in surface sediments of the Tropical and Southeast Atlantic. *Marine Micropaleontology*, 10: 165-188.

Pufahl, P.K. Maslin, M.A., Anderson, L., Brüchert, V., J ansen, F., Lin, H., Perez, M., Vidal , L., Shipboard Scientific Party, 1998. Lithostratigraphic summary for Leg 175: Angola-Benguela upwelling system. In Wefer, G., Berger, W.H., and Richter, C., et al., Proc. ODP, Initial Reports, 175: College Station TX (Ocean Drilling Project), 533-542.

Romero, O.E., Lange, C.B., Fischer, G., Treppke, U.F., and Wefer, G., 1999a. Variability in export production documented by downward fluxes and species composition of marine planktonic diatoms: observations from the tropical and equatorial Atlantic. *In* Fischer, G., and Wefer, G. (Eds.), *Use of proxies in paleoceanography: examples from the South Atlantic*: Berlin Heidelberg (Springer-Verlag), pp. 365-392.

Romero, O.E., Lange, C.B., Swap, R.J., and Wefer, G., 1999b. Eolian transported freshwater diatoms and phytoliths across the equatorial Atlantic record of temporal changes in Saharan dust transport patterns. *Journal of Geophysical Research*, 104: 3211-3222.

Runge, F., 1999. The opal phytolith inventory of soils in central Africa -quantites, shapes, classification, and spectra. *Review of Paleobotany and Palynology*, 107: 23-53.

Schneider, R., 1991. Spätquartäre Produktivitätsänderungen im östlichen Angola-Becken: Reaktion auf Variationen im Passat-Monsun-Windsystem und in der Advektion des Benguela-Küstenstroms [Ph.D. thesis]. *Berichte Fachberreich Geowissenschaften Nr. 21*, 198 pp. Univ. Bremen, Bremen, Germany.

Schneider, R., Müller, P.J., and Wefer, G., 1994. Late Quaternary productivity changes off the Congo deduced form stable carbon isotopes of planktonic foraminifera. *Palaeogeography, Palaeoclimatology, Palaeoecology*, 110: 255-274.

Schneider, R.R., Müller, P.J., and Ruhland, G., 1995. Late Quaternary surface circulation in the east equatorial South Atlantic: evidence from alkenone sea surface temperatures. *Paleoceanography*, 10(2): 197-219.

Schneider, R.R. Müller, P.J., Ruhland, G., Meinecke, G., Schmidt , H., and Wefer, G., 1996. Quaternary surface temperatures and productivity in the Equatorial South Atlantic: Response to changes in Trade Monsoon wind forcing and surface water advection. In Wefer, G., Berger, W.H., Siedler, G., and Webb, D.J. (Eds.), The South Atlantic: Present and past circulation: Berlin, Heidelberg (Springer-Verlag), p. 527-551.

Table 2. Depth in meters below seafloor (mbsf), meters composite depth (mcd), Grape density, Sedimentation rate, and concentration of the different siliceous organisms from Site 1077

Depth (mbsf)	Depth (mcd)	Site	Hole	Core	Sect.	Top (cm)	Bottom (cm)	Age (ka)	Density (g/cc)	Sed. rate (cm/kyr)	Marine Diatoms	Silicoflagellates	Radiolarians	Freshwater Diatoms	Chrysophyceans cysts	Phytoliths
											(organisms per gram dry sediment)					
0.05	0.05	1077	B	1H	1	5	8	0.3	1.22	17.86	34903365	1116037	808165	1260352	780011	548398
0.45	0.45			1H	1	45	48	2.5	1.20	17.86	37661737	827546	652006	2557870	335126	150463
0.85	0.85			1H	1	85	88	4.8	1.27	17.86	35051701	798477	573905	1048001	444612	399238
1.25	1.25			1H	1	125	128	7.0	1.27	22.00	20588570	190972	503472	746528	446835	104167
1.65	1.65			1H	2	5	8	8.8	1.29	22.00	31448727	417711	504734	1348858	559944	139237
2.05	2.05			1H	2	45	48	10.6	1.25	22.00	41625785	531080	969798	958253	222860	253995
2.45	2.45			1H	2	85	88	12.5	1.24	22.00	35428195	406108	744531	396439	783921	183715
2.85	2.85			1H	2	125	128	14.3	1.26	22.00	26930703	731197	885133	375219	557151	327114
3.25	3.25			1H	3	5	8	16.1	1.26	22.00	53147979	1339913	777765	877874	1159452	508243
3.65	3.65			1H	3	45	48	17.9	1.26	22.00	107908693	1813847	927078	927078	555765	376205
4.05	4.05			1H	3	85	88	19.7	1.25	22.00	39034355	771605	395448	376157	781962	250772
4.65	4.65			1H	3	125	128	22.6	1.24	18.08	165933057	1420367	700587	643004	444612	393480
5.05	5.05			1H	4	5	8	24.8	1.07	18.08	64529574	1128472	462963	829475	558544	154321
5.45	5.45			1H	4	45	48	27.0	1.27	18.08	136197372	1981928	413703	1481635	891442	105831
5.85	5.85			1H	4	85	88	29.2	1.26	18.08	81677466	1398534	607639	906636	893670	135031
5.45	5.89	1077	A	2H	1	45	46	29.4	1.22	18.08	65087979	2378632	444785	1489062	1679831	154708
5.85	6.29			2H	1	85	86	31.6	1.24	18.08	95218935	2353395	443673	1832562	1452214	135031
6.25	6.69			2H	1	125	126	33.8	1.23	18.08	82951049	1851852	308642	655864	1563923	250772
6.55	6.99			2H	2	5	6	35.5	1.24	18.08	92950172	1566416	765803	7188109	1903809	156642
6.95	7.39			2H	2	45	46	37.7	1.23	18.08	86821280	2083333	798611	729167	781962	416667
7.35	7.79			2H	2	85	86	39.9	1.23	18.08	55413251	1232639	156250	86806	670253	138889
7.75	8.19			2H	2	125	126	42.1	1.25	18.08	64109208	2320587	658077	1350790	1114302	346356
8.05	8.49			2H	3	5	6	43.8	1.28	18.08	112165708	3202451	1438782	3562146	2239775	742597
8.45	8.89			2H	3	45	46	46.0	1.24	18.24	73214405	2424494	502217	1316154	2005744	173178
8.85	9.29			2H	3	85	86	48.2	1.25	19.90	45157221	1044277	504734	1209621	671933	156642
9.25	9.69			2H	3	125	126	50.2	1.26	19.90	40325869	1131300	591757	983361	335966	34809
9.55	9.99			2H	4	5	6	51.7	1.27	19.90	62469528	1000585	750439	2097380	891442	192420
9.95	10.39			2H	4	45	46	53.7	1.26	19.90	77739039	1273148	655864	4639275	1005379	327932
10.35	10.79			2H	4	85	86	55.7	1.26	19.90	70135953	831554	734862	1121631	671933	212723
11.14	11.14	1077	B	2H	4	104	105	57.5	1.27	19.90	59202575	1319444	601852	3472222	0	462963
11.54	11.54			2H	4	144	145	59.5	1.26	19.90	53742031	727238	702160	2282022	446835	927855
11.95	11.95			2H	5	35	36	61.6	1.24	19.90	62927788	1885718	846649	2924787	780011	865891
12.35	12.35			2H	5	75	76	63.6	1.23	19.90	56518145	2666944	656153	2137788	780011	613820
12.75	12.75			2H	5	115	116	65.6	1.25	19.90	26921723	1655093	526620	1780478	223418	225694
13.14	13.14			2H	6	4	5	67.5	1.27	19.90	35503891	1253858	551698	1429398	893670	275849
13.54	13.54			2H	6	44	45	69.6	1.25	19.90	42334113	1053241	902778	2156636	1117088	200617
13.94	13.94			2H	6	84	85	71.6	1.26	19.90	25294548	1450848	750439	3727179	780011	425249
14.35	14.35	1077	C	3H	1	105	106	73.6	1.30	19.90	8727198	42545	293945	351960	111989	69618

Table 2. continued

Depth (mbsf)	Depth (mcd)	Site	Hole	Core	Sect.	Top (cm)	Bottom (cm)	Age	Density (g/cc)	Sed. rate	Marine Diatoms	Silicoflagellates	Radiolarians	Freshwater Diatoms	Chrysophyceans cysts	Phytoliths
											(organisms per gram dry sediment)					
14.75	14.75			3H	1	145	146	75.6	1.29	19.90	9740010	100560	529874	760002	223978	162443
14.98	15.42	1077	A	3H	1	48	50	79.0	1.24	15.85	21492044	279707	356867	887346	335126	77160
15.35	15.79			3H	1	85	88	81.3	1.27	15.85	51128420	1729681	752315	2617027	372363	128601
15.78	16.22			3H	1	128	130	84.0	1.28	15.85	75154084	1863426	756173	1903935	223418	67515
16.05	16.49			3H	2	5	8	85.8	1.28	15.85	154750272	3703704	1882716	1820988	1117088	123457
16.45	16.89			3H	2	45	48	88.3	1.27	15.85	47854884	1104492	646532	1562452	1002872	80816
16.85	17.29			3H	2	85	88	90.8	1.30	15.85	67560305	2619599	1809414	486111	670253	108025
17.25	17.69			3H	2	125	128	93.3	1.27	15.85	19302773	588349	395448	501543	223418	19290
17.55	17.99			3H	3	5	8	95.2	1.33	15.85	64900355	2102623	1388889	1099537	446835	77160
17.95	18.39			3H	3	45	48	97.7	1.29	15.52	24875813	309796	484899	619593	111430	94286
18.35	18.79			3H	3	85	88	100.3	1.26	15.20	71346166	1242284	1134259	3294753	0	162037
18.75	19.19			3H	3	125	128	102.9	1.28	15.20	16306953	526620	661651	1620370	167563	13503
19.05	19.49			3H	4	5	8	104.9	1.29	15.20	72007786	972222	945216	2673611	335126	27006
19.48	19.92			3H	4	48	48?	107.8	1.26	15.20	58612237	774491	700409	1602860	891442	67347
19.85	20.29			3H	4	85	88	110.2	1.27	15.20	121921012	555556	1087963	1516204	670253	92593
20.25	20.69			3H	4	125	128	112.8	1.31	15.20	37255130	474537	694444	740741	390981	115741
20.55	20.99			3H	5	5	8	114.8	1.34	15.20	52545387	1242284	2052469	1498843	670253	270062
20.95	21.39			3H	5	45	48	117.4	1.33	15.20	9531475	144676	482253	265239	167563	48225
21.35	21.79			3H	5	85	88	120.1	1.32	15.20	11920466	212191	1446759	1051312	446835	173611
21.75	22.19			3H	5	125	128	122.7	1.32	15.20	4451904	98380	248843	717593	55854	57870
22.05	22.49			3H	6	5	8	125.2	1.34	8.55	339506	17361	416667	77160	3858	32793
22.45	22.89			3H	6	45	48	129.8	1.34	8.55	10128898	92593	590278	99826	279272	219907
22.85	23.29			3H	6	85	88	134.5	1.31	8.55	27584620	617284	1302083	149498	502690	376157
23.25	23.69			3H	6	125	128	139.2	1.27	8.55	23241407	352045	472608	250772	2178321	38580
23.55	23.99			3H	7	5	8	142.7	1.29	8.55	45335237	702160	1512346	729167	2681011	297068
23.99	24.43			4H	2	5	8	147.9	1.21	8.55	85205503	1282793	1822917	1323302	893670	445602
25.55	25.99			4H	2	43	45	166.1	1.24	8.55	35300406	378086	499614	985725	251345	209298
25.93	26.37			4H	2	85	88	170.5	1.26	8.55	89187103	987654	1095679	1990741	726107	462963
26.35	26.79			4H	2	125	128	175.5	1.28	8.55	10359698	49190	144676	81019	55854	107060
26.75	27.19			4H	3	5	8	180.1	1.29	8.55	35401195	594136	1633873	148534	1619777	418596
27.43	27.87			4H	3	43	45	188.1	1.28	8.55	7616749	66551	231481	46296	223418	156250
27.85	28.29			4H	3	85	88	193.0	1.25	10.43	37254288	771605	896991	260417	1843195	298997
28.25	28.69			4H	3	125	128	196.8	1.25	10.43	38974437	706019	694444	601852	1954904	231481
28.55	28.99			4H	4	5	8	199.7	1.23	10.43	62402680	648148	941358	1041667	1899049	262346
28.93	29.37			4H	4	43	45	203.4	1.25	10.43	26261938	391590	580633	479360	5138604	54012
29.35	29.79			4H	4	85	88	207.4	1.26	10.43	49787651	1201775	1120756	1161265	2681011	256559
29.75	30.19			4H	4	125	128	211.2	1.27	10.43	37640484	981427	663310	595625	783921	135369
30.05	30.49			4H	5	5	8	214.1	1.27	10.43	37683754	787037	501543	540123	865743	185185

Table 2. continued

Depth (mbsf)	Depth (mcd)	Site	Hole	Core	Sect.	Top (cm)	Bottom (cm)	Age	Density (g/cc)	Sed. rate	Marine Diatoms	Silicoflagellates	Radiolarians	Freshwater Diatoms	Chrysophyceans cysts	Phytoliths
											(organisms per gram dry sediment)					
30.45	30.89			4H	5	45	48	217.5	1.25	13.33	39534144	601852	516975	493827	1298615	208333
30.85	31.29			4H	5	85	88	220.5	1.27	13.33	72032653	391590	499614	337577	55854	310571
31.25	31.69			4H	5	1225	128	223.5	1.27	13.33	42181452	626929	501543	260417	335126	482253
31.55	31.99			4H	6	5	8	225.8	1.25	13.33	55154329	711806	486111	625000	1117088	503472
31.98	32.42			4H	6	48	50	229.0	1.25	13.33	40387826	482253	925926	1157407	1117088	289352
32.35	32.79			4H	6	85	88	231.8	1.27	13.33	33760246	555556	590278	989583	2345885	399306
32.75	33.19			4H	6	125	128	234.8	1.29	13.33	41985507	694444	597994	1292438	1899049	462963
33.05	33.49			4H	7	5	8	237.0	1.29	13.33	64649030	964506	733025	3086420	2234176	540123
33.45	33.89			4H	7	45	48	240.0	1.29	22.31	36493198	1064815	925926	1921296	1452214	115741
33.55	33.99			5H	1	5	8	240.4	1.27	22.31	41670778	270062	1060957	1369599	1228797	347222
33.95	34.39			5H	1	45	48	242.2	1.29	22.31	27567452	270062	756173	938465	1452214	243056
34.35	34.79			5H	1	85	88	244.0	1.23	22.31	29882733	200617	570988	1257716	1228797	185185
34.75	35.19			5H	1	125	128	245.8	1.28	22.31	36772636	416667	833333	486111	1172942	277778
35.05	35.49			5H	2	5	8	247.2	1.28	22.31	44899106	366512	1060957	2189429	1452214	443673
35.45	35.89			5H	2	45	48	249.0	1.18	22.31	76391166	324074	763889	486111	2010758	208333
35.85	36.29			5H	2	85	88	250.8	1.27	22.31	15808770	135031	434028	115741	893670	347222
36.25	36.69			5H	2	125	128	252.6	1.16	22.31	32994697	127315	520833	81019	1061233	231481
36.55	36.99			5H	3	5	8	253.9	1.28	22.31	32940230	193385	541477	541477	1903809	348092
36.93	37.37			5H	3	43	45	255.6	1.15	22.31	41309666	193385	367431	212723	1903809	96692
37.35	37.79			5H	3	85	88	257.5	1.26	22.31	86906876	347222	833333	1064815	3462972	555556
37.75	38.19			5H	3	125	128	259.3	1.16	22.31	65268212	96451	462963	308642	2457593	192901
38.05	38.49			5H	4	5	8	260.6	1.28	22.31	71760777	277778	771605	1087963	3127846	354938
38.45	38.89			5H	4	45	48	262.4	1.21	22.31	47565531	135031	405093	607639	446835	154321
38.85	39.29			5H	4	85	88	264.2	1.29	22.31	58759661	632716	324074	455247	1452214	262346
39.25	39.69			5H	4	125	128	266.0	1.26	20.12	51809667	1280864	493827	2291667	2010758	493827
39.55	39.99			5H	5	5	8	267.5	1.24	20.12	104774511	1574074	679012	2376543	1899049	478395
39.93	40.37			5H	5	43	45	269.4	1.24	20.12	84768266	729167	270062	877701	446835	135031
40.35	40.79			5H	5	85	88	271.5	1.22	20.12	55370868	462963	254630	439815	781962	277778
40.75	41.19			5H	5	125	128	273.5	1.25	20.12	63617246	462963	231481	270062	1787341	366512
41.05	41.49			5H	6	5	8	274.9	1.29	20.12	50852639	439815	462963	439815	1899049	185185
41.45	41.89			5H	6	45	48	276.9	1.23	20.12	101724822	810185	729167	1620370	1340505	189043
41.85	42.29			5H	6	85	88	278.9	1.19	20.12	52293422	740741	578704	439815	1340505	138889
42.25	42.69			5H	6	125	128	280.9	1.20	20.12	84979508	810185	567130	945216	2904429	162037
42.55	42.99			5H	7	5	8	282.4	0.99	20.12	77033464	837191	432099	1336806	2234176	432099
42.95	43.39			5H	7	45	48	284.4	1.24	20.12	99262200	1053241	526620	326003	2792720	275849
43.05	46.37			6H	1	5	8	299.20	1.26	20.12	108437140	406108	966923	1218324	1791820	232062
44.25	47.57			6H	1	125	128	305.16	1.30	20.12	111214234	648148	787037	1782407	2345885	162037
45.35	48.67			6H	2	85	88	310.63	1.26	20.12	74939153	350205	431021	457960	1560023	323266

Table 2. continued

Depth (mbsf)	Depth (mcd)	Site	Hole	Core	Sect.	Top (cm)	Bottom (cm)	Age	Density (g/cc)	Sed. rate	Marine Diatoms	Silicoflagellates	Radiolarians	Freshwater Diatoms	Chrysophyceans cysts	Phytoliths
											(organisms per gram dry sediment)					
46.65	49.97			6H	3	65	68	317.09	1.28	20.12	99733670	270062	189043	769676	781962	54012
47.75	51.07			6H	4	25	28	322.55	1.30	20.76	44134648	208333	393519	717593	3909808	46296
49.05	52.37			6H	5	5	8	329.01	1.33	20.76	54889272	243056	675154	1728395	1675632	54012
50.25	53.57			6H	5	125	1228	336.31	1.29	11.14	37627783	831255	669622	854346	2228604	738894
51.35	54.67			6H	6	85	88	343.61	1.26	11.14	80145136	619593	646532	1804901	1448593	1131431
52.65	55.97			6H	7	65	68	352.23	1.25	11.14	81793547	1624431	487329	5766732	671933	1245397
53.75	57.95			7H	1	125	128	365.37	1.29	11.14	89725611	1858779	862042	7839198	1448593	431021
55.05	59.25			7H	2	105	108	373.99	1.30	19.82	55988817	371299	208855	1578019	1231876	208855
57.49	61.69			7H	4	45	48	390.18	1.23	19.82	15034630	324886	812216	920511	895910	189517
58.59	62.79			7H	5	5	8	397.48	1.35	19.82	75278015	270062	810185	1107253	1675632	162037
59.79	63.99			7H	5	125	128	405.44	1.31	19.82	43933944	189517	433182	297812	1119888	81222
61.09	65.29			7H	6	105	108	414.06	1.22	19.82	65919295	348092	626566	417711	3359663	812216
62.26	66.46			8H	1	25	28	422.27	1.20	8.72	86344964	1574074	393519	1203704	1340505	277778
63.46	67.66			8H	1	145	148	431.04	1.22	8.72	80856979	974659	406108	893437	1679831	460256
64.55	68.75			8H	2	105	108	439.00	1.28	11.43	95161439	1276339	649773	928247	2463753	580154
65.85	70.05			8H	3	85	88	456.06	1.29	11.43	112497755	594136	378086	783179	2569302	270062

Table 4. Concentration of the different marine diatom groups from Site 1077

Site	Hole	Core	Sect.	Top (cm)	Bottom (cm)	Age (ka)	Neritic	Littoral	Warm	Oc. Temp.	High nutrients (*Chaetoceros spp. RS*)	High nutrients (*T. nitzschioides*)	Low Salinity
							(valves per gram dry sediment)						
1077	B	1H	1	5	8	0.3	4098550	360788	1664435	67347	10551842	8858702	8580126
		1H	1	45	48	2.5	3999807	401235	1128472	463927	12103303	12399676	6814236
		1H	1	85	88	4.8	3081621	174667	873334	212095	10734204	14672199	4779580
		1H	1	125	128	7.0	2213542	225694	529514	243056	9048412	5808857	2345885
		1H	2	5	8	8.8	3863826	417711	730994	382902	14533573	8287168	3023697
		1H	2	45	48	10.6	7123395	923617	1246883	554170	16184493	8580126	6574383
		1H	2	85	88	12.5	3693648	522139	870231	183715	8101868	21165876	503949
		1H	2	125	128	14.3	3502047	336735	894754	384840	6488227	11310167	3677197
		1H	3	5	8	16.1	2233188	177115	1047288	577549	6807878	31216029	10881016
		1H	3	45	48	17.9	5871491	376205	1679488	403077	12452789	37680875	48907330
		1H	3	85	88	19.7	2989969	289352	607639	154321	8354126	11729423	14745560
		1H	3	125	128	22.6	2888720	326301	690989	652601	54625143	77029045	29566704
		1H	4	5	8	24.8	2353395	192901	569059	192901	9655181	30384791	20554417
		1H	4	45	48	27.0	9467310	202041	952480	481050	5977170	75326824	43569213
		1H	4	85	88	29.2	3337191	163966	540123	327932	24670091	33400928	19102203
1077	A	2H	1	45	46	29.4	8721650	415777	937916	1286008	11019361	14054589	28053185
		2H	1	85	86	31.6	10146605	231481	790895	1813272	10836622	19102203	51777024
		2H	1	125	126	33.8	11612654	250772	713735	6587577	10691235	12399676	40271018
		2H	2	5	6	35.5	4542607	409009	1018170	11330409	24962937	9183078	41155870
		2H	2	45	46	37.7	4652778	381944	963542	9192708	17391137	17147299	36640483
		2H	2	85	86	39.9	2595486	121528	642361	3203125	18642560	6702527	23123719
		2H	2	125	126	42.1	5204004	380992	1030410	4589221	15708679	9192993	27188972
		2H	3	5	6	43.8	21976237	1403973	2889167	7135895	38903516	11422854	28109179
		2H	3	45	46	46.0	4268842	519534	961139	4286160	28959080	14541643	19054566
		2H	3	85	86	48.2	3689780	313283	461223	1705653	19311285	10862910	8343163
		2H	3	125	126	50.2	4281537	313283	713590	1801378	16934555	8399157	7447253
		2H	4	5	6	51.7	5330039	317493	1250731	2366768	33203917	9638713	9861574
		2H	4	45	46	53.7	3886960	250772	694444	2266590	35566877	17929261	16700464
		2H	4	85	86	55.7	6052941	290077	1005600	1624431	36235299	11142882	13494646

Table 4. continued

Site	Hole	Core	Sect.	Top (cm)	Bottom (cm)	Age (ka)	Neritic	Littoral	Warm	Oc. Temp.	High nutrients (*Chaetoceros spp. RS*) (*T. nitzschioides*)		Low Salinity
							(valves per gram dry sediment)						
1077	B	2H	4	104	105	57.5	2592593	162037	1053241	3750000	23663147	8322305	19381475
		2H	4	144	145	59.5	4977816	225694	1128472	4689429	24407224	17314862	446835
		2H	5	35	36	61.6	6705843	240525	1260352	5762985	24258192	23957496	222860
		2H	5	75	76	63.6	7990248	275161	1471052	7535174	20549861	17048823	780011
		2H	5	115	116	65.6	4024884	125386	802469	1592400	11086524	8043033	670253
		2H	6	4	5	67.5	5918210	476466	727238	1956019	14016030	11338442	670253
		2H	6	44	45	69.6	3347801	451389	1103395	1918403	17841483	15862648	1508069
		2H	6	84	85	71.6	5228056	175102	1175687	1225717	8607412	8134406	222860
1077	C	3H	1	105	106	73.6	825753	11603	133435	114097	3247674	3247674	1119888
		3H	1	145	146	75.6	1349825	11603	175980	212723	2127786	4927505	895910
1077	A	3H	1	48	50	79.0	2970679	135031	723380	501543	5156313	5585439	6255692
		3H	1	85	88	81.3	2977109	122171	752315	1118827	8999949	12213494	24873824
		3H	1	128	130	84.0	8574460	283565	1026235	850694	21324093	14968978	27815488
		3H	2	5	8	85.8	11913580	740741	1944444	2314815	24170114	16532901	96516393
		3H	2	45	48	88.3	4835519	188572	727348	1212247	15310007	5682941	19723148
		3H	2	85	88	90.8	8344907	351080	999228	2349537	30723569	7372780	17203153
		3H	2	125	128	93.3	2459491	48225	453318	559414	8361320	4356643	3016137
		3H	3	5	8	95.2	8198302	424383	983796	2121914	23137554	11170879	18767077
		3H	3	45	48	97.7	3084496	67347	552246	956328	9143397	5237220	5794371
		3H	3	85	88	100.3	7048611	702160	1215278	2214506	14453394	9830373	35746812
		3H	3	125	128	102.9	3969907	297068	742670	675154	2775533	2345885	5473731
		3H	4	5	8	104.9	10964506	607639	1350309	1485340	11525643	5920566	39991746
		3H	4	48	48?	107.8	3044087	87551	747552	255919	13004884	9638713	31813326
		3H	4	85	88	110.2	5115741	254630	1585648	219907	12993463	5138604	96404685
		3H	4	125	128	112.8	3043981	104167	746528	405093	11091129	2681011	19102203
		3H	5	5	8	114.8	4712577	216049	1309799	756173	15075160	14633851	15639230
		3H	5	45	48	117.4	1572145	72338	260417	289352	3063355	2262103	1982831
		3H	5	85	88	120.1	916281	19290	260417	202546	3798099	3016137	3630536
		3H	5	125	128	122.7	280671	23148	124421	52083	1982831	1368433	530617

Table 4. continued

Site	Hole	Core	Sect.	Top (cm)	Bottom (cm)	Age (ka)	Neritic	Littoral	Warm	Oc. Temp.	High nutrients (*Chaetoceros spp. RS*)	(*T. nitzschioides*)	Low Salinity
							(valves per gram dry sediment)						
		3H	6	5	8	125.2	20255	3858	12539	7716	42438	81983	170718
		3H	6	45	48	129.8	711806	66551	206887	214120	2234176	6660637	0
		3H	6	85	88	134.5	2165316	86806	477431	327932	14968978	8797067	558544
		3H	6	125	128	139.2	2850116	127797	419560	274884	7344566	11952840	223418
		3H	7	5	8	142.7	7413194	229552	648148	553627	16248103	19995873	111709
		4H	2	5	8	147.9	2822145	357832	789931	1228781	14618506	58926386	6367401
		4H	2	43	45	166.1	1110629	121528	324074	793306	6212880	25441677	1228797
		4H	2	85	88	170.5	2546296	694444	879630	2530864	3915682	56357084	22062486
		4H	2	125	128	175.5	791377	31829	173611	580150	592258	5697148	2429666
		4H	3	5	8	180.1	2018711	337577	708912	958719	5004182	22453467	3798099
		4H	3	43	45	188.1	339988	69444	120081	257523	1843195	4719696	223418
		4H	3	85	88	193.0	3428819	366512	390625	602816	6868509	24073244	1340505
		4H	3	125	128	196.8	4346065	370370	995370	1018519	10154447	20610272	1340505
		4H	4	5	8	199.7	3973765	462963	1003086	1103395	28632694	25581313	1228797
		4H	4	43	45	203.4	2849151	587384	573881	749421	6255692	14075307	1117088
		4H	4	85	88	207.4	4104938	553627	958719	1633873	9813186	32172131	335126
		4H	4	125	128	211.2	1637968	263970	609162	967890	17078286	17022292	0
		4H	5	5	8	214.1	3086420	432099	520833	1481481	10152258	20275145	1619777
		4H	5	45	48	217.5	2982253	459105	462963	1331019	9179585	10668189	14354579
		4H	5	85	88	220.5	3672840	270062	904707	8898534	2177400	9104266	46694274
		4H	5	1225	128	223.5	2734375	376157	1147762	9823495	951541	5082750	21448087
		4H	6	5	8	225.8	5434028	520833	1979167	11319444	6662540	9606956	18711222
		4H	6	48	50	229.0	14795525	607639	1485340	1938657	7511843	12399676	1340505
		4H	6	85	88	231.8	4192708	538194	902778	1284722	6593095	19381475	502690
		4H	6	125	128	234.8	8622685	694444	1263503	1755401	10077113	18543659	893670
		4H	7	5	8	237.0	10204475	771605	1977238	1861497	12669737	36417065	670253
		4H	7	45	48	240.0	9409722	451389	706019	983796	7195659	15862648	1675632
		5H	1	5	8	240.4	6008873	279707	569059	1215278	6814236	16086066	10388917
		5H	1	45	48	242.2	3564815	364583	452353	560378	4718775	14522143	3127846

Table 4. continued

Site	Hole	Core	Sect.	Top (cm)	Bottom (cm)	Age (ka)	Neritic	Littoral	Warm	Oc. Temp.	High nutrients (*Chaetoceros spp. RS*)	(*T. nitzschioides*)	Low Salinity
							(valves per gram dry sediment)						
		5H	1	85	88	244.0	3888889	270062	578704	347222	5392886	14745560	4412497
		5H	1	125	128	245.8	3883102	277778	520833	549769	7602246	16086066	7540343
		5H	2	5	8	247.2	5970293	289352	752315	1138117	5458472	16197774	14745560
		5H	2	45	48	249.0	5983796	266204	729167	682870	9060508	36975609	22230049
		5H	2	85	88	250.8	2121914	96451	236304	260417	2900831	8210596	1731486
		5H	2	125	128	252.6	4641204	347222	248843	468750	2492316	17538280	6702527
		5H	3	5	8	253.9	6903834	212723	415777	502800	6105408	13662629	4479550
		5H	3	43	45	255.6	7590349	125700	464123	454454	5487449	23517640	2799719
		5H	3	85	88	257.5	5462963	277778	636574	1354167	9117856	51274334	18320241
		5H	3	125	128	259.3	3269676	221836	318287	356867	8829026	44571807	7372780
		5H	4	5	8	260.6	6226852	246914	378086	671296	7746835	48034779	7931324
		5H	4	45	48	262.4	2826003	115741	356867	424383	4580060	34685579	4133225
		5H	4	85	88	264.2	1728395	61728	331790	648148	6590819	42225922	6925945
		5H	4	125	128	266.0	1666667	246914	841049	1782407	4753498	39656620	2569302
		5H	5	5	8	267.5	3657407	246914	632716	2060185	4607240	90037284	3239555
		5H	5	43	45	269.4	21132330	189043	378086	850694	2399897	56301230	3462972
		5H	5	85	88	271.5	7997685	462963	428241	520833	3992842	35523395	6143983
		5H	5	125	128	273.5	7320602	212191	376157	626929	5716438	33624345	14968978
		5H	6	5	8	274.9	7141204	231481	335648	682870	4225818	28709159	9271829
		5H	6	45	48	276.9	8912037	108025	580633	891204	12453688	57753444	20107582
		5H	6	85	88	278.9	9120370	277778	451389	844907	6641147	26698401	7819615
		5H	6	125	128	280.9	12287809	378086	378086	1188272	9633962	42337631	18208533
		5H	7	5	8	282.4	11329090	445602	621142	985725	13959914	30943334	18208533
		5H	7	45	48	284.4	11460262	200617	589313	752315	11594914	42896175	31166752
		6H	1	5	8	299.20	9350150	541477	928247	406108	16358443	60921886	19486044
		6H	1	125	128	305.16	24803241	717593	729167	1412037	7604262	57753444	17314862
		6H	2	85	88	310.63	6977156	552246	660001	0	7208675	38443424	20558874
		6H	3	65	68	317.09	11072531	648148	904707	1242284	11059170	48816741	25693021
		6H	4	25	28	322.55	7025463	439815	590278	1550926	19437329	13516763	1273148

Table 4. continued

Site	Hole	Core	Sect.	Top (cm)	Bottom (cm)	Age (ka)	Neritic	Littoral	Warm	Oc. Temp.	High nutrients (*Chaetoceros spp. RS*) (*T. nitzschioides*) (valves per gram dry sediment)		Low Salinity
		6H	5	5	8	329.01	17500000	297068	1147762	378086	12677105	21671505	893670
		6H	5	125	1228	336.31	6430683	150088	1477787	785074	10766572	17605974	111430
		6H	6	85	88	343.61	5805317	323266	1198778	2101228	22393798	48026422	0
		6H	7	65	68	352.23	3668508	216591	988196	1813948	19316215	55546425	0
		7H	1	125	128	365.37	11193082	646532	1980004	1050614	16707182	56606548	1002872
		7H	2	105	108	373.99	7031468	440917	719391	162443	18300580	27885201	1007899
		7H	4	45	48	390.18	8257527	568551	1299545	1597358	1903809	0	270739
		7H	5	5	8	397.48	11315586	324074	1890432	1917438	29453062	26698401	3462972
		7H	5	125	128	405.44	5116959	446719	920511	1597358	15477829	20157977	0
		7H	6	105	108	414.06	2332219	92825	545345	2065349	25421449	34940493	335966
		8H	1	25	28	422.27	6979167	312500	543981	2337963	22073087	53843636	185185
		8H	1	145	148	431.04	5834416	433182	744531	2274204	21869796	49051077	514403
		8H	2	105	108	439.00	10674835	278474	777406	1786875	31067299	50506931	0
		8H	3	85	88	456.06	4064429	189043	540123	22604167	23224376	61551543	0

7.2

Evidence for Congo River freshwater load in Late Quaternary sediments of ODP Site 1077 (5°S, 10°E)

Uliana, E., Lange, C. B., and Wefer, G.

Submitted for publication in *Palaeogeogr., Palaeoclimat., Palaeoecol.* (March, 2001)

Evidence for Congo River freshwater load in Late Quaternary sediments of ODP Site 1077 (5°S, 10°E)

Uliana, E.[1], C. B. Lange[2], and G. Wefer[1]

[1]Fachbereich Geowissenschaften, Klagenfurter Strasse, Universität Bremen, 28359 Bremen, Germany.

[2]Scripps Institution of Oceanography, University of California at San Diego, Geosciences Research Division and Marine Life Research Group, La Jolla, CA 92093-0244, U.S.A.

Abstract Late Quaternary fluctuations in the intensity of Congo River freshwater load were reconstructed using three different proxies (marine and freshwater diatoms, and the $\delta^{18}O$ record of *Globigerinoides ruber*) preserved in the sediments of ODP Site 1077, located at the northern rim of the Congo River fan (5°10'S, 10°26'E). An abrupt change in the diatom assemblage is evident since Termination II: a two to four-fold increase in a) the relative abundance of a marine planktonic diatom tolerant of low salinity conditions (*Cyclotella litoralis*), and b) in the concentration of freshwater diatoms. The microfossil data suggest a change in the environmental conditions surrounding Site 1077 from predominantly marine to mixed marine/brackish/fresh. The $\delta^{18}O$ record of the planktic foraminifera *Globigerinoides ruber* (pink) revealed negative deviations from the global oxygen isotope signal since Termination II which occurred during warm Stage 1 and substages 3.2, 5.1, 5.3, and 5.5. Comparison of the isotopic signal of ODP Site 1077 with the record from a pelagic location (Core GeoB1041 at 3°48'S, 7°05'W) confirms these results.

The construction of an artificial $\delta^{18}O$ curve using alkenone-derived sea surface temperature (SST) data from a nearby core (GeoB 1008 at 6°S, 10°E) allowed us to estimate salinity and temperature effects on the ODP Site 1077 isotopic signal. Although increased SSTs may account for lighter $\delta^{18}O$ values during warmer periods, they do not explain the extremely light values documented in the sediments of Site 1077. We used the oxygen isotope difference ($\Delta\delta^{18}O$) between our site and GeoB1041 as a proxy for freshwater input. A general trend in the $\Delta\delta^{18}O$ was observed, with more negative values since Termination II. In addition, conspicuous $\Delta\delta^{18}O$ negative pulses coincided with periods of Northern Hemisphere summer insolation maxima over the African continent, suggesting an increase in the freshwater discharge from the Congo River due to enhanced precipitation on the hinterland.

Here we propose that the abrupt change in environmental conditions at Site 1077 since Termination II is a consequence of a major reorganization in the depositional environment of the Congo River delta. This reorganization involved sustained equatorward displacement of the Angola-Benguela Front causing a northward deflection of the Congo River plume thus moving plume waters further north than normal and over Site 1077.

Keywords: Late Quaternary, Congo fan area, diatoms, oxygen isotopes

Introduction

During Ocean Drilling Program (ODP) Leg 175, the Lower Congo Basin (LCB) off west Africa was the target for three drilling Sites 1075, 1076, and 1077, along a transect on the northern rim of the Congo Fan (Shipboard Scientific Party, 1998, "Introduction"). Here the second largest river in the world in terms of freshwater discharge joins an oceanic high-fertility area. The regional environment is dominated by seasonal coastal upwelling and associated filaments and eddies moving offshore, by river input from the Congo River, and by incursions of open-ocean waters.

Sedimentation within the LCB is dominated by rainout of suspended clay derived from the Congo River and by pelagic settling of biogenic debris. Sediments are dominated by diatomaceous, partially carbonate-bearing clays (Shipboard Scientific Party, 1998, "Site 1077"). Kaolinite and smectite are the most important clay minerals in the surface sediments of the Congo Fan (van der Gaast and Jansen, 1984; Gingele et al., 1998). Other important particles of terrestrial origin include fresh- and brackish-water diatoms, plant remains, chrysophyte cysts, and phytoliths. The marine biogenic components include marine diatoms, coccoliths, planktic and benthic foraminifers, silicoflagellates, radiolarians, dinoflagellate cysts, ebridians, and sponge spicules (e.g., Jansen et al., 1984; Mikkelsen, 1984; van Iperen et al., 1987; Jansen and van Iperen, 1991, Uliana et al., 2001). High opal contents (5 to 25 wt%) with large amounts of diatoms characterize late Quaternary Congo Fan sediments (van Iperen et al., 1987; Müller and Schneider, 1993; Schneider et al., 1997; Uliana et al., 2001). Total organic carbon (TOC) values range from 1.9 to 4.7 wt% over the past 500,000 years (Shipboard Scientific Party, 1998, "Site 1077"). Schneider et al. (1997) have shown that variations of total organic carbon in the Congo Fan (Core GeoB1008) are mainly a result of changes in marine organic carbon with values between 0.5 and 4 wt%. Schneider et al. (1997) also suggested that enhanced opal production in the region during warm humid climates was the result of an additional supply of dissolved silica due to more intense chemical weathering on the continent. Total paleoproductivity derived from oceanic upwelling, on the other hand, was high in periods of increased zonal trade wind intensity at precessional minima during cold and more arid glacial climate conditions (Schneider et al., op. cit.).

A long-term trend within the past 450,000 years was recorded by Uliana et al. (2001) who studied siliceous microfossils from ODP Site 1077. They reported an abrupt change in the siliceous signal at 120-130 ka (Termination II) when the environmental conditions in the Congo area seemed to have changed from predominantly marine to mixed marine/brackish/freshwater. Here we take Uliana's results a step further and compare changes in the freshwater signal derived from freshwater diatoms at Site 1077 with concomitant changes in the oxygen isotope ratios of planktonic foraminifers from the Congo Fan area and nearby sites in the east equatorial Atlantic. We also relate these changes to present-day upper water column characteristics of the region. Possible causes and consequences of an increased freshwater signal in the past 120-130 kyr are discussed, including local enhancement of monsoonal precipitation, latitudinal migration of the Inter-Tropical Convergence Zone (ITCZ), and regional movements of oceanic fronts.

Regional Setting

In the eastern Angola Basin (0° to 20°S), the surface and shallow subsurface circulation is dominated by the Angola Current (AC) and the Benguela Coastal Current (BCC) (Fig.1). The AC flows southward along the African coast and is fed by the eastward-flowing, shallow-subsurface warm South Equatorial Countercurrent (SECC). The BCC transports cold and nutrient-rich waters northward across the Walvis Ridge. The two currents converge and form a strong temperature and productivity gradient called the Angola Benguela Front (ABF; Fig. 1). The position of the ABF depends on the intensity of both currents (Meeuwis and Lutjeharms, 1990), which in turn is strongly associated with the latitudinal movements of the ITCZ. Satellite images of sea surface temperature (SST) reveal that the ABF moves from its northernmost location at 14°S in July-August to 16°S during January-February (Meeuwis and Lutjeharms, 1990). The ABF delineates the northern boundary of the zonally directed tradewind field. North of the ABF, winds weaken and change to a meridional direction (summary in Schneider et al., 1995). High coastal productivity is restricted to two narrow areas north and south of the Congo estuary and is considered to be the result of upwelling of colder waters of the Equatorial Undercurrent.

In a zone between 10° and 16°S, the interaction between SECC, AC, and BCC creates a complicated pattern of fronts, gyres, and a thermal dome (Angola Dome), bringing nutrient-rich shallow subsurface waters into the euphotic zone (oceanic upwelling). North of the ABF, the BCC can be traced as a shallow subsurface current to 5°S (van Bennekom and Berger, 1984).

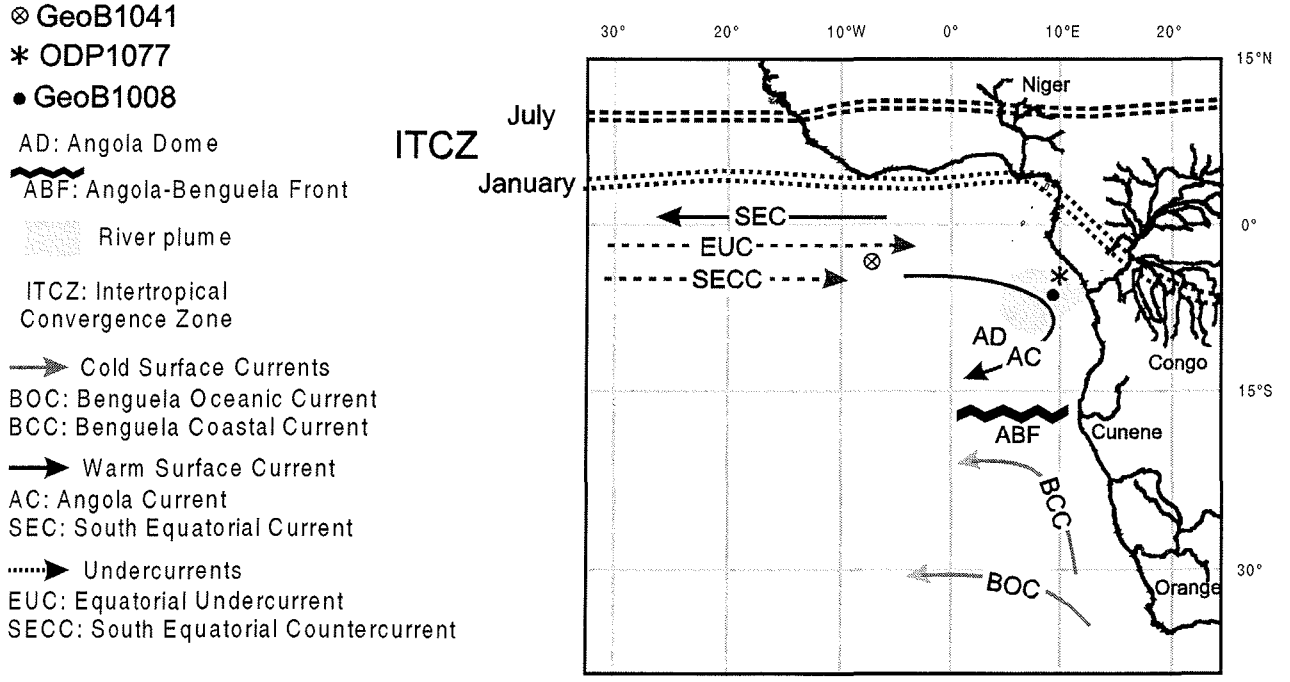

Fig. 1: Location of coring sites, seasonal migrations of the Inter-Tropical Convergence Zone (ITCZ, from Barret, 1974), main surface, and subsurface currents.

Superimposed on the system described above is the influence of the Congo River and fan area which supplies freshwater, nutrients (including large amounts of dissolved SiO_2), and terrigenous particles to the ocean. The Congo River discharge regime is associated with monsoonal circulation and precipitation

(Eisma and van Bennekom, 1978; van Bennekom and Berger, 1984; Gasse, 2000); maximum river discharge is in December (Fig. 2). A major feature is the river plume which has its maximum extension in February-March (van Bennekom and Berger, 1984). Salinity is below 30‰ in the inner plume area. Farther offshore (150-200 km from the river mouth) the plume broadens and salinity rises to about 30‰ (van Bennekom and Berger, 1984). The main direction of the plume is always WNW near the river mouth. Offshore the direction of the plume axis changes to SW or SSW in February and March, to W or WSW from April to August, while in October and November the plume spreads in a NW direction (van Bennekom and Berger, 1984).

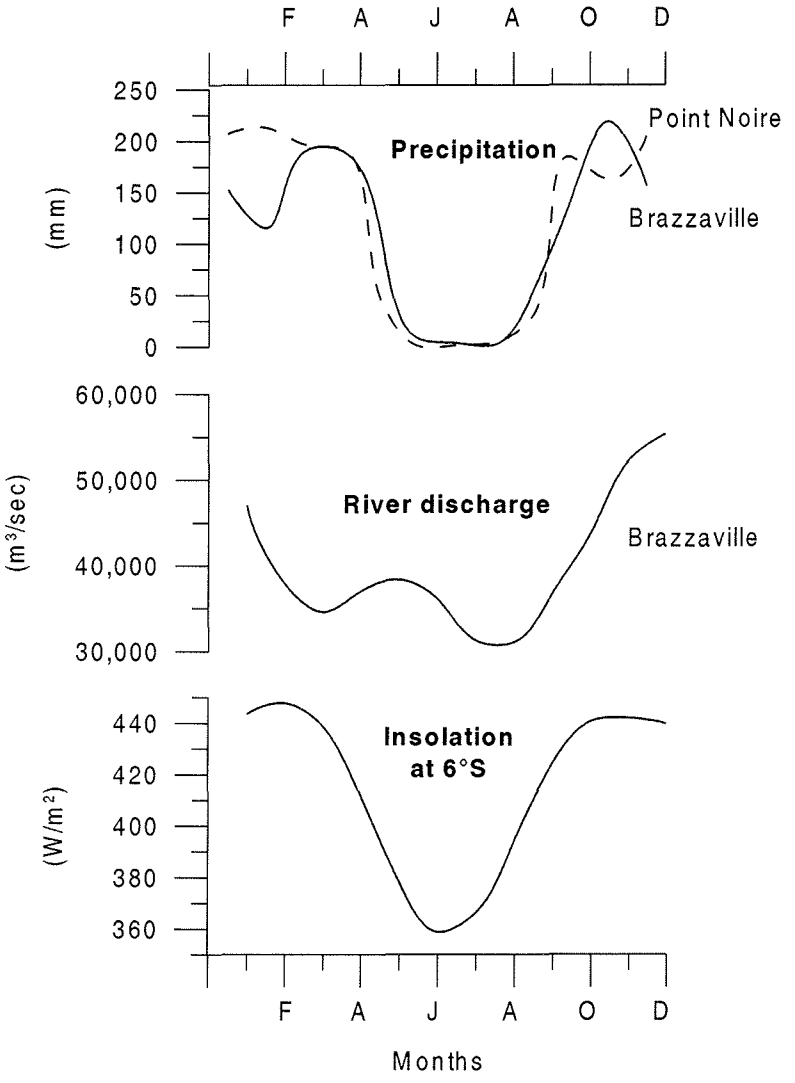

Fig. 2: Monthly precipitation data: at Brazzaville (4°S, 15° E), and at Point Noire (5°S, 12° E); monthly averages from IRI/LDEO Climate Data Library (Baker et al., 1994). River discharge at Brazzaville (Vorosmarty et al., 1998), and 10-year average of monthly insolation at 6°S (from Laskar, 1990).

In summary, modern primary productivity in the area is high in the surface waters off the Congo. Berger et al. (1989) give values of 90-125 gC/m²/yr. High rates of primary productivity are assumed to be the result of 1) nutrient input from the river that carries large amounts of dissolved silica to the ocean (van Bennekom and Berger, 1984; Schneider et al., 1997), and 2) upwelling of subsurface oceanic waters rich in nitrate and phosphate within the estuary and the inner plume area. Especially, it is the input of silica that determines the dominant group within the primary producers of the region. Diatoms are the dominant group within the river plume, small flagellates dominate the area north of the plume (Cadée, 1978, 1984) and coccolithophores and dinoflagellates play an important role further south in the oceanic upwelling area off Angola (Shannon and Pillar, 1986).

Material and Methods

We investigated samples of ODP Site 1077 (5°10'S, 10°26'E) spanning the last 450,000 years. The site is located at 2,382 m water depth, at the northern edge of the Congo River plume (Fig. 1). Sedimentological records suggest that Site 1077 is not affected by turbidity currents (Pufahl et al., 1998).

We used abundances of siliceous microfossils published by Uliana et al. (2001) for ODP Site 1077. Stable oxygen isotope data measured on the planktonic foraminifer *Globigerinoides ruber* (pink) (size >150 μm) were used to generate the oxygen isotope stratigraphy for ODP Site 1077. *G. ruber* pink variety was sufficiently abundant in most samples. A Finnigan MAT 251 micromass spectrometer equipped with a Kiel automated carbonate preparation device was used. Calibration to the PDB standard was via the VNBS19, and the internal standard SHK Bremen. Analytical precision during the measurements from working standards was ± 0.07‰. Stratigraphic pointers were obtained by tuning the $\delta^{18}O$ record of Site 1077 to the $\delta^{18}O$ record of Site 677 (Panama Basin, Shackleton et al., 1990). Control points and detailed information about the age model are published in Uliana et al. (2001). The $\delta^{18}O$ record is shown in some of the figures to allow comparison of biological proxy patterns with global climate change. All data are presented versus sediment age derived from $\delta^{18}O$ -based stratigraphy rather than versus original depth in the cores. For this we refer to the PANGAEA server (http://www.pangaea.de/Projects/SFB261/EUliana_et_al_2000/).

Results and Discussion

Siliceous microfossil record

Marine taxa account for 95% of the siliceous microfossil signal in the sediments of Site 1077 (Uliana et al., 2001). For the three main marine siliceous groups (marine diatoms, radiolarians, sillicoflagellates), concentrations tend to be higher (although highly variable) during glacial stages and cooler conditions of substages 5.2 and 5.4. In contrast, freshwater diatoms which dominate the siliceous signal derived from the continent (followed by chrysophycean cysts and phytoliths), show highest contributions within interglacial stages (Uliana et al., 2001).

An abrupt change in the siliceous microfossil assemblages preserved in the sediments of Site 1077 is evident at Termination II (Fig. 3A). While the marine taxa *Thalassionema nitzschioides* var. *nitzschioides* and *Chaetoceros* spp. in average account for 80% of the marine diatom signal between 450 and 130 ka, their relative abundance is reduced to about 55% during the last 130 ka (Uliana et al., 2001). Times of extremely reduced contribution of these species correspond to cold substages within warm stages 5 and 3 (5.4, 5.2, and 3.2). In these periods *Cyclotella litoralis* dominates (Fig. 3A), a species known to tolerate lower salinity environments (C. Lange, unpubl. obs.). The distinct change in marine environmental conditions at Site 1077 since ca. 130 ka is also implied from increasing concentrations of the freshwater diatom genus *Aulacoseira* (Fig. 3B). This genus seems to reflect temporal fluctuations in the intensity of Congo River discharge (van Iperen et al., 1987; Uliana et al., 2001). Although the two proxies are not perfectly correlated throughout the whole record, their general trend is similar, and times of concentration maxima of *Aulacoseira* coincide with high relative abundances of *C. litoralis* during the above mentioned cold substages.

What caused this remarkable change in environmental conditions from predominantly marine to mixed marine/brackish/fresh documented in the siliceous deposits at Site 1077 near Termination II? We

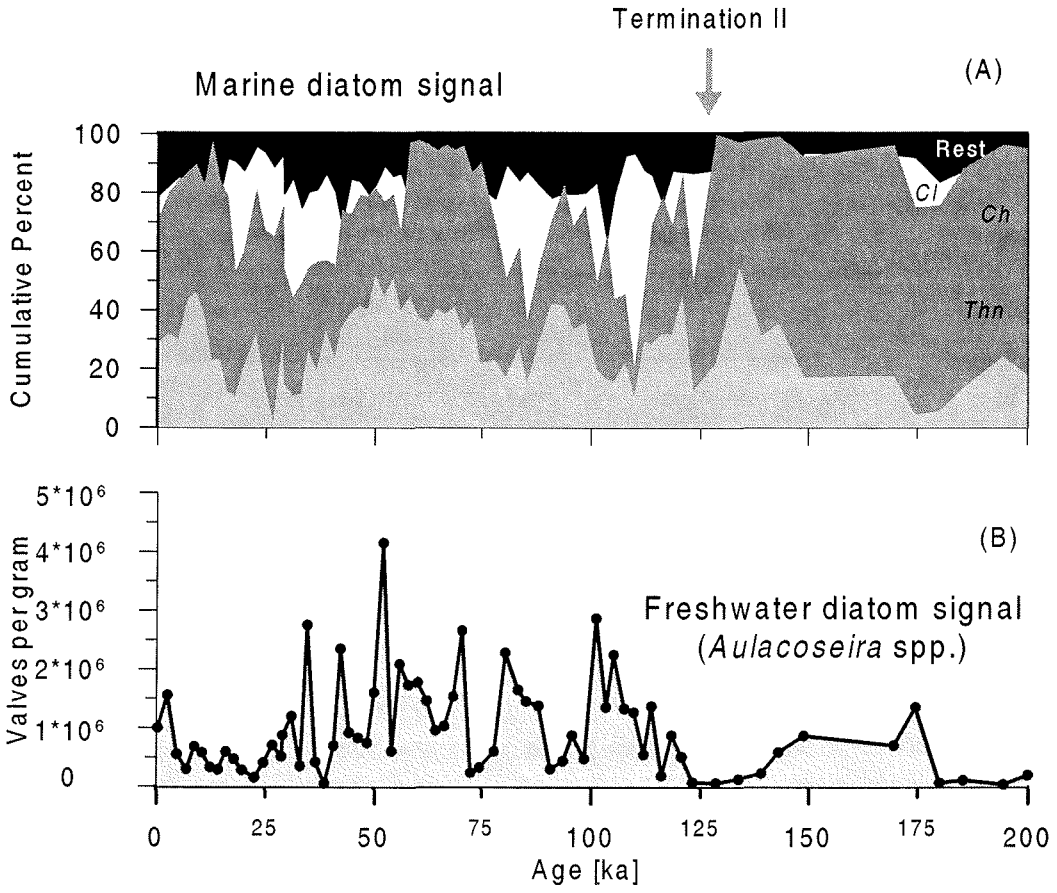

Fig. 3: (A) Relative contribution of the three most abundant marine (*Ch*: *Chaetoceros* spp., and *Th: Thalassionema nitzschioides* var. *nitzschioides*) and marine-brackish (*Cl: Cyclotella litoralis*) diatom taxa. (B) Concentration of freshwater diatom species *Aulacoseira* spp. (in valves per gram dry sediment) at ODP Site 1077.

hypothesize that this change is the result of a freshening of the ambient water masses. To test this hypothesis we now turn to the oxygen isotope record of Site 1077.

Oxygen isotope records

The oxygen isotopic composition recorded in the tests of planktonic foraminifers is determined mainly by the temperature and isotopic composition of the water mass in which they calcified (e.g. Emiliani, 1954); thus, $\delta^{18}O$ values of their carbonate tests are useful tools for reconstructing hydrological conditions of the upper water column. The $\delta^{18}O$ value of oceanic waters is mainly related to (1) global ice volume and (2) salinity. Marine waters diluted by freshwater are isotopically more negative since continental rainwater is relatively poor in ^{18}O.

One approach to estimate the effect of isotopically lighter waters discharged into the ocean by the Congo River is to compare the $\delta^{18}O$ record of our study site with the one from a nearby location which is free of any freshwater influence (Fig. 4). For this purpose we selected core GeoB1041 located at 3°48'S and 7°05'W (Fig. 1). The oxygen isotope curve of GeoB 1041 is also based on the planktonic foraminifer *G. ruber* pink (Meinecke, 1992)

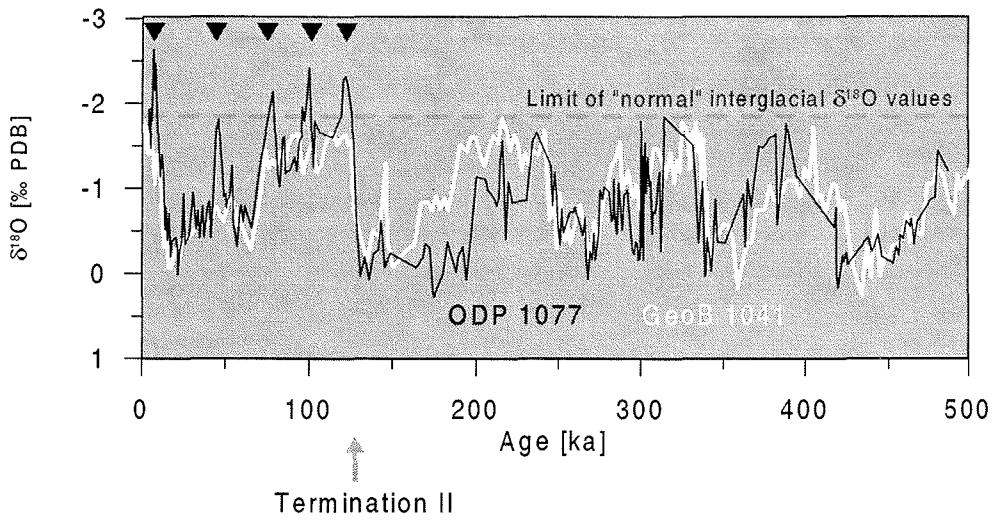

Fig. 4: $\delta^{18}O$ data of the planktic foraminifer *G. ruber* (pink) vs. age at ODP Site 1077 (black line, this study) and in core GeoB1041 (white line, Meinecke et al., 1992). Black triangles denote times of lightening effect at ODP Site 1077.

The two $\delta^{18}O$ curves shown in Fig. 4 vary within nearly identical glacial and interglacial limits in the older part of the record; small deviations may be related to local effects or stratigraphic discrepancies. This similarity vanishes after Termination II when Site 1077 systematically shows much lighter values during warm phases. Marked peaks in substages 5.5, 5.3, 5.1 and Stage 1 are up to 0.6‰ lighter than the "normal" interglacial limit (Fig. 4). The latter is even reached during stage 3. Glacial values of both records are similar (Fig. 4), and differences in the isotopic signal of surface sediments from these two areas are inconspicuous (Mulitza, 1994).

The lightening effect of enhanced local freshwater input on the $\delta^{18}O$ signal of certain foraminifer species has been reported previously from this and other areas. In the Congo fan region, negative deviations in $\delta^{18}O$ records of *G. ruber* pink were described in cores GeoB 1007 (6°S, 10°E) and GeoB1008 (6°S, 10°E) during Stage 1 (Schneider, 1991; Mulitza and Rühlemann, 2000), and at Termination II in GeoB 1008 (Schneider, 1991). For GeoB 1007, Mulitza and Rühlemann (2000) constructed an alkenone-derived SST record and concluded that the observed negative deviations were not caused by an increase in temperature but were due to regionally lower $\delta^{18}O$ of surface waters. Pastouret et al. (1978) showed a strong depletion in oxygen isotopes ratios of *G. ruber* pink in the Niger fan, where $\delta^{18}O$ values as low as nearly -3‰ were attributed to an increase in freshwater discharge and high precipitation over the drainage area between 13-11.8 ka and 11.5-4.5 ka. Showers and Bevis (1988) used the isotopic record of *Globigerinoides sacculifer* from the Amazon fan and reported a negative deviation from the "global" $\delta^{18}O$ signal during MIS Stage 1. They interpreted this as an enhanced deglacial discharge of the Amazon River at the end of the Younger Dryas.

To test for freshwater and temperature effects on the observed differences between Site 1077 and GeoB 1041 (Fig. 4), we evaluated in which way temperature and salinity control the present-day oxygen isotope ratio in the working area. Monthly equilibrium $\delta^{18}O_{calcite}$ values were calculated for an east-west transect along 5°S (10°W to 12°E) including the two core locations (Table 1; Fig. 5). Calculations were based on temperature and salinity data from Conkright et al. (1998) and the Epstein et al. (1953) equation, and on the salinity relationship for the eastern equatorial Atlantic of Fairbanks et al. (1992). At the location of Site 1077 the timing of maxima as well as minima of SST, salinity and resulting $\delta^{18}O_{calcite}$ differs by no more than one month (Table 1).

Profiles of SST, salinity and equilibrium $\delta^{18}O_{calcite}$ for the two most contrasting months are shown in Fig. 5. East-west differences in temperature within a given month are rather small and vary by maximal 1.4°C (Fig. 5A). Salinity variations, on the other hand, are conspicuous, especially in austral summer (February) when an east-west gradient of about 5‰ is observed (Fig. 5B). At this time, $\delta^{18}O_{calcite}$ values are shifted toward lighter values close to the African coast (Fig. 5C). They are the result of enhanced freshwater input from the Congo River which in turn is related to a maximum in summer precipitation on land (compare Table 1 and Fig. 2). East-west differences in $\delta^{18}O_{calcite}$ are small during austral winter (July). If we now assume a constant salinity of open ocean waters of 35‰ (Brown et al., 1995) (dotted line in Fig. 5C), and re-calculate $\delta^{18}O_{calcite}$, we see that the freshwater effect on the isotopic signal is by far more important for the deviations seen in $\delta^{18}O_{calcite}$ between both sites. It accounts for a difference of about 0.50‰ in February and 0.24‰ in July (Fig. 5C).

$\Delta\delta^{18}O$ record and freshwater input

It hence seems obvious that the observed lighter values in the foraminiferal oxygen isotope record of Site 1077 are a consequence of freshwater discharge pulses of the Congo River. However, we need to consider the possibility that they may be related to much stronger temperature contrasts than the seasonal SST gradients found today. To test this, we calculated an equilibrium $\delta^{18}O_{calcite}$ record for the last 200,000 years (Fig. 6) following the same procedure as the one used for the monthly equilibrium $\delta^{18}O_{calcite}$ calculations discussed above. We based these calculations on alkenone-derived SST data of Schneider et al. (1995) generated for nearby core GeoB1008 (Fig. 1), and on the annual average salinity from Conkright et al. (1998) for our site (Table 1). A global ice effect was subsequently added using the SPECMAP Stack (Imbrie et al., 1984).

Month	SST (°C)	Salinity (PSU)	eq. $\delta^{18}O$ calcite	eq. $\delta^{18}O$ ((S= 35
1	28.01	31.63	-2.03	-1.7
2	**28.42**	**28.80**	**-2.33**	-1.8
3	28.82	29.84	-2.33	-1.9
4	27.71	30.56	-2.05	-1.7
5	26.48	31.65	-1.72	-1.4
6	23.37	33.40	-0.93	-0.8
7	**22.22**	**32.02**	**-0.80**	-0.5
8	22.55	33.43	-0.75	-0.6
9	22.63	33.47	-0.77	-0.6
10	25.14	32.43	-1.38	-1.1
11	26.05	32.07	-1.60	-1.3
12	26.26	29.59	-1.84	-1.4
Average	25.64	31.57	-1.54	-1.2

Table 1: Monthly averages in sea surface temperature (SST) and salinity (in PSU) at 5°S, 10.5°E taken from the Levitus Atlas (Conkright et al., 1998), equilibrium $\delta^{18}O_{calcite}$, and equilibrium $\delta^{18}O_{calcite}$ calculated with constant salinity values. Values are based on the Epstein et al.'s (1953) equation.

With these settings, the "constant-salinity" $\delta^{18}O$ reconstruction for the Congo fan area merely reaches lightest values of the open ocean reference record GeoB 1041 during warm substages 5.5, 5.3, 5.1 and Stage 1 (Fig. 6). Although increased SSTs may account for lighter $\delta^{18}O$ values during these warmer periods, they do not explain the extremely light values documented in the sediments of Site 1077. Thus, we now return to

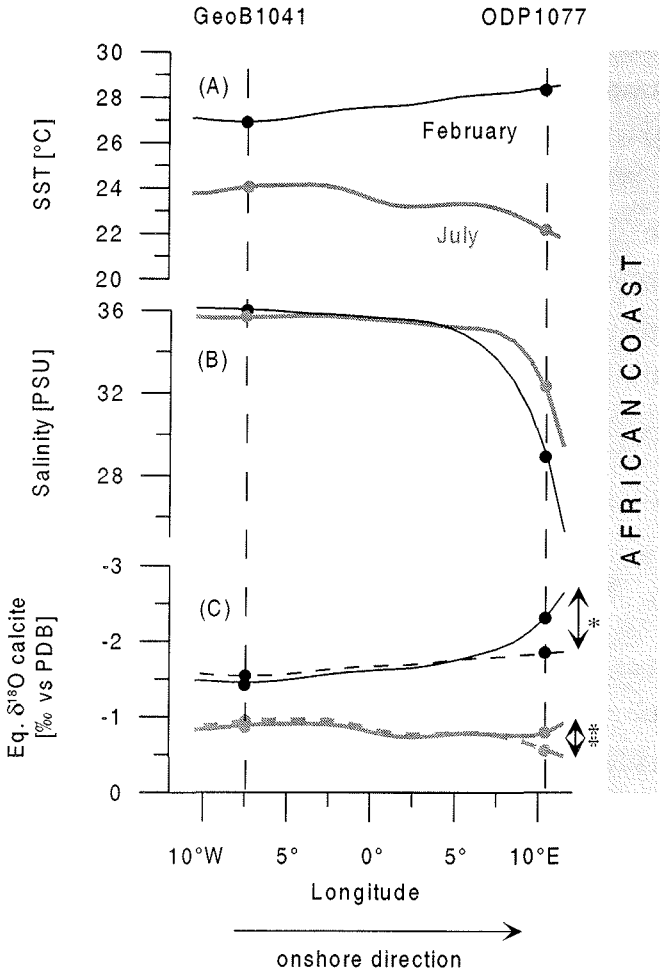

Fig. 5: Monthly averages in A) sea surface temperature (SST), and B) salinity for February (black thin line) and July (gray thick line) in a transect along 5°S between 12°W and 12°E (monthly averages since 01 January 1960 from Levitus Atlas; Conkright et al., 1998). C) Equilibrium $\delta^{18}O_{calcite}$ values calculated for February and July (continuous line) and annual mean salinity (dotted line) using the equations of Epstein et al. (1953) and Fairbanks et al. (1992). Approximate position of core GeoB 1041 and ODP Site 1077 are marked for reference. Difference between both equilibrium $\delta^{18}O_{calcite}$ calculated with monthly and annual mean salinity in February (*, 0.50‰), and July (**, 0.24‰).

our initial hypothesis and confirm that the observed differences between Site 1077 and GeoB 1041 are caused by enhanced freshwater influence over Site 1077. The timing of these freshwater pulses can be extracted by computing the difference between the isotopic records of both sites ($\Delta\delta^{18}O$ in Fig. 7). For building the $\Delta\delta^{18}O$ curve, both records were previously interpolated into intervals of 1 ka. When we compare the $\Delta\delta^{18}O$ record with summer insolation at 10°N it is obvious that almost all pulses (with the exception of the negative peak in stage 3.2) are linked to maxima in Northern Hemisphere insolation (Fig. 7). This suggests that they may be coupled with increased freshwater discharge from the Congo River due to enhanced precipitation in the hinterland.

A long-term trend is also obvious in the $\Delta\delta^{18}O$ record; it shows an abrupt shift toward sustained negative values since Termination II. Why do we not find such fresh pulses prior to Termination II? The Congo River has existed since the Pliocene and no substantial changes in the catchment area have been reported for at least the Late Quaternary (Beadle, 1974). Pollen records from marine and terrestrial sites of equatorial Africa indicate more or less similar glacial and interglacial vegetation conditions over the last 150,000 years (Dupont et al., 2000).

Do latitudinal shifts of the Angola Benguela Front affect the location of the Congo River plume?

We suggest that the changes observed at Site 1077 since Termination II may not be directly linked to environmental conditions on land but rather may be related to rearrangements of the oceanographic setting. Site 1077 is located at the northern rim of the Congo River plume, an area characterized by steep nutrient and salinity gradients (van Benekom and Berger, 1984). Thus, slight movements of the river plume would result in significant changes of plume water supply to the study site. We were interested in knowing whether latitudinal shifts of the Angola-Benguela Front (ABF) could have influenced the geographical location of the Congo River plume. Present-day seasonal changes in the direction of the river plume

closely follow ABF movements with time lags of four to eight weeks (see "Regional Setting").

Jansen et al. (1996) reconstructed the late Quaternary history of the ABF based on assemblages of foraminifers, and stated that the ABF underwent several large latitudinal shifts during the past 200,000 years. These shifts were linked to movements of the Subtropical and Polar Fronts with northward migrations resulting in increased advection of relatively cold BC waters. The model of Jansen et al. (1996) is reproduced in Fig. 7 and clearly shows an overall trend to more sustained northerly positions since Termination II. We could speculate that northward shifts of the ABF would move the river plume further north and thus closer to our site. This would then result in enhanced advection of river plume waters over Site 1077 (especially since Termination II), independently of any local precipitation/freshwater load discussed above.

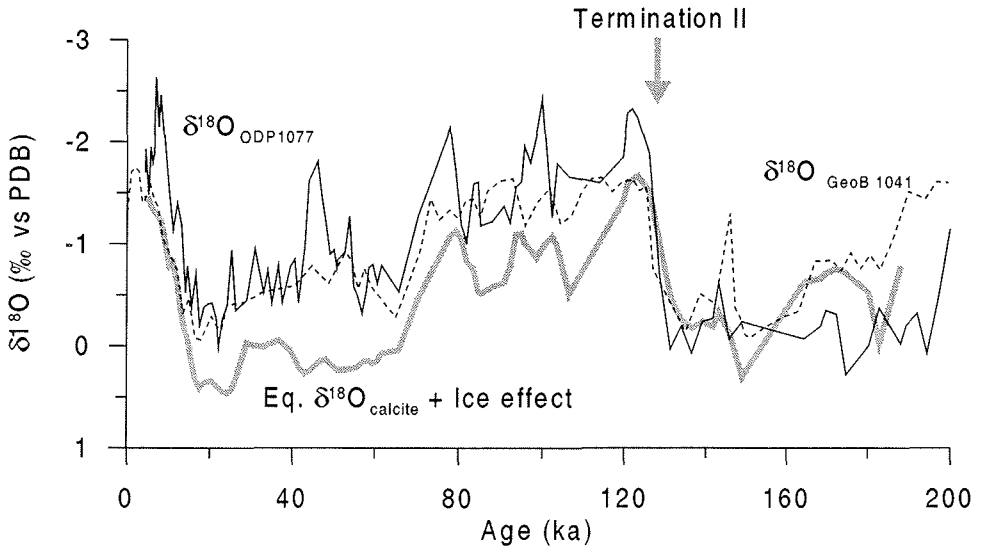

Fig. 6: Comparison between $\delta^{18}O$ of ODP Site 1077 (black thin line), equilibrium $\delta^{18}O_{calcite}$ calculated using the equation of Epstein et al. (1953) and corrected for the global ice effect using the SPECMAP Stack (Imbrie et al., 1984) (grey thick line), and $\delta^{18}O$ of GeoB 1041 (dotted line).

In Figure 7 three proxies for freshwater influence at Site 1077 are compared to Northern Hemisphere summer insolation and the ABF reconstruction of Jansen et al. (1996). In general terms, the freshening of the system since Termination II implied from the diatom signal (percent of brackish *C. litoralis* and abundance of freshwater *Aulacoseira* species) and from the $\Delta\delta^{18}O$ signal coincides with a trend of equatorward migration of the ABF.

Support for this hypothesis also comes from seismic investigations of Neogene sediments of the Congo Fan. Based on a set of high-resolution seismic lines, Uenzelmann-Neben (1998) built a model for the evolution of Neogene and Quaternary sedimentation in this area. She found that since the early Quaternary the Congo River has been the prevailing sediment source. A marked modification in the sediment composition was documented by a prominent reflector near Stage 6 (Uenzelmann-Neben, op. cit.). As a consequence, the Congo Canyon has guided the material from the Congo River farther to the west onto the lower fan. Sediments as well as freshwater from the river have since been deflected northward by the BCC.

Peak-to-peak correlation of our "freshening parameters" (Fig. 7), on the other hand, points to both local and regional effects acting together implying a rather complex interaction of mechanisms. For example, we discussed above that higher percentages of *C. litoralis* correspond with colder periods within Stages 5 and 3 (Fig. 3A). A more detailed look, however, reveals that this species becomes more abundant during periods of increasing or maximal insolation at 10°N (Fig. 7). These times are characterized by

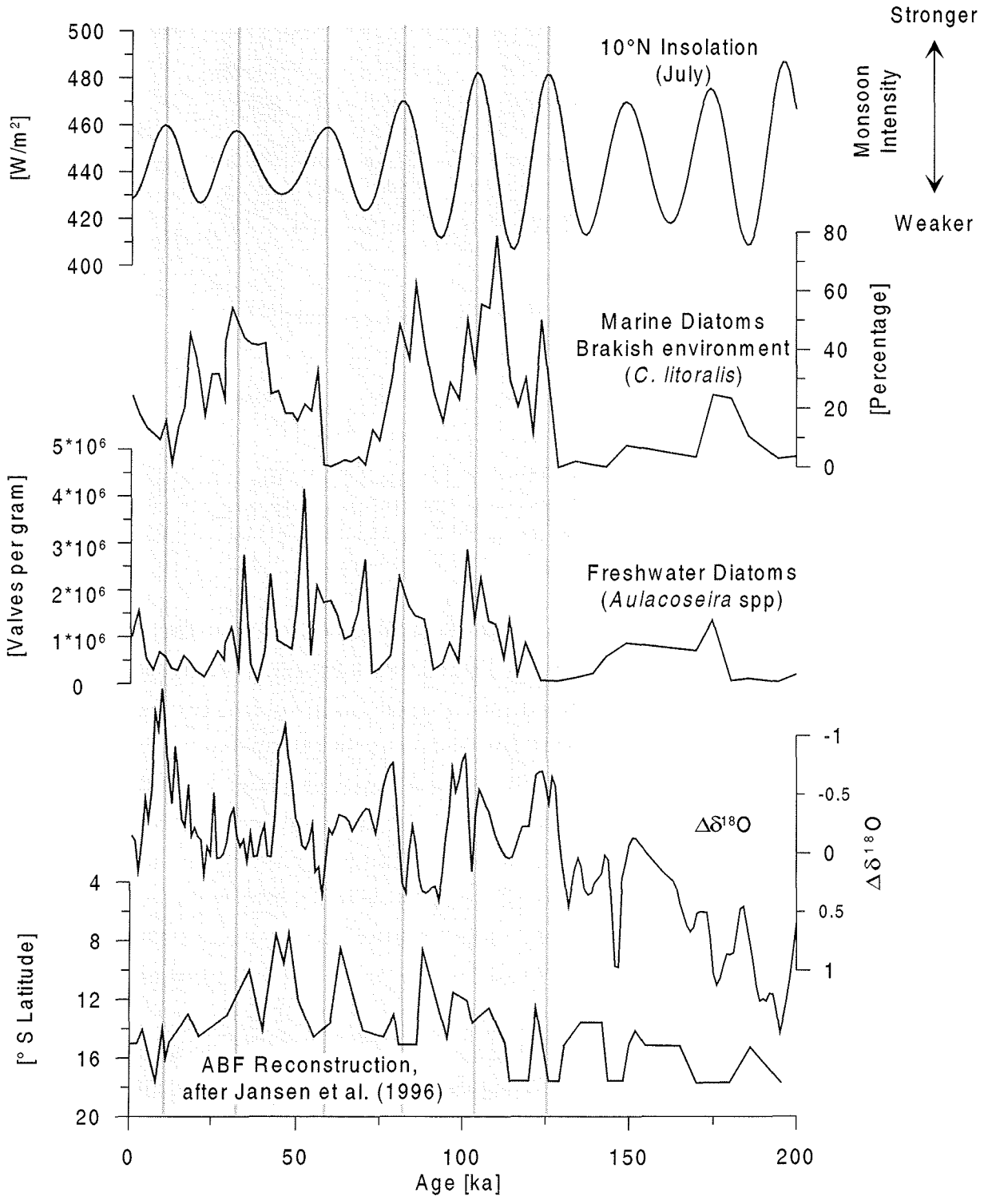

Fig. 7: Comparison between $\Delta\delta^{18}O$ (black line) and of summer insolation (July) at 10°N (white line) (data from Berger and Loutre, 1991), percentage of the marine-brackish diatom species *C. litoralis*, and concentration of freshwater diatoms at ODP Site 1077, and reconstruction of the average position of the Angola-Benguela Front (ABF; modified from Jansen et al., 1996). Vertical gray lines denote maxima in insolation.

increased monsoon intensity and decreased southeast trade winds in the equatorial Atlantic (McIntyre et al., 1989). A more intense monsoon over Central Africa drives enhanced precipitation in the hinterland and hence causes stronger freshwater discharge (Schneider et al., 1997; Gingele, et al., 1998). Fluctuations of *C. litoralis* follow the pattern of summer insolation with higher amplitudes during stage 5 and less promi-

nent cycles since Stage 4. However, enhanced abundances of *C. litoralis* near 5.4 and 5.2 do not exactly coincide with times of maximal monsoons, they occur somewhat earlier. We interpret this out-of-phase relation as follows: It is well known that enhanced upwelling during times of stronger trade winds generally intensifies marine paleoproductivity in the Congo Fan area during cold stages or colder interglacial substages (Schneider et al., 1994). Thus, times of enhanced nutrient concentrations in surface waters followed by strong freshwater inputs seem to provide optimal conditions for *C. litoralis* growth.

Also the freshwater diatom signal does not always correlate with maxima in Northern Hemisphere summer insolation, as would be expected. This may be explained by the fact that planktonic freshwater diatoms are produced exclusively in continental waters. A key limiting factor for their growth and abundance is the availability of nutrients (especially silicate, Round et al., 1990). Thus, a large river discharge does not necessarily imply high productivity of the freshwater community.

In summary, the variations in oxygen isotopes, marine and freshwater diatoms observed at Site 1077 give evidence that although Congo River discharge may have fluctuated following glacial-interglacial cycles, the abrupt change at Termination II does not seem to be directly related to climatic processes (i.e. insolation forcing). Rather, a major reorganization in the depositional environment of the Congo River fan must have taken place.

Conclusions

Marine and freshwater diatoms, and the $\delta^{18}O$ record of planktic foraminifer *G. ruber* pink from the Congo fan area (ODP Site 1077; 5°10'S, 10°26'E) were used to reconstruct Late Quaternary fluctuations in the intensity of Congo River freshwater load. Our findings are:

1) An abrupt change in the diatom assemblage is evident at Termination II. Since that time, the relative abundance of *C. litoralis* (a marine diatom tolerant of lowered salinity) and the concentration of freshwater diatoms (genus *Aulacoseira*) increased dramatically, suggesting a change in environmental conditions from predominantly marine to mixed marine/brackish/fresh.
2) Comparison of the oxygen isotope record of *G. ruber* from Site 1077 with another record from a pelagic area in the equatorial Atlantic (GeoB 1041), revealed persistent deviations of the "global" $\delta^{18}O$ signal since Termination II (during warm Stages 5.5, 5.3, 5.1, 3 and 1) at the Congo site.
3) An artificial $\delta^{18}O$ (equilibrium $\delta^{18}O_{calcite}$) curve was constructed to estimate salinity and temperature effects on the observed differences between Site 1077 and GeoB 1041, for present times and for the past 200,000 years. This showed that freshwater inputs have caused negative deviations in the $\delta^{18}O$ signal at the Congo site.
4) Using the oxygen isotope difference between both locations ($\Delta\delta^{18}O$) as a proxy for freshwater input, a general trend in the $\Delta\delta^{18}O$ record was observed, with sustained negative values since Termination II.
5) Significant negative pulses in $\Delta\delta^{18}O$ during Northern Hemisphere summer insolation maxima are attributed to increased Congo River freshwater discharge due to enhanced precipitation on land.

6) We suggest that the apparent change to a less saline environment at Site 1077 since Termination II is a consequence of a sustained equatorward displacement of the Angola-Benguela Front. This migration was responsible for a northward deflection of the Congo River plume moving plume waters further north than normal and over Site 1077.

Acknowledgments

We would like to acknowledge fruitful discussions with Frank Schmieder and Helge Arz during the preparation and earlier versions of this manuscript. We are grateful to Stefan Mulitza and Wolfgang Berger for their constructive criticisms and comments that helped improve the first draft. This research was funded by the Deutsche Forschungsgemeinschaft (Sonderforschungsbereich 261 at the Bremen University).

References

Baker, C.B., Eischeid, J.K., Karl, T.R., Diaz, H.F., 1994. The quality control of long-term climatological data using objective data analysis. Preprints of AMS Ninth Conference on Applied Climatology, Dallas, TX., January, 15-20.

Barret, E.C., 1974. Part V: Satellite data analyses in regional climatology. In: Barret, E.C. (ed.), Climatology from satellites. Methuen & Co Ltd, London, 221-260.

Beadle, L.C., 1974. Chapter 9: the great rivers of Africa. In: Beadle, L.C. (ed.), The inland waters of tropical Africa: an introduction to tropical limnology. Longman, London, 346 pp.

Berger, A., and Loutre, M.F., 1991. Insolation values for the climate of the last 10 million years. *Quaternary Sci. Rev.*, 10: 297-317.

Berger, W. H., Smetacek, V. S., Wefer, G., 1989. Ocean productivity and paleoproductivity -an overview. In: Berger, W. H., Smetacek, V.S., and Wefer, G. (eds.), Productivity of the oceans: present and past. John Willey & Sons, New York, pp 1-34.

Brown E., Colling, A., Park, D., Phillips, J., Rothery, D., Wright, J., 1995. Chapter 3: Salinity in the oceans. In: Bearman, G. (ed.), Seawater: its composition, properties and behaviour. Ocean circulation. Oxford. Pergamon Press, pp 30-37.

Cadée, G. C., 1978. Primary production and Chlorophyll in the Zaire River, estuary and plume. Neth. J. Sea Res. 12(3/4), 368-381.

Cadée, G. C., 1984. Particulate and dissolved organic carbon and Chlorophyll a in the Zaire River, estuary and plume. Neth. J. Sea Res. 17(2-4), 426-440.

Conkright, M., Levitus, S., O'Brien, T., Boyer, T., Antonov, J. and Stephens, C., 1998. World Ocean Atlas. Available online and on CD-ROM Data Set Documentation.. Tech. Rep. 15, NODC Internal Report, Silver Spring, MD, 16pp.

Dupont, L.M., Jahns, S., Marret, F., Ning, S., 2000. Vegetation change in equatorial West Africa: time-slices for the last 150 ka. Palaeogeogr., Palaeoclimatol., Palaeoecol. 155, 95-122.

Eisma, D. and van Bennekom, A. J., 1978. The Zaire river and estuary and the Zaire outflow in the Atlantic Ocean. Neth. J. Sea Res. 12(3/4), 255-272.

Emiliani, C., 1954. Depth habitat of some species of pelagic foraminifera as indicated by oxygen isotopic ratio. Amer. Jour. of Sci. 252, 149-158.

Epstein, S., Buchsbaum, R., Lowenstam, H.A., Urey, H.C., 1953. Revised carbonate-water isotopic temperature scale. Bull. Geol. Soc. Amer. 64, 1315-1325.

Fairbanks, R.G., Charles, C.D., Wright, J.D., 1992. Origin of global meltwater pulses. In: Taylor, R.E., Long, A., Kra, R. (eds.), Radiocarbon after four decades; an interdisciplinary perspective. Springer-Verlag, New York, pp. 473-500.

Gasse, F., 2000. Hydrological changes in the African tropics since the Last Glacial Maximum. Quater. Sci. Rev. 19, 189-211.

Gingele, F. X., Müller, P. M., Schneider, R.R., 1998. Orbital forcing of freshwater input in the Zaire Fan area-clay mineral evidence from the last 200 kyr. Palaeogeogr., Palaeoclimatol., Palaeoecol. 138, 17-26.

Imbrie, J., Hays, J.D., Martinson, D.G., McIntyre, A., Mix, A.C., Morley, J.J, Pisias, N.G., FPrell, W.L., Shackleton., N.J., 1984. The orbital theory of Pleistocene climate: support from a revised chronology of the marine d^{18}O record. In: Berger, A., Imbrie, J., Hays, J., Kukla, G., Saltzman, B. (eds.), Milankovitch and climate. D. Reidel Publishing Company, Palisades, NY, pp. 269-305.

Jansen, J. H. F., Ufkes, E., Schneider, R.R., 1996. Late Quaternary Movements of the Angola-Benguela front, SE Atlantic, and implications for advection in the Equatorial Ocean. In: Wefer, G., Berger, W.H., Siedler, G., Webb, D.J. (eds.), The South Atlantic: Present and past circulation. Springer-Verlag, Berlin, Heidelberg, pp. 553-575.

Jansen, J. H. F., van Iperen, J. M., 1991. A 220,000-year climatic record for the East Equatorial Atlantic Ocean and Equatorial Africa: evidence from diatoms and opal phytolits in the Zaire (Congo) deep-sea fan. Paleoceanography 6(5), 573-591.

Jansen, J. H. F., van Weering, T. C. E., Gieles, R., van Iperen, J., 1984. Middle and Late Quaternary oceanography and climatology of the Zaire-Congo fan and adjacent eastern Angola Basin. Neth. J. Sea Res. 17, 201-249.

Laskar, J., 1990. The chaotic motion of the solar system: A numerical estimate of the chaotic zones. Icarus, 88: 266-291.

McIntyre, A., Ruddiman, W.F., Karlin, K., Mix, A.C., 1989. Surface waters response of the Equatorial Atlantic Ocean to orbital forcing. Paleoceanography 4, 19-55.

Meeuwis, J. M., Lutjeharms, J. R. E., 1990. Surface thermal characteristics of the Angola-Benguela Front. S. Afr. J. Mar. Sci. 9, 261-279.

Meinecke, G., 1992. Spätquartäre oberflächenwassertemperaturen im Östlichen Äquatorialen Atlantik. Bericht aus dem Fachbereich Geowissenschaften. Ph.D. Thesis, Universität Bremen, Germany.

Mikkelsen, N., 1984. Diatoms in the Zaire deep-sea fan and Pleistocene palaeoclimatic trends in the Angola Basin and west equatorial Africa. Neth. J. Sea Res. 14(2-4), 280-292.

Mulitza, S., 1994. Spätquartäre variationen der oberflächennahen Hydrographie im westlichen äquatorialen Atlantik. Bericht aus dem Fachbereich Geowissenschaften. Ph.D. Thesis, Universität Bremen, Germany.

Mulitza, S., Rülehmann, C., 2000. African monsoonal precipitation modulated by interhemispheric temperature gradients. Quater. Res. 53, 270-274.

Müller, P. J., Schneider, R., 1993. An automated leaching mehtod for the determination of opal in sediments and particulate matter. Deep-Sea Res. I 40(3), 425-444.

Pastouret, L., Chamley, H., Delibrias, G. Duplessy, J.C., Thiede, J., 1978. Late Quaternary climatic changes in Western Tropical Africa deduced from deep-sea sedimentation off the Niger delta. Oceanol. Acta 1(2), 217-232.

Pufahl, P. K., Maslin, M. A., Anderson, L., Brüchert, V., Jansen, F., Lin, H., Perez, M., Vidal, L., Shipboard Scientific Party, 1998. Lithostratigraphic summary for Leg 175: Angola-Benguela upwelling system. In: G. Wefer, Berger, W.H., Richter, C., et al. (eds.), Proc. ODP Initial Reports. College Station TX, Ocean Drilling Project. 175, 533-542.

Round , F. E., Crawford, R. M., Mann, D. G., 1990. The Diatoms. Biology & Morphology of the Genera. Cambridge University Press, Cambridge, U.K. 747 pp.

Schneider, R. R., 1991. Spätquartär Produktivitätsänderungen im östlichen Angola-Becken: Reaktion auf Variationen im Passat-Monsun-Windsystem und in der Advektion des Benguela-Küstenstroms. Berichte Fachberreich Geowissenschaften Nr. 21. Ph.D. Thesis, Universität Bremen, Germany.

Schneider, R.R., Müller, P.J., Wefer, G., 1994. Late Quaternary paleoproductivity changes off the Congo deduced from stable carbon isotopes of planktonic foraminifera. Palaeogeogr., Palaeoclim., Palaeoecol. 110, 255-274.

Schneider, R. R., Müller, P. J., Ruhland, G., 1995. Late Quaternary surface circulation in the east equatorial South Atlantic: evidence from alkenone sea surface temperatures. Paleoceanography 10(2), 197-219.

Schneider, R. R., Price, B., Müller, P.J., Kroon, D., Alexander, I., 1997. Monsoon related variations in Zaire (Congo) sediment load and influence of fluvial silicate supply on marine productivity in the east equatorial Atlantic during the last 200,000 years. Paleoceanography 12(3), 463-481.

Shackleton, N. J., Berger, A., Peltier, W.R., 1990. An alternative astronomical calibration of the lower Pleistocene timescale based on ODP Site 677. Trans. of the Royal Soc. of Edinburgh: Earth Sci. 81, 251-261.

Shannon, L.V., Pillar, S.C., 1986. The Benguela Ecosystem Part III. Plankton. Oceanogr. Mar. Biol. Ann. Rev. 24, 65-170.

Shipboard Scientific Party, 1998. Chapter 1: Introduction: background, scientific objectives, and principal results for Leg 175 (Benguela Current and Angola-Benguela upwelling systems). In: G. Wefer, Berger, W.H., Richter, C., et al. (eds.), Proceedings of the Ocean Drilling Program, Initial Reports, 175, College Station, TX (Ocean Drilling Program), 7-25.

Shipboard Scientific Party, 1998. Chapter 5: Site 1077. In: G. Wefer, Berger, W.H., Richter, C., et al. (eds.), Proceedings of the Ocean Drilling Program, Initial Reports, 175, College Station, TX (Ocean Drilling Program), 115-141.

Showers, W. J. and Bevis, M., 1988. Amazon cone isotopic stratigraphy: evidence for the source of the tropical freshwater spike. Palaeogeogr., Palaeoclim., Palaeoecol. 64, 189-199.

Uenzelmann-Neben, G., 1998. Neogene sedimentation history of the Congo Fan. Mar. and Petroleum Geol. 15, 635-650.

Ufkes, E., Jansen, J.H.F., Brummer, G.A., 1998. Living planktonic foraminifera in the eastern South Atlantic during spring: indicators of water masses, upwelling and the Congo (Zaire) River plume. Mar. Micropal. 33, 27-53.

Uliana, E., Lange, C. B., Donner, B., Wefer, G., 2001. Siliceous phytoplankton productivity fluctuations in the Congo Basin over the past 460,000 years: marine vs. riverine influence, ODP Site 1077. In: G. Wefer, W. H. Berger and C. Richter (eds.), Proc. ODP, Sci. Res., 175.

van Bennekom, A. J., Berger, G. W., 1984. Hydrography and silica budget of the Angola Basin. Neth. J. Sea Res. 17(2-4), 149-200.

van der Gaast, S. J., Jansen, J. H. F., 1984. Mineralogy, opal and manganese of Middle and Late Quaternary sediments of the Zaire (Congo) deep-sea fan: origin and climatic variation. Neth. J. Sea Res. 14(2-4), 313-341.

van Iperen, J. M., van Weering, T. C. E., Jansen , J.H.F., van Bennekom, A.J., 1987. Diatoms in surface sediments of the Zaire deep-sea fan (SE Atlantic Ocean) and their relation to overlying water masses. Neth. J. Sea Res. 21(3), 203-217.

Vorosmarty, C.J., Fekete, B.M., Tucker, B.A., 1998. Global River Discharge Database (RivDIS) V. 1.1. Available online [http://www-eosdis.ornl.gov] and on CD-ROM from the ORNL Distributed Active Archive Center, Oak Ridge National Laboratory, Oak Ridge, TN, USA.

7.3

Opal sedimentation at the northern rim of the Congo Fan: A 1 Myr record from ODP Site 1077 (5°S, 10°E)

Uliana, E, Lange, C. B., and Wefer, G.

To be submitted to *Paleoceanography* (June, 2001)

Opal sedimentation at the northern rim of the Congo Fan: A 1 Myr record from ODP Site 1077 (5°S, 10°E)

Uliana, E.*, C. B. Lange§, and G. Wefer*

*Fachbereich Geowissenschaften, Klagenfurter Strasse, Universität Bremen, 28359 Bremen, Germany.
§Scripps Institution of Oceanography, University of California at San Diego, Geosciences Research Division and Marine Life Research Group, La Jolla, CA 92093-0244, U.S.A.

Abstract: We present Late Quaternary (1 Myr) biogenic opal and diatom records from the northern rim of the Congo River Fan (ODP Leg 175, Site 1077). Opal sedimentation in the area reflects surface ocean productivity, with marine microorganisms (especially diatoms) driving the biogenic opal signal. We find that opal has fluctuated in tune with eccentricity variations (100 kyr), with higher values during glacial stages reaching 25 wt % at the LGM. No evidence of forcing in the obliquity band and only a very slight response in the precessional band could be observed. A correlation with ODP Site 677 benthic oxygen isotope data (ice-volume proxy) indicates that the phase lock between opal and orbital eccentricity began at ca. 1 Myr, earlier than the establishment of large ice sheets in the Northern Hemisphere. Comparison of the Congo area with other opal records from the equatorial Atlantic (ODP Site 663) and the subtropical South Atlantic off Namibia (ODP Site 1084) suggests a greater resemblance with the equatorial site for the last 500 kyr. This similarity breaks down in the older part of the record, when opal fluctuations at Site 1077 were synchronized with those from off Namibia.

Keywords: Opal sedimentation, diatoms, Congo Fan, glacial-interglacial cycles, eccentricity periodicity, Late Quaternary.

Introduction

Silicon (Si) is an important component of the marine biogenic matter that accumulates in coastal and abyssal sediments (27% of the lithosphere; Tréguer et al., 1995). Dissolved silica in seawater occurs mostly as silicic acid ($Si(OH)_4$). The $Si(OH)_4$ content in the modern ocean is determined by the balance between geological and biological cycles of silica (Tréguer et al., 1995). It is produced by chemical weathering and enters the upper ocean via two different pathways: fluvial and eolian transport. According to Tréguer et al. (1995) the flux of silica into the ocean through rivers is five times larger than by wind (5.6 ± 0.6 against 0.5 ± 0.5 Tmol Si per year).

The transfer of $Si(OH)_4$ from the marine hydrosphere to the biosphere initiates the biological cycle of Si (see fig. 1 in Tréguer et al., 1995). Marine microorganisms like diatoms, silicoflagellates and radiolarians

build up their skeletons by taking up $Si(OH)_4$ from seawater. Diatoms, in particular, have an absolute requirement for Si (Lewin, 1961), without which frustules are not formed and the cell cycle is not completed (e.g. Brzezinski, 1992). Once $Si(OH)_4$ is incorporated into their shells, and after these organisms die, the fraction of accumulated biogenic silica that escapes dissolution (see Ragueneau et al., 2000, for factors governing the dissolution of biogenic opal formed in surface waters), sinks through the water column as phytoplankton particulate silicon (biogenic Si) or $Si(OH)_4$-rich fecal pellets (e.g. Dugdale et al., 1995; Tréguer et al., 1995), and reaches the seafloor where dissolution continues. According to Tréguer et al. (1995), 90% of the dissolution occurs in the euphotic zone (above 1,000 m water depth; e.g. Takahashi, 1986), and 10% in the seabed.

Paleoproductivity studies often interpret the formation of opal-rich sediment as evidence of high diatom productivity. Indeed, opal sediment formation is clearly associated with high primary productivity in coastal areas at both high and low latitudes (e.g. Lyle et al., 1988; Herbert et al., 1989; Mortlock et al., 1991; Sancetta, 1995). However, Nelson et al. (1995) have shown that the relationship between opal sediment accumulation and total primary productivity (or diatom productivity) is not simple, and that regional differences in silica preservation dominate over regional productivity differences.

Here we present a 1 m.y. biogenic opal record from the northern rim of the Congo River Fan (ODP Leg 175 Site 1077, Shipboard Scientific Party, 1998), an environment which is dominated by seasonal coastal upwelling and associated filaments and eddies moving offshore, by riverine input from the Congo River, and by incursions of open-ocean waters (Fig. 1). The Congo River is the second most important river in the world in terms of mean annual flow (1300 km^3); its waters are characterized by high contents of dissolved silica (185 mmol L^{-1}) (Giresse et al., 1990). This silica is biologically available and part of it

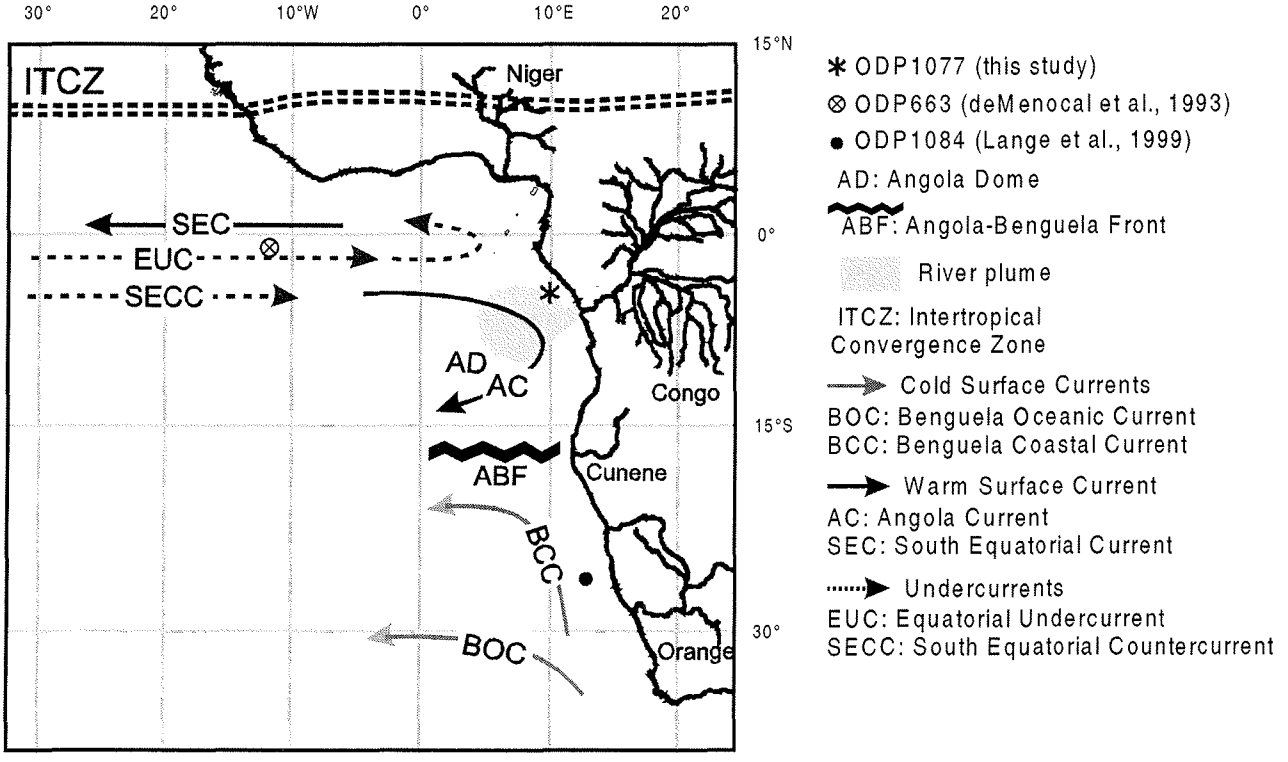

Figure 1: Location of ODP sites, main surface and subsurface currents, and extension of the Congo River plume.

(38 mmol L^{-1}, Giresse et al., 1990) are already utilized within the river by freshwater organisms like diatoms. The siliceous material is then exported to the ocean where a large quantity of it is deposited and buried in the sediments (van der Gaast and Jansen, 1984). The rest is recycled in surface waters and enters the marine biological silica cycle. Marine silica production in the area profits from an additional silicate supply due to intensified dissolution in salty waters (Barker et al., 1994). The dissolution rate of diatoms increases by a factor of 4 from freshwater to average oceanic salinities (Hurd, 1983).

Although skeletal remains of both freshwater and marine siliceous organisms do contribute to the biogenic opal sedimentation in the Congo Fan area, Uliana et al. (2001) have shown that opal sedimentation at Site 1077 is strongly dominated by marine organisms. Their abundance is by two orders of magnitude greater than the one of freshwater organisms. Even if we follow Conley et al. (1990) and consider that freshwater planktonic diatoms contain up to one order of magnitude more silica in their frustules than their marine counterparts, the marine opal contribution in the Congo Fan area would be at least 10 times higher than the continental one.

Modern Marine Productivity

Marine productivity in the Congo Fan area is under the influence of coastal upwelling, incursions of South Equatorial Counter Current waters, and the presence of the Angola Dome (Voituriez, 1981; Hay and Brock, 1992). The latter is a perennial feature located at 10°S which influence can be detected in the underlying sediments as an enrichment of amorphous silica (Gorshkov, 1977). Superimposed on this scenario, is the influence of the Congo River supplying large amounts of terrigenous material to the ocean (including $Si(OH)_4$).

Satellite pictures show high values in chlorophyll all along the year, while oceanic surface waters data from Conkright et al. (1998) indicate that a maximum in chlorophyll takes place at the Site 1077 location during August, when high nutrients and low sea surface temperatures (SST) are observed. It is during boreal summer (August) when the Inter-tropical Convergence Zone (ITCZ) reaches its northernmost position, and the intensity of the southeast Trade winds increases, and produces strengthening of the upwelling along the southwest coast of Africa (Philander and Pacanowski, 1986). Atmospheric circulation reverses during boreal winter (February-March), the ITCZ moves to its southward position and the wind system is relaxed, then a minimum in productivity is observed.

Regional Paleoclimatology

In the equatorial Atlantic, surface waters are directly controlled by Trade wind intensity. Trade winds in turn are a function of the seasonal interaction between the low-latitude oceanic cyclones, the continental anticyclones, and the monsoonal cyclones over Africa (Prell and Kutzbach, 1987; McIntyre et al., 1989). On a geological timescale strong monsoonal winds and enhanced precipitation over the African continent are induced by maximal Northern Hemisphere insolation when boreal summer coincides with minima in the Earth-sun distance (Pokras and Mix, 1985; deMenocal et al., 1993). This setting leads to a decrease in the strength of zonal Trade winds along the eastern tropical Atlantic and consequently reduces upwelling

intensity (McIntyre et al., 1989, deMenocal et al., 1993). On the other hand, when boreal summers coincide with maximal Earth-sun distance, solar insolation over North and Central Africa and hence African monsoon intensity is reduced. The responsible orbital mechanism behind this insolation-driven scenery is precession of the Earth's rotational axis with periodicities of 19 and 23 kyr (Berger, 1978; and Berger and Loutre, 1992). Consequently, monsoon related paleoclimate proxies in low latitudes generally vary at precessional periodicities (Rossignol-Strick, 1983; Pokras and Mix, 1985; Pokras, 1987; deMenocal et al., 1993; Schneider et al., 1997). In particular, these cycles have been recognized in sediments from the Congo river mouth for the last 200,000 years by terrigenous input elements (Schneider et al., 1997) as well as clay minerals (Gingele et al., 1998). The 23-kyr signal recorded in these parameters is considered to be a proxy of weathering of the central African hinterland and subsequent fluctuations in the composition of the Congo River sediment load. This assumption implies that fluvial input and hence the availability of dissolved silicate in the Fan area follows the monsoonal regime. However, productivity of opaline microorganisms strongly depends on changes in the supply of other nutrients as well. In the Congo Fan area productivity is mainly driven by two different mechanisms, coastal and river induced upwelling. Coastal upwelling results from shallowing of the thermocline and nutricline due to stronger Trades linked to precessional variations and probably, episodically, from northward advection of cold nutrient-rich Benguela Current waters (Schneider et. al, 1997). Hydrographic studies carried out in the area by the Netherlands Institute for Sea Research (van Bennekom and Berger, 1984; Cadée 1978, 1984; van der Gaast and Jansen, 1984) have shown that river-induced upwelling strongly influences the annual variability of present day marine productivity. This mechanism could also be assumed to have affected marine productivity on geological timescales.

Here we examine fluctuations in opal concentration from the Congo Fan area in relation to orbital forcing and global climate change during the past one million year. It is intriguing that in some areas of the world opal preservation tends to emphasize different Milankovitch frequencies than does calcite preservation (e.g. Eastern Tropical Pacific: Lyle et al., 1988; Central Equatorial Pacific: Rea et al., 1991),

Material and Methods

Site 1077 is located at the northern rim of the Congo River Fan (5°10'S, 10°26'E; 2,394 m water depth). This site together with Sites 1075 and 1076, form a depth transect in the eastern Angola Basin (Shipboard Scientific Party, 1998). Of the three sites, Site 1077 is the closest to the Congo River mouth. Previous results have shown that calcium carbonate is a minor component of the sediments (average: 3.1 %, Shipboard Scientific Party, 1998, "Site 1077"), total organic carbon content (TOC) is rather high (average: 2.3 %, Shipboard Scientific Party, 1998, "Site 1077"), and that variations of TOC are mainly a result of changes in marine organic carbon, thus reflecting elevated primary production in the area (Schneider et al., 1997).

Samples (n = 240) were taken at an average resolution of 4,000 years and analyzed for biogenic opal. Biogenic opal mainly reflects the abundance of diatomaceous silica (Uliana et al., 2001), and was determined using a sequential leaching technique (DeMaster, 1981) modified by Müller and Schneider (1993). Opal content from the samples was extracted with 1 M NaOH at 85°C during one hour. Concen-

tration of silica was simultaneously measured by continuous flow analysis with molibdate-blue spectrophotometry. This method has a precision of ± 0.5 % (Müller and Schneider, 1993). We neglected the problem of the method not being able to discriminate between biogenic opal and volcanic glass, because no volcanic ash layers have been reported in earlier extensive sedimentological investigations (e.g. Jansen et al, 1984, van der Gaast and Jansen, 1984). Data are given as weight percentages (wt %) of biogenic silica. Since accumulation records are highly dependent on sedimentation rates and are highly susceptible to artifacts of age modeling, we prefer not to present accumulation rate data. In these fan environments, calculation of accumulation rates of marine biogenic components from fan sediments can lead to erroneous estimates due to rapid fluctuations in terrigenous sediment supply (Schneider et al., 1997). Furthermore, Archer et al. (1993) and Verardo and McIntyre (1994) have presented evidences that opal accumulation rates from tropical sediments are affected by the supply or dissolution of other sediments components and thus may not match other paleoproductivity indicators.

Microscope slides for counting the abundances of siliceous organisms (mainly marine and freshwater diatoms) were prepared following the methods of Schrader and Gersonde (1978) and Lange et al. (1994).

An oxygen isotopic stratigraphy is available for Site 1077, and is based on stable isotope data of the planktic foraminifer *Globigerinoides ruber* (pink). Control points and detailed information about the age model are published in Dupont et al. (2001) and Uliana et al. (2001). The $\delta^{18}O$ record of Site 1077 was correlated to the one of ODP Site 677 (1°N 83°W) (Shackleton et al., 1990).

To inspect for responses of the opal signal to orbital forcing, spectral analyses were performed using the program Spectrum (Schulz and Stattegger, 1997). We used the Lomb-Scargle method (window type: Welch-overlapped-segment averaging, three segments, level of significance = 0.05, lineal detrend, 6 dB Bandwidth = 0.003 kyr^{-1}).

On the basis of the results obtained in the frequency domain and to examine the timing and evolution of the opal response with respect to eccentricity, a bandpass filtering was carried out with the MatLab program version 5.1. The eccentricity-related component was extracted in the frequency band 85-135 kyr for opal, and 90-120 kyr for oxygen isotopes, applying a Butterworth bandpass filter.

A cross-spectral analysis between opal concentration and the eccentricity orbital parameter (Laskar, 1990) was conducted (Welch-overlapped-segment averaging, three segments, level of significance = 0.05, lineal detrend, 6 dB Bandwidth = 0.002 kyr^{-1}). The coherency (κ) estimated is a measure of the degree to which the analyzed signals (opal and eccentricity) are linearly related at a given periodicity. Positive phase values indicate that the opal signal lags eccentricity; conversely, negative values denote opal leading eccentricity.

Results

The opal record of Site 1077 is shown in Figure 2 plotted together with the planktic oxygen isotope record of the site and the benthic oxygen isotope record of ODP Site 677. $\delta^{18}O$ values of *G. ruber* at Site 1077 are related to hydrological conditions of the upper water column (SST and salinity) and global ice volume (Uliana et al., submitted). $\delta^{18}O$ values of Site 677 provide constraints on the evolution of deep-sea temperature and continental ice volume.

High opal contents characterize the Congo Fan area, ranging from 3 % during oxygen isotope stage 5.5 to 25 % during the last glacial maximum (Fig. 2). The record clearly follows ice age cycles with maxima during glacial and minima during interglacial times. A closer look reveals that biogenic opal maxima and minima tend to lead $\delta^{18}O$ by several thousand years (ca. 8 kyr). The variability is largest in the youngest and oldest part of the record, while between ca. 600 and 350 ka it is reduced, as manifested by a relatively low standard deviation of 2.5 % compared to 4.2 % for the whole record. The average opal content during this mid-Pleistocene interval of about 13.6 % is similar to that of the whole record (13.2 %). The reduced variability is essentially expressed in less pronounced minima in warm stage 13 and especially in stage 11, a time when oxygen isotopes imply extremely warm conditions. However, stage 11 is still controversially discussed, because insolation variations during that interval are too small to explain the exceptionally light $\delta^{18}O$ values (Imbrie et al., 1993; Howard, 1997).

A high correspondence between percent opal (Fig. 3), and opal accumulation rates (not shown) implies that changes in percent opal reflect changes in deposition and are not merely the result of variable dilution by other sedimentary components (i.e. at Site 1075: average $CaCO_3$ over 1 Myr. = 2.25 % ; terrigenous organic fraction comprises ca. 30 % of the bulk organic matter; Holtvoeth et al., 2001). High total diatom abundances characterize the sediments of Site 1077 with values ranging between 10^5 and 10^8 valves/g of dry sediment (Fig. 3). Uliana et al. (2001) reported that abundances of other siliceous organisms (e.g. radiolarians, silicoflagellates, phytoliths) never exceeded 10^7 individuals/g of dry sediment, rang-

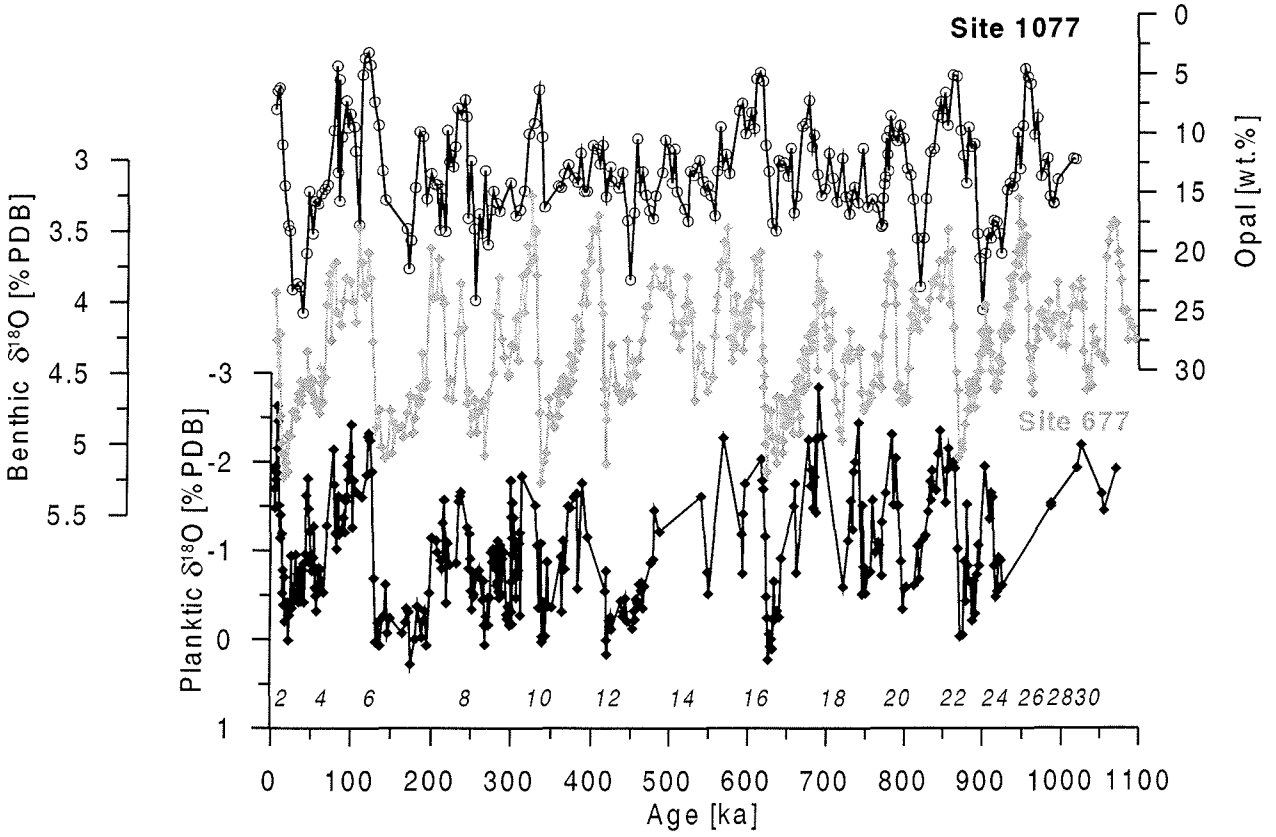

Figure 2: Site 1077 opal record (black line, open circles), oxygen isotope records of Site 1077 based on planktic foraminifer *G. ruber* (pink) (black line, black diamonds), and Site 677 based on benthic foraminifer *Cibicidoides wuellerstorfi* (gray line, gray diamonds) (Shackleton et al., 1990). Note that the scale for opal percent is inverted. Numbers 2, 4, 6, etc. refer to even marine cold oxygen isotopes.

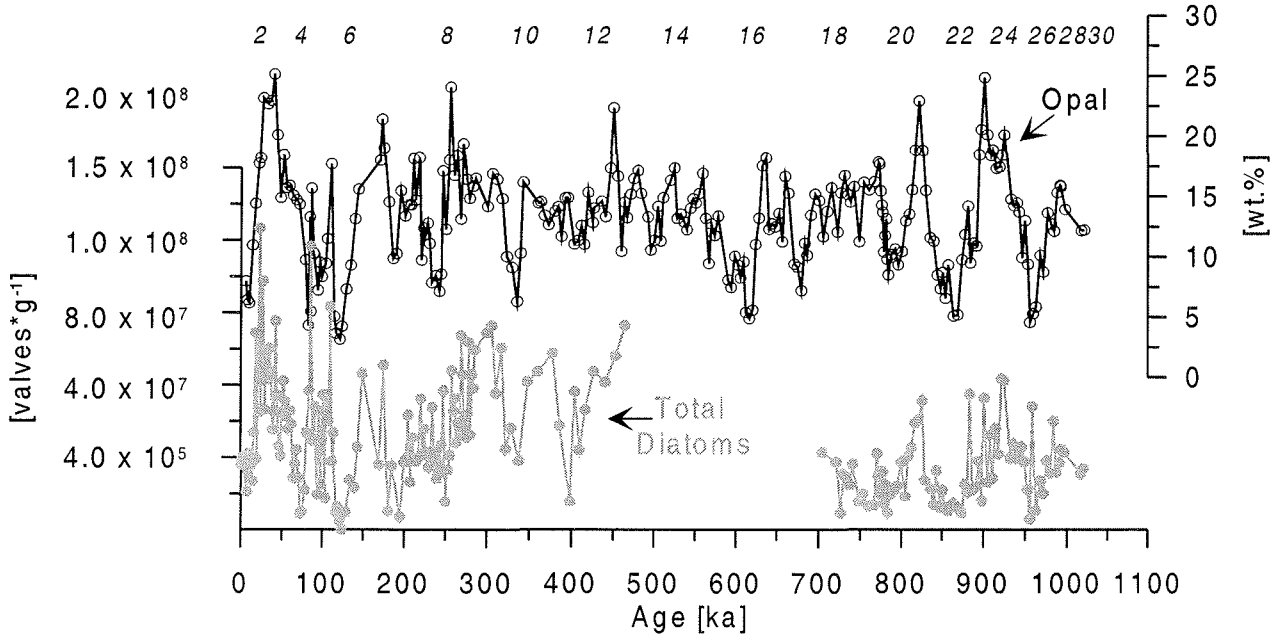

Figure 3: Comparison between opal percent and total diatom concentration at Site 1077. Numbers 2, 4, 6, etc. denote oxygen isotope stages as in Fig. 2.

ing in general 10^4-10^6 individuals/g. Within the diatom signal, marine species (mainly *Thalassionema nitzschioides* var. *nitzschioides* and *Chaetoceros* resting spores) compose >90% of the diatom assemblage.

Spectral analysis over the entire Site 1077 record (1,000 ka; Dt = 4.0 kyr) was performed to investigate for cyclicities that might drive opal variability in the Congo Fan area. Figure 4 compares the power spectrum of Site 1077 opal record (Fig. 4A) with the spectra of the $\delta^{18}O$ curves for Site 1077 (Fig. 4B) and Site 677 (Fig. 4C). The opal record is dominated by variance at the 100 kyr periodicity, with distinct peaks exactly at the eccentricity periods near 95 and 124 kyr (Fig. 4A). These cyclicities represent a quarter of the whole variance (Table 1) indicating that the deposition of biogenic silica in the study area is largely controlled by the 100 kyr ice age cycle, hence by high-latitude variations. Strong power in the eccentricity and obliquity band in both ice volume-related oxygen isotope records indicates high latitude forcing (Figs. 4B, 4C; Table 1). As we do not find a comparably strong obliquity forcing in the opal spectrum we propose that opal sedimentation in the area responds only to extreme contrasting changes of the boundary conditions.

Precessional frequencies near 1/19 and especially 1/23 kyr are more pronounced in the $\delta^{18}O$ record of Site 1077 (4B) than that of Site 677 (4C). They contribute with 13.0 % to the total variance while at Site 677 only 6.7 % of the variance is related to precession (Table 1). Strong low-latitude forcing of $\delta^{18}O$ in the Congo Fan area has been reported by Uliana et al. (subm.), and explained as a result of freshwater pulses initiated by stronger monsoonal precipitation which cyclically enlighten the oxygen isotope values. The opal record (Fig. 4A), on the other hand, shows a mild response in the precession band (8 %, Table 1). It is not as clearly centered at the marked Milankovitch frequencies as in the spectrum of the Site 1077 oxygen isotopes (Figs. 4B), but for these high frequencies this may partly result from uncertainties of the age model. Nevertheless, even if we consider a broader frequency band the response is quite weak for an equatorial region and by far not as strong as in the respective $\delta^{18}O$ record.

Discussion

Variations in opal sedimentation in the Congo Fan area

Earth's climate is known to be driven by orbitally induced variations in the distribution of solar radiation (Milankovitch 1930; Hays et al., 1976). Primarily, regional components of the equatorial climate system like wind intensities directly respond to precessional driven variations which dominate in low latitudes (Berger, 1978). Additionally, and especially during the Pleistocene, the indirect influence of more obliquity-related high latitude variability with a period of 41 kyr (Berger, 1978) and the not yet fully understood 100 kyr cycle (Imbrie et al., 1993) have to be taken into account.

The strong 100 kyr power in the opal record of Site 1077 reflects the overwhelming effects of high-latitude forcing. In this view, opal sensitivity off the Congo seems to be modulated by glacial-interglacial cyclicity which in turn is linked to variations in the North Atlantic SST field. This would suggest that other factors in conjunction with (or in addition to) upwelling intensity may be regulating the deposition of biogenic opal in these sediments. We assume that enhanced opal concentrations in the Congo Fan area during glacial periods must have been the result of increased silica availability in the surface waters. It is known that glacial-interglacial changes in the nutrient content of intermediate waters can affect the nutrient content of the upwelled waters (e.g. Boyle and Keigwin, 1987; Charles et al., 1991; deMenocal et al., 1992; Pollock, 1997) and that intermediate water production was enhanced during glacial stages (deMenocal et al., 1992). If we follow Pollock's ideas and speculate that Antarctic Intermediate Waters could have been the source of advected nutrients during glacials (northward displacement of the silica front) coinciding with enhanced Benguela Current circulation, and increased vertical mixing which in turn was induced by the strengthening of the Trade winds (e.g. Sarnthein et al., 1987; Schneider et al., 1995; Jansen et al., 1996).

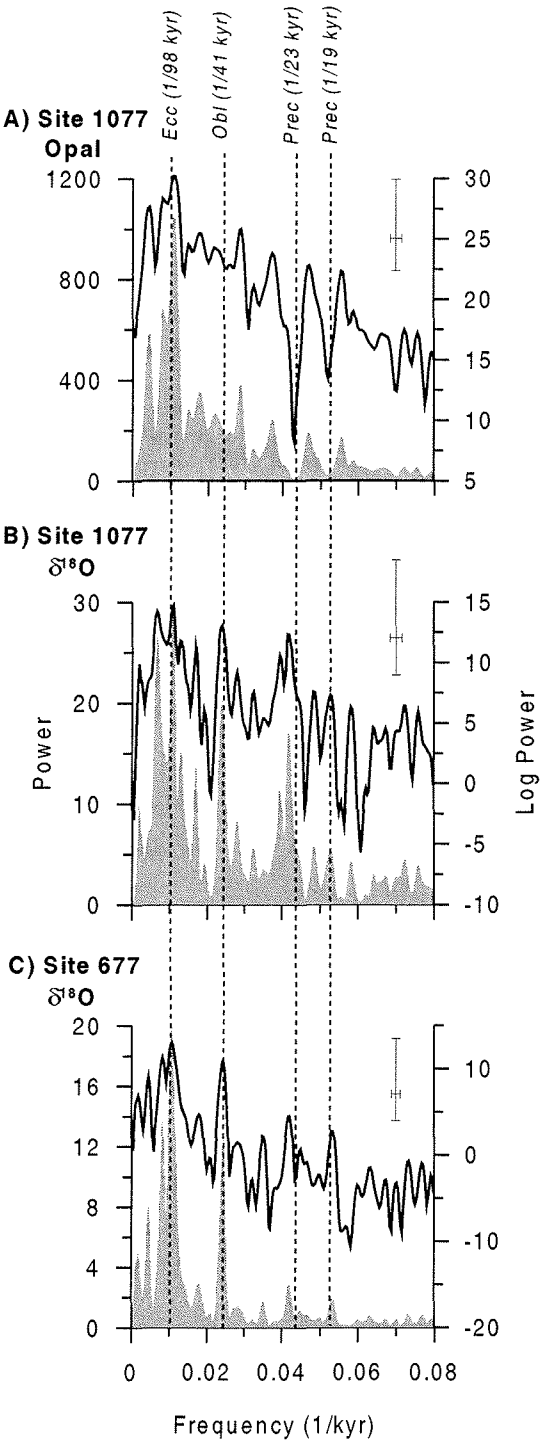

Fig. 4: Power spectra of opal sedimentation (A), and the $\delta^{18}O$ records of Site 1077 (B) and Site 677 (Shackleton et al., 1990) (C), on linear (gray area) and logarithmic (black line) scale. The cross in the upper right corner of each panel denotes 6 dB bandwidth (horizontal bar) at 80 % confidence interval (vertical bar) for the logarithmic scale of each spectrum.

We have shown that opal sedimentation in the Congo Fan area is not strongly influenced by precessional variations of insolation (Fig. 4A). This is somewhat surprising because upwelling in the eastern equatorial Atlantic is thought to be closely related to precession which controls the intensity of monsoons (McIntyre 1989; Molfino and McIntyre, 1990; Meinecke, 1992). Many proxies used to reconstruct paleoclimate in the African region are influenced by precessional forcing (e.g. oxygen isotopes: Pastouret et al., 1978; freshwater diatoms: Pokras and Mix, 1985; phytoliths: deMenocal et al., 1993; clay minerals: Gingele et al., 1998, pollen: Dupont et al., 1999). Furthermore, paleoproductivity changes based on organic carbon variations in the Congo Fan area during the last 200,000 years varies at the 23-19 kyr precessional periodicities (Schneider et al., 1994, 1997). The precessional driven monsoon system also modulates upwelling in the Congo Fan area (Rossignol-Strick, 1983; Prell and Kutzbach, 1987). Consequently, we would have expected a stronger effect of precessional frequencies on opal productivity as well. But the anticipated low latitude forcing is obviously far less important at Site 1077, at least for the sedimentation of opal. Thus, the Site 1077 opal record is curious in that it does not covary with published estimates of eastern equatorial Atlantic upwelling intensity variations.

Three features of the opal record indicate that its strong 100 kyr (Fig. 4A) component is not a simple consequence of changes in global ice volume, and may shed some light on its origin: (1) the lack of a well-defined obliquity peak in the opal spectrum; (2) the evolution of the amplitude of the 100 kyr component; and (3) the timing of its maxima and minima.

In both oxygen isotope records discussed (Sites 1077 and 677) high-latitude forcing manifests itself not only in a strong 100 kyr component but also in a distinct peak in the obliquity band (Figs. 4B, 4C) contributing 10.5 and 8.7 % variance respectively (Table 1). A clearly expressed 41 kyr peak is missing in the spectrum of the Site 1077 opal record and unlike the smaller deviations in the precession band discussed above the peak near 36 kyr can probably not be attributed to uncertainties in the age model (Fig. 4A). Taking into account that part of this peak is included in the 5.2 % variance calculated for the interval 38 to 45 kyr we may assume that there is only a very weak link to orbital obliquity.

The other two points raised above (evolution and timing) may be clarified in the time domain. The 100 kyr component in the opal content record at Site 1077 and in the $\delta^{18}O$ record of Site 677 has been extracted by bandpass filtering, and their evolution during the last 1,100 kyr is compared to eccentricity variations in Figure 5. The oxygen isotopes show the well-known increasing amplitude of the 100 kyr

	Eccentricity 150 – 80 kyr	Obliquity 45 – 38 kyr	Precession 24.7 – 17.5 kyr
Site 677 $\delta^{18}O$	30.9 %	10.5 %	6.7 %
Site 1077 $\delta^{18}O$	19.4 %	8.7 %	13.0 %
Site 1077 Opal	25.2 %	5.2 %	8.0 %

Table 1: Percentage of partial contribution of orbital parameters to the whole spectra calculated for records of oxygen isotopes (Sites 677 and 1077) and opal (Site 1077).

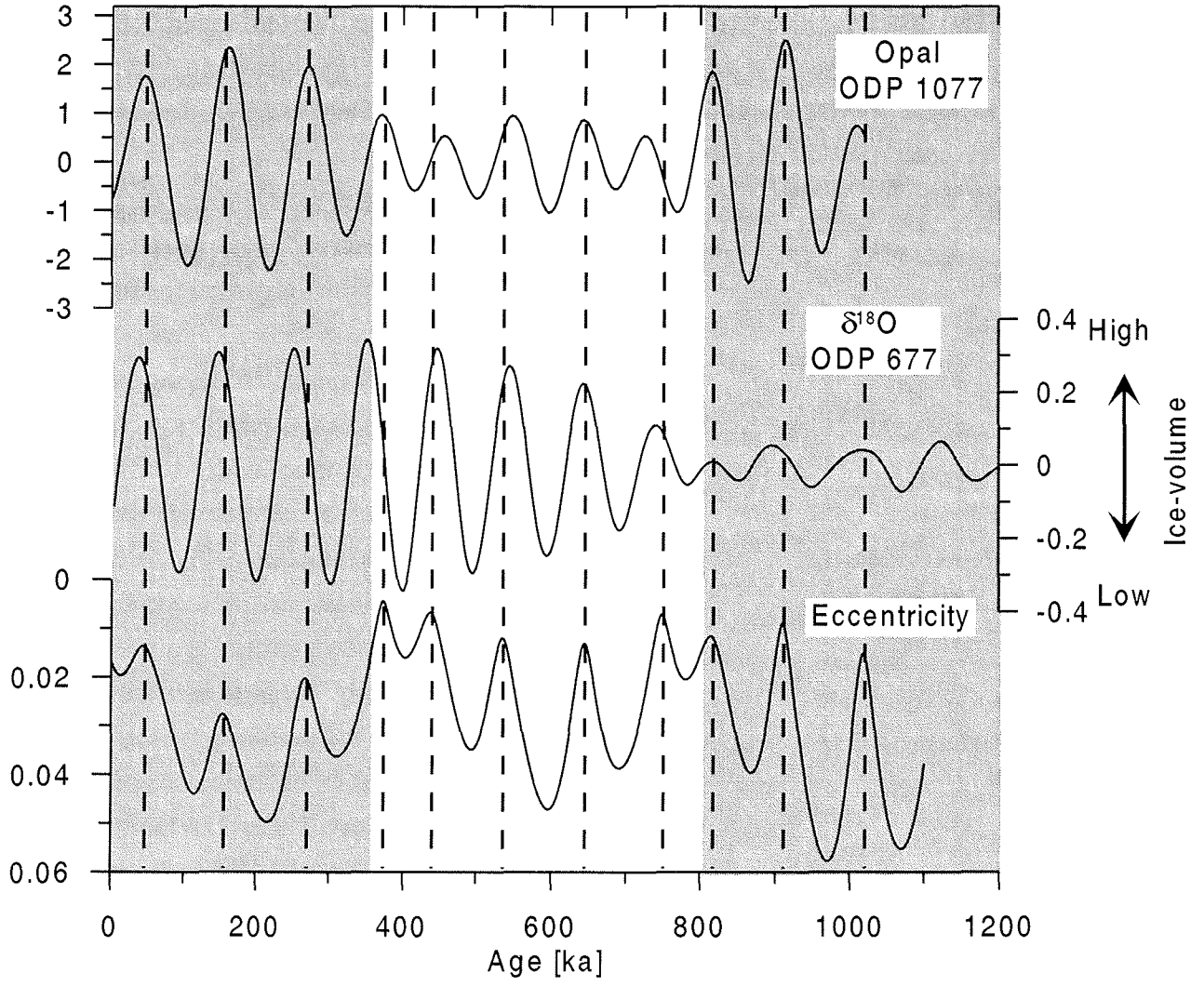

Fig. 5: Comparison between the Butterworth band-pass filter (85-135 kyr) signals of opal at Site 1077 (upper curve), and oxygen isotopes of Site 677 (middle curve), to isolate variance associated with the 100-kyr eccentricity cycles. The lower curve represents eccentricity from Laskar (1990); note that the Y-axis is reversed. The gray bars indicate time intervals with high amplitude in the opal signal. Vertical lines refer to minima in eccentricity.

component since about 900 ka (Mid-Pleistocene Transition; e.g. Raymo, et al., 1997) and are particularly strong in the past 650 kyr (Fig. 5). The manifestation of these 100-kyr cycles is thought to be related to the appearance of large Northern Hemisphere ice sheets that played an important role by amplifying the weak eccentricity forcing (Imbrie et al., 1993; Raymo et al., 1997; Raymo, 1998). Surprisingly, the bandpass filtered opal signal shows a strong 100-kyr cyclicity between 1,100 and 800 ka, earlier than in the oxygen isotopes. Several Pleistocene and pre-Pleistocene climate records show 100-kyr fluctuations in times when no large ice sheets existed to help establish the 100-kyr cyclicity (Miller et al., 1991; Wright and Miller, 1992; Zachos et. al, 1997). For example, Rutherford and D'hont (2000) reported the onset of 100-kyr glacial cycles as early as 1,200 ka in the oxygen isotope record of Site 659 from the tropical Atlantic. They concluded that the tropics played a major role in the initiation and maintenance of the 100kyr cycles, suggesting that increased heat flow across the equator or from the tropics to higher latitudes strengthened the semiprecession cycle in the Northern Hemisphere, and triggered the transition to sustained 100-kyr glacial cycles. This observation could be considered consistent with early onset of

strong 100 kyr cycles in the opal record of Site 1077. It is curious, however, that the amplitude in the opal signal decreases significantly exactly at the time of globally increasing 100 kyr cycles in oxygen isotopes, between 800 and 350 ka. This interval is followed by an increase in opal amplitudes in the Late Quaternary but not earlier than about 350 ka (Fig.5).

A closer look at the timing of the maxima and minima in Figure 5 strengthens the hypothesis that the 100 kyr cycles observed in the opal record do not exactly coincide with the evolution of global ice mass (as is the case in the $\delta^{18}O$ signal): opal leads ice volume. In fact, unlike the lagging oxygen isotope response, the extracted 100 kyr component seems to be directly timed with orbital eccentricity. Maxima in opal contents coincide with minima in eccentricity and vice versa (Fig. 5). To further examine this relationship in the frequency domain, we performed a cross-spectral analysis between opal and eccentricity. The phasing results are illustrated in Fig. 6, and demonstrate that the opal record is, in general, in phase with eccentricity. High coherence is observed near 124 (κ= 0.97) and 95 kyr (κ= 0.92) (Table 2). Within the error range, the phase angle calculated for these two periods confirms synchronized cycles or even a slight lead of opal. However, by inspecting this (Fig. 5), it is obvious that the negative phase angle is concentrated in the interval of strongly reduced amplitudes in the opal record (between 800 and 350 ka).

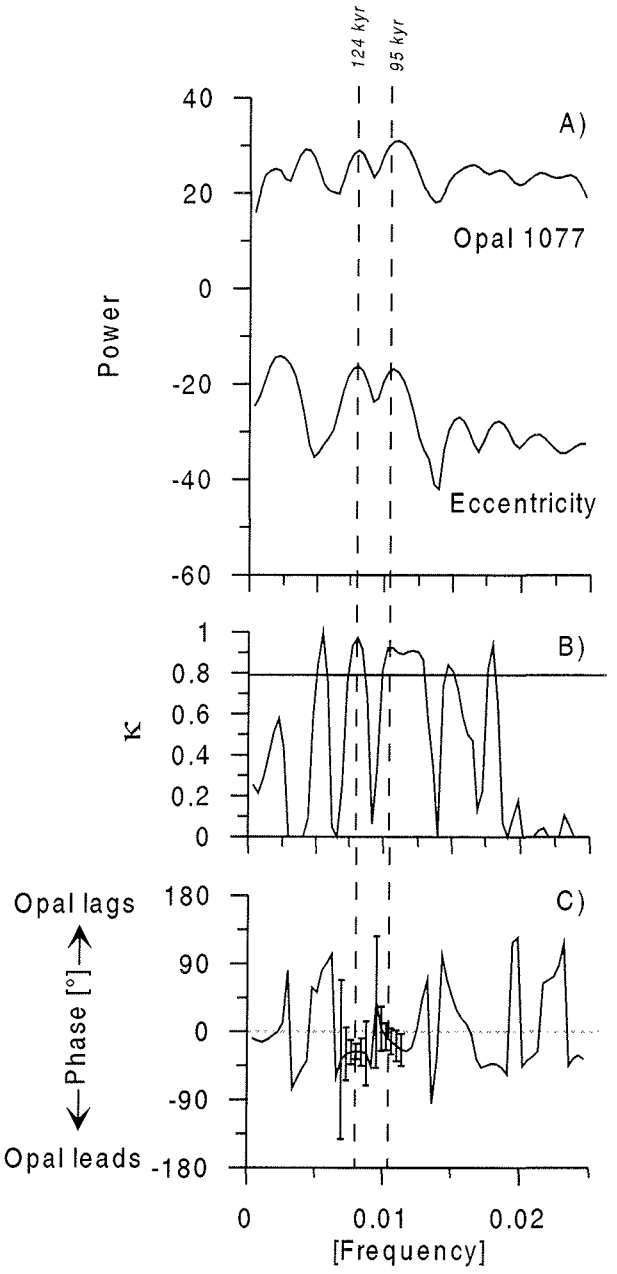

Figure 6: Cross-spectra of the Site 1077 opal record with respect to eccentricity (Laskar, 1990). A) Autospectra of both records; B) coherency (κ, horizontal line represents the 0.8 confidence level); and C) phasing in degrees (horizontal line at zero indicates that both parameters are in phase). Vertical lines denote peaks in eccentricity according to Berger and Loutre (1992). Vertical bars represent 95 % confidence interval.

Comparison of the Congo Fan opal record with adjacent areas

A comparison of opal sedimentation in the Congo Fan area (Sites 1077, this study; and 1075 from Holtvoeth unpub. obs.) with other locations in the equatorial and tropical eastern Atlantic to the north (Site 663) and south (Site 1084) is shown in Figure 7. Present day surface water conditions of these three hydrologically different areas are displayed in Table 3. It is obvious that the Congo Fan is the most productive, showing the highest values of

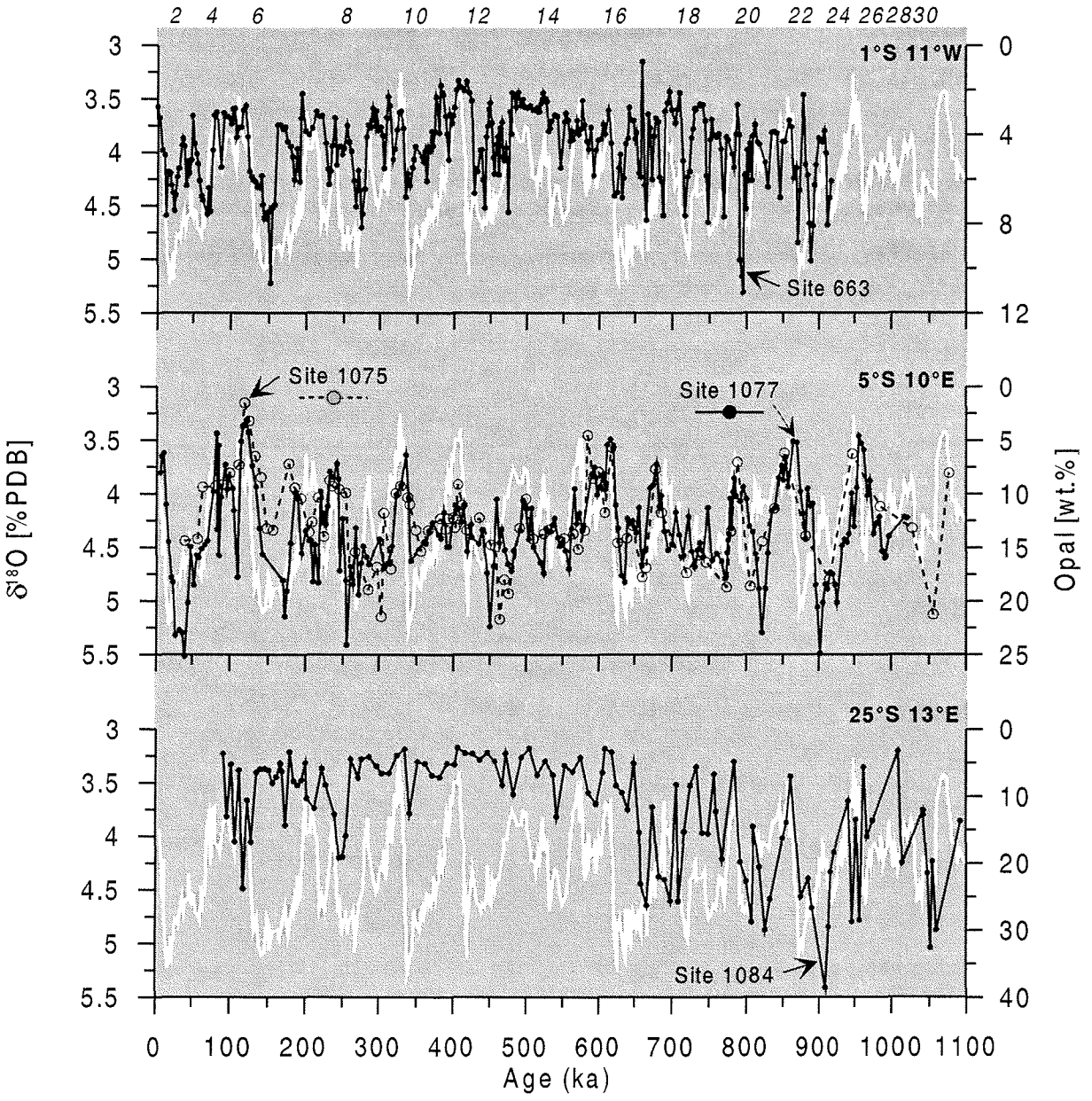

Figure 7: Comparison of opal records: equatorial Site 663 (from deMenocal et al., 1992; upper panel), Congo Fan Sites 1077 (present study) and 1075 (from Holtvoeth, unpub. data), and off Namibia Site 1084 (from Lange et al., 1999). White line in the background of each panel corresponds to benthic oxygen isotope record of Site 677 (Shackleton et al., 1990).

annual chlorophyll and silicate (Table 3). This higher amount of silicate observed at Site 1077 is mainly due to an additional input from the river. Preservation in the sediments, on the other hand, is enhanced at the Namibia Site 1084 (average opal content 22 %), followed by the Congo Fan (ca. 13 %), and is lowest at the Equator, Site 663 (4.6 %).

During the last 500 kyr, Sites 663 and 1077 show the same pattern with distinct maxima in opal concentrations during glacial intervals and minima during interglacials (Fig. 7). The pattern at Site 1084 is somewhat more erratic with high values (>15 %) in either glacials (MIS 8) or interglacials (MIS 5). In addition, a conspicuous long-term trend at this site is a significant drop in opal values at about 650 ka (mean value: 17.0 ± 8.6 % between 1,100-600 ka vs. 7.6 ± 4.5 % between 600-100 ka). Reduced vari-

Frequency	κ	Phase in degrees	Phase in kyr
95 kyr	0.92	-12 (±17)	-3.2 (±4.5)
124 kyr	0.97	-26 (±10)	-8.9 (±3.4)

Table 2: Results of cross spectral analysis in the eccentricity band (inverted) for the opal record of Site 1077. Coherency (κ), phase in degrees and in kyr (error in parenthesis).

	Site 663	Site 1077	Site 1084
Latitude	1°S	5°S	25°S
Longitude	11°W	10°E	13°E
Water Depth (m)	3708	2381	1992
Area	Equat. Atlantic	Congo River Fan	off Namibia
Chlorophyll *a* ($\mu mol*L^{-1}$)	0.25	0.37	0.13
Salinity (PSU)	35.64	32.87	35.03
Silicate ($\mu mol*L^{-1}$)	3.78	5.89	2.46
Phosphate ($\mu mol*L^{-1}$)	0.25	0.24	0.65
Nitrate ($\mu mol*L^{-1}$)	0.39	0.85	2.75
Benthic silicon release ($\mu mol*m^{-2}*a^{-1}$)	20-30	100-125	125-150
Upwelling	Divergence	Coastal and river induced	Coastal
Main silicate input	Eolian	Riverine	Benguela Current

Table 3: Environmental setting for ODP Sites 663 (DeMenocal et al., 1993), 1077 (present study), and 1084 (Lange et al., 1999). Surface water data are from Conkright et al. (1998), and benthic silicon release from Zabel et al. (2000).

ability between 650 and 300 ka is observed at Site 1084 as was also the case for Site 1077 (Fig. 5). Low amplitude variations between 620 and 475 ka were also reported by deMenocal et al. (1993) for Site 663.

In the older part of the opal record (older than approx. 650 ka) a distinct spiky pattern which is related to strong obliquity and/or precessional forcing (deMenocal et al., 1993) characterizes the equatorial Site 663. The record at Site 1084 (Lange et al., 1999), on the other hand, shows low frequency fluctuations (mainly in the eccentricity band; Gorgas et al., 2001), as is the case for the entire opal record of Site 1077.

Considering these observations, the response of the opal system at Site 1077 seems to be more similar to the equatorial Atlantic than to the Namibia area for the younger part of the record. This similarity in the deposition is reversed in the older sediments.

Conclusions

Here we present a 1 Myr record of biogenic opal for Site 1077 in the Congo Fan area. This record shows that:

1) Opal sedimentation reflects surface ocean productivity, with marine microorganisms (especially diatoms) driving the biogenic opal signal.
2) Glacial stages are characterized by high opal values reaching 25 wt % at the LGM.
3) A dominance in the 100 kyr periodicity, and phasing calculations implicate high latitude forcing. Surprisingly, no evidence of forcing in the obliquity band and only a very slight response in the precessional band could be observed.
4) The phase lock between opal and orbital eccentricity began earlier than the establishment of large ice sheets in the Northern Hemisphere, at ca. 1 Myr.
5) Despite the sensitivity to high-latitude forcing, the timing in the opal record is not exactly synchronized with ice-volume fluctuations estimated from oxygen isotopes, but is coincident with eccentricity.
6) Comparison of the Congo area with other records from the equatorial (Site 663) and subtropical South Atlantic (Site 1084) suggests a greater similarity with the equatorial site for the last 500 kyr. This similarity breaks down in the older part of the record.

Acknowledgements

We would like to thank Frank Schmieder, Helge Arz, Britta Jahn, Jens Holtvoeth and Lydie Dupont for fruitful discussions regarding sedimentary patterns and African paleoclimatology that significantly improved an earlier version of this manuscript. J. Holtvoeth kindly made available unpublished opal data for Site 1075. We also thank Marco Klann for advice and technical support during opal measurements. This research was funded by the Deutsche Forschungsgemeinschaft (Sonderforschungsbereich 261 at the Bremen University).

References

Archer, D., Lyle, M., Rodgers, K., and Froelich, B., 1993. What controls opal preservation in tropical deep-sea sediments. *Paleoceanography,* **8**: 7-22.

Barker, P., Fontes, J–C., Gasse, F., and Druart, J.-C, 1994. Experimental dissolution of diatom silica in concentrated salt solutions and implications for paleoenvironmental reconstruction. *Limnol. Oceanogr.*, **39**: 99-110.

Berger, A.L., 1978. Long term variations of daily insolation and Quaternary climatic change. *J. Atmosph. Sci.*, **35**: 2362-2367.

Berger, A.L. and Loutre M.F., 1992. Astronomical solutions for paleoclimates studies over the last 3 million years. *Earth and Planet. Sci. Lett.*, **111**: 369-382.

Boyle, E., and Keigwin, L.D., 1987. North Atlantic thermohaline circulation during the last 200,000 years linked to high latitude surface temperature. *Nature*, **330**: 35-40.

Brzezinski, M.A., 1992. the Si:C:N ratio of marine diatoms: interespecific variability and the effect of some environmental variables. *J. Phycol.*, **21**: 347-357.

Cadée, G.C., 1978. Primary production and Chlorophyll in the Zaire River, estuary and plume. *Neth. J. Sea Res.*, **12**(3/4): 368-381.

Cadée, G.C. , 1984. Particulate and dissolved organic carbon and Chlorophyll a in the Zaire River, estuary and plume. *Neth. J. Sea Res.*, **17**: 426-440.

Charles, C.D., Froelich, P.N., Zibello, M.A., Mortlock, R.A., and Morley, J.J., 1991. Biogenic opal in southern ocean sediments over the last 450,000 years: implications for surface water chemistry and circulation. *Paleoceanography*, **6**: 697-728.

Conkright, M., Levitus, S., O'Brien, T., Boyer, T., Antonov, J. and Stephens, C., 1998. *World Ocean Atlas.* Available online and on CD-ROM Data Set Documentation.. Tech. Rep. 15, NODC Internal Report, Silver Spring, MD. 16pp.

Conley, D.J., Zimba, P.V., and Theriot, E., 1990. Silica content of freshwater and marine benthic diatoms. *11th Diatom Symposium*, 95-101.

DeMaster, D.J., 1981. The supply and accumulation of silica in the marine environment. *Geochim. Cosmochim. Acta*, **45**: 1715-1732.

deMenocal, P.B., Oppo, D.W., Fairbanks, R.G., and Prell, W.L., 1992. Pleistocene variations in North Atlantic intermediate water $\delta^{18}O$. *Paleoceanography*, **7**: 229-250.

deMenocal, P.B., Ruddiman, W.F., and Pokras, E.M. , 1993. Influences of high- and low latitude processes on African terrestrial climate: Pleistocene eolian records from Equatorial Atlantic Ocean Drilling Program Site 663. *Paleoceanography*, **8**: 209-242.

Dugdale, R.C., Wilkerson, F.P., and Minas, H.J., 1995. the role of a silicate pump in driving new production. *Deep Sea-Res.*, **42**: 697-719.

Dupont, L.; Schneider, R.R., Schmüser, A. and Jahns, S., 1999. Marine-terrestrial interaction of climate changes in west equatorial Africa of the last 190,000 years. *Palaecology of Africa*, **26**: 61-84.

Dupont L.M., Donner B., Schneider R., Wefer G. (2001) Mid-Pleistocene environmental change in tropical Africa began as early as 1.05 Ma. *Geology*, **29**: 195-198.

Gorgas, T.J., Kronen Jr., J.D., and Wilkens, R.H:, 2001. 9. Data report: sedimentation rates from Milankovitch periodicity in Log and GAR bulk density records of Southwest Africa, Sites 1081, 1082, and 1084. In: Wefer, G., Berger, W.H., and Richter, C. (Eds.), *Proc. ODP, Sci. Results*, **175**, 1-23 [Online]. Available from World Wide Web: <http://www-odp.tamu.edu/publications/175_SR/chap09.pdf>.

Gingele, F.X., Müller, P.M., and Schneider, R.R., 1998. Orbital forcing of freshwater input in the Zaire Fan area- clay mineral evidence from the last 200 kyr. *Palaeoceanogr., Palaeoclimat., Palaeoecol.*, **138**: 17-26.

Giresse, P., Ouetiningue, R., Barusseau, J.-P., 1990. Minéralogie et microgranulométrie des suspensions et des alluvions du Congo et de L'Oubangui. *Sci. Gèol. Bull.*, **43**: 151-173.

Gorshkov, S.G., 1977. Atlas Okeanov, Atlanticheskiy I Indiyskiy Okean'i. Ministerstvo Oboronyi SSSR, *Voenno-Morskoe Flot*, Leningrad.

Hay, W.W., and Brock, J.C., 1992. Temporal variations in intensity of upwelling off southwest Africa. In:

Prell, C.P., and Emeis, K.C. (eds.). *Upwelling systems: evolution since the early Miocene.* Geological Society Special Publication, London No 65, 463-497.

Hays, J.D., Imbrie, J., Shackleton, N.J., 1976. variations in the Earth's orbit: pacemaker of the ice ages. *Science*, **194**: 1121-1132.

Herbert, T.D., Curry, W.B., Barron, J.A., Codispoti, L.A:, Gersonde, R., Keir, R.S., Mix, A.C., Mycke, B., Schrader, H., Stein, R., and Thierstein, H.R., 1989. Geological reconstruction of marine productivity. In: Berger, W.H., Smetacek, V.S., and Wefer, G. (eds.). *Productivity of the Ocean: present and past.* John Willey (New York), pp 409-428.

Holtvoeth, J., Wagner, T., Horsfield, B., Schubert, C.J., Wand, U., 2001. Late-Quaternary supply of terrigenous organic matter to the Congo deep-sea fan (ODP site 1075): implications for equatorial African paleoclimate. *Geo-Marine Letters.* [Online]. Available from World Wide Web:

http://link.springer.de/link/service/journals/00367/contents/01/00060/paper/s003

Howard, W.R., 1997. Paleoclimatology: A Warm future in the past. *Nature*, **388**: 418-419.

Hurd, D.C., 1983. Physical and chemical properties of siliceous skeletons. In Aston, S.R. (ed.), *Silicon geochemistry and biogeochemistry.* London (Academic Press), pp. 187-244.

Imbrie, J., Berger, A., Boyle, E.A., Clemens, S.C., Duffy, A., Howard, W.R., Kukla, G., Kutzbach, J., Martinson, D.G., McIntyre, A., Mix, A.C., Molfino, B., Morley, J.J., Peterson, L.C., Pisias, N.G., Prell, W.L., Raymo, M.E., Shackleton, N.J., and Toggweiler, J.R., 1993. On the structure and origin of major glaciation cycles 2. the 100,000-year cycle. *Paleoceanography*, **8**: 699-735.

Jansen, J. H. F., van Weering, T. C. E., Gieles, R., van Iperen, J., 1984. Middle and Late Quaternary oceanography and climatology of the Zaire-Congo fan and adjacent eastern Angola Basin. *Neth. J. Sea Res.* **17**, 201-249.

Jansen, J.H.F., Ufkes, E., Schneider, R.R., 1996. Late Quaternary Movements of the Angola-Benguela front, SE Atlantic, and implications for advection in the Equatorial Ocean. In: Wefer, G., Berger, W.H., Siedler, G., and Webb, D.J. (eds.). *The South Atlantic: Present and past circulation.* Springer-Verlag (Berlin, Heidelberg), pp. 553-575.

Lange, C.B., Treppke, U.F., and Fischer, G., 1994. Seasonal diatom fluxes in the Guinea Basin and their relationship to trade winds, hydrography and upwelling events. *Deep-Sea Res. I*, **41**: 859-878.

Lange, C. B., Berger, W. H., Lin, H.-L., Wefer, G., and Shipboard Scientific Party Leg 175, 1999. The early Matuyama diatoms maximum off SW Africa, Benguela Current System (ODP Leg 175). *Marine Geology*, **161**: 93-114.

Laskar, J., 1990. The chaotic motion of the solar system: A numerical estimate of the chaotic zones. *Icarus*, **88**: 266-291.

Lewin, J.C., 1961. The dissolution of silica from diatom walls. *Geochim. Cosmochim. Acta*, **21**: 182-195.

Lyle, M., Murray, D:W., Finney, B.P., Dymond, J., Robbins, J.M., Brooksforce, K., 1988. The record of late Pleistocene biogenic sedimentation in the Eastern Tropical Pacific Ocean. *Paleoceanography*, **3**: 39-5.

McIntyre, A., Ruddiman, W.F., Karlin, K., and Mix, A., 1989. Surface water response of the Equatorial Atlantic Ocean to orbital forcing. *Paleoceanography*, **4**: 19-55.

Meeuwis, J.M., and Lutjeharms, J.R.E., 1990. Surface thermal characteristics of the Angola-Benguela Front. *S. Afr. J. Mar. Sci.*, **9**: 261-279.

Meinecke, G., 1992. Spätquartäre Oberflächenwassertemperaturen im Östlichen Äquatorialen Atlantik. Bericht aus dem Fachbereich Geowissenschaften. Ph.D. Thesis, Universität Bremen, Germany.

Milankovitch, M., 1930. Mathematische Klimalehre und astronomische Theorie der Klimaschwankungen. *Handbuch der Klimatologie, Bd1, Teil A. Bornträger*, Berlin.

Miller, K.G., Wright, J.D., Fairbanks, R.G., 1991. Unlocking the ice house: Oligocene-Miocene oxygen isotopes, eustacy and margin erosion. *J. Geophys. Res.*, **96**: 6829-6848.

Molfino, B., and McIntyre, A., 1990. Nutricline variations in the equatorial Atlantic coincident with the Younger Dryas. *Paleoceanography*, **5**: 997-1008.

Mortlock, R.A:, Charles, C.D., Froelich, P.N., Zibello, M.A., Saltzman, J., Hays, J.D., Burckle, L.H., 1991. Evidence of lower productivity in the Antarctic Ocean during the last glaciation. *Nature*, **351**: 220-223.

Müller, P.J. and Schneider, R., 1993. An automated leaching method for the determination of opal in sediments and particulate matter. *Deep-Sea Res.I*, **40**: 425-444.

Nelson, D. M., P. Tréguer, Brzenzinski, M.A., Leynaert, A., Quéguiner, B., 1995. Production and dissolution of biogenic silica in the ocean: Revised global estimates, comparison with regional data and relationship to biogenic sedimentation.. *Global Biogeochem. Cycle*, **9**: 359-372.

Pastouret, L., Chamley, H., Delibrias, G., Duplessy, J.C., Thiede, J., 1978. Late Quaternary climatic changes in Western Tropical Africa deduced from deep-sea sedimentation off the Niger delta. *Oceanol. Acta*, **1**: 217-232.

Peterson, R.G., and Stramma, L., 1991. Upper-level circulation in the South Atlantic Ocean. *Progr. Oceanogr.*, **26**: 1-73.

Philander, S.G., and Pacanowski, R.C., 1986. A model of the seasonal cycle in the tropical Atlantic Ocean. *J. of Geophys. Res.*, **77**: 5255-5265.

Pokras, E.M. , 1987. Diatom record of the Late Quaternary climatic change in the Eastern Equatorial Atlantic and Tropical Africa. *Paleoceanography*, **2**: 273-286.

Pokras, E.M. and Mix, A.C., 1985. Eolian evidence for spatial variability of Late Quaternary climates in Tropical Africa. *Quaternary Res.*, **24**: 137-149.

Pollock, D.E., 1997. The role of diatoms, dissolved silicate and Antarctic glaciation in glacial/interglacial climatic change: a hypothesis. *Global and Planetary Change*, **14**: 113-125.

Prell, W.L., and J.E. Kutzbach , 1987. Monsoon variability over the past 150,000 years. *J. of Geophys. Res.*, **92**: 8411-8425.

Ragueneau, O., Tréguer, P. Leynaert, A., Anderson, R.F., Brzezinski, M.A., DeMaster, D.J., Dugdale, R.C., Dymond, J., Fischer, G., Francois, R., Heinze, C., Maier-Reimer, E., Martin-Jézéquel, V., Nelson, D.M., and Quéguiner, B., 2000. A review of the Si cycle in the modern ocean: recent progress and missing gaps in the application of biogenic opal as a paleoproductivity proxy. *Global and Planetary Change*, **26**: 317-365.

Raymo, M.R., Oppo, D.W., and Curry, W., 1997. The timing of major climate terminations. *Paleoceanography*, **12**: 557-585.

Raymo, M.E. , 1998. Glacial puzzles. *Science*, **281**: 1467-1468.

Rea, D. K., Pisias, N.G., and Newberry, T., 1991. Late pleistocene paleoclimatology of the central equatorial Pacific: flux patterns of biogenic sediments. *Paleoceanography,* **6**: 227-244.

Rossignol-Strick, M., 1983. African monsoons, an intermediate climate response to orbital insolation. *Nature*, **304**(7): 46-49.

Rutherford, S. and D'hont, S., 2000. Early onset and tropical forcing of 100,000-year Pleistocene glacial cycles. *Nature*, **408**: 72-75.

Sancetta, C., 1995. diatoms in the Gulf of California: seasonal flux patterns and the sediment record for the last 15,000 years. *Paleoceanography*, **10**: 67-84.

Sarnthein, M., Win, K., and Zahn, R., 1987. Paleoproductivity of oceanic upwelling and the effect on atmospheric CO_2 and climate change during deglaciation times. In: Berger, W.H., and Labeyrie, L.D. (eds.), *Abrupt climatic change- evidence and implications*. Reidel, Hingham (Mass.), NATO ASI Ser., C216, pp 311-341.

Schneider, R., Müller, P.J., and Wefer, G., 1994. Late Quaternary productivity changes off the Congo deduced form stable carbon isotopes of planktonic foraminifera. *Palaeogeogr., Palaeoclimat., Palaeoecol.*, **110**: 255-274.

Schneider, R. R., Müller, P. J., Ruhland, G., 1995. Late Quaternary surface circulation in the east equatorial South Atlantic: evidence from alkenone sea surface temperatures. *Paleoceanography,* **10**: 197-219.

Schneider, R.R. Müller, P.J., Ruhland, G., Meinecke, G., Schmidt , H., and Wefer, G., 1996. Quaternary surface temperatures and productivity in the Equatorial South Atlantic: Response to changes in Trade Monsoon wind forcing and surface water advection. In: Wefer, G., Berger, W.H., Siedler, G., and Webb, D.J. (eds.), *The South Atlantic: Present and past circulation.* Springer-Verlag (Berlin, Heidelberg), pp. 527-551.

Schneider, R.R., Price, B., Müller, P.J., Kroon, D., Alexander, I., 1997. Monsoon related variations in Zaire (Congo) sediment load and influence of fluvial silicate supply on marine productivity in the east equatorial Atlantic during the last 200,000 years. *Paleoceanography*, **12**: 463-481.

Schrader, H.J., and Gersonde, R., 1978. Diatoms and sillicoflagellates. *Utrecht Micropaleontology Bulletin*, 17: 129-176.

Schulz, M. and Stattegger, K., 1997. Spectrum: spectral analysis of unevenly spaced paleoclimatic time series. *Computers & Geosciences*, **23**: 929-945.

Shackleton, N.J., Berger, A., Peltier, W.R., 1990. An alternative astronomical calibration of the lower Pleistocene timescale based on ODP Site 677. *Transaction of the Royal Soc. of Edinburgh*: Earth Sciences, **81**: 251-261.

Shipboard Scientific Party , 1998. Chapter 5: Site 1077. In: Wefer, G., Berger, W.H., Richter, K., and Shipboard Scientific Party (eds.), *Proc. of the Ocean Drilling Progr., Initial Reports,* **175**, College Station, TX (Ocean Drilling Program), 115-141.

Takahashi, K., 1986. Seasonal fluxes of pelagic diatoms in the subarctic Pacific, 1982-1983. *Deep-Sea Res.*, **33**: 1225-1251.

Tréguer, P., Nelson, D.M., Van Bennekom, A.J., DeMaster, D.J., Leynaert, A., and Quéguiner, B., 1995. The silica balance in the World ocean: a reestimate. *Science*, **268**: 375-379.

Uliana, E., Lange, C.B., Donner, B., and Wefer, G., 2001. Siliceous phytoplankton productivity fluctuations in the Congo Basin over the past 460,000 years: marine vs. riverine influence, ODP Site 1077. In: Wefer, G., Berger, W.H., and Richter, C. (Eds.), *Proc. ODP, Sci. Results*, **175**, 1-32 [Online]. Available from World Wide Web:

<http://www-odp.tamu.edu/publications/175_SR/chap_11chap_11.htlm>.

Uliana, E., Lange, C.B., and Wefer, G.. Evidence for Congo River freshwater load in Late Quaternary sediments of ODP Site 1077 (5°S, 10°E). Submitted for publication in *Palaeogeogr., Palaeoclimat., Palaeoecol.*.

van Bennekom, A. J. and Berger, G.W., 1984. Hydrography and silica budget of the Angola Basin. *Neth. J. of Res.*, **17**: 149-200.

van der Gaast, S.J. and Jansen, J.H.F., 1984. Mineralogy, opal and manganese of Middle and Late Quaternary sediments of the Zaire (Congo) deep-sea fan: origin and climatic variation. *Neth. J. of Sea Res.*, **14**: 313-341.

Verardo, D.J., and McIntyre, A. 1994. Production and destruction: Control of biogenous sedimentation in the tropical Atlantic 0-300,000 years B.P. *Paleoceanography*, **9**: 63-86.

Voituriez, B., 1981. Les sous-courants équatoriaux nord et sud et la formation des dômes thermiques tropicaux. *Oceanol. Acta*, **4** : 497-506.

Wright, J.D. and Miller, K.G., 1992. Miocene stable isotopes stratigraphy, Site 747, Kerguelen Plateau. *Proc. ODP Sci. Res.*, **120**: 855-866.

Zabel, M., Hensen, C., and Schlüter, M., 2000. Chapter 12.5.2. Balancing the diffusion controlled flux of benthic silicate in the South Atlantic- Application of kriging. In: Schulz, H.D: and Zabel, M. (eds.), *Marine Geochemistry*, Springer, Berlin: pp. 388-391.

Zachos, J.C., Flower, B.P., and Paul, H., 1997. Orbitally paced climate oscillations across the Oligocene/ Miocene boundary. *Nature*, **388**: 567-570.

8- Conclusions

It is the intention of this work to give a generalized picture of the temporal fluctuations in siliceous phytoplankton productivity in the Congo Basin over the past 1 Myr, and to examine the interplay between marine productivity and Congo River freshwater outflow in relation to African climate variability. From this investigation the following conclusions can be drawn:

1. Sediments from the northern rim of the Congo Fan contain large amounts of biogenic opal (3 to 25 wt %) and siliceous microfossils. The marine signal dominates and marine diatoms are the most abundant siliceous microfossils group, followed by silicoflagellates and radiolarians.

2. Opal sedimentation reflects surface ocean productivity, with marine microorganisms (especially diatoms) driving the biogenic opal signal. The record clearly follows ice age cycles with maxima during glacial and minima during interglacial times. The variability is largest in the youngest and oldest part of the record, while between ca. 600 and 350 ka it is reduced.

3. Glacial stages are characterized by high opal values as well as high abundances of diatoms, silicoflagellates, and radiolarians. *Thalassionema nitzschioides* var. *nitzschioides* dominates the diatom signal, and abundance peaks are associated with glacial periods.

4. A dominance in the 100 kyr periodicity, and phasing calculations implicate high latitude forcing. No evidence of forcing in the obliquity band and only a very slight response in the precessional band could be observed. The phase lock between opal and orbital eccentricity began earlier than the establishment of large ice sheets in the Northern Hemisphere, at ca. 1 Myr.

5. Comparison of the Congo area with other opal records from the equatorial Atlantic (ODP Site 663) and the subtropical South Atlantic off Namibia (ODP Site 1084) suggests a greater resemblance with the equatorial site for the last 500 kyr. This similarity breaks down in the older part of the record, when opal fluctuations at Site 1077 were synchronized with those from off Namibia.

6. An abrupt change in the amplitude of the siliceous signal as well as in the diatom assemblages is evident at Termination II. Since that time, the relative abundance of *Cyclotella litoralis* (a marine diatom tolerant of lowered salinity) and the concentration of freshwater diatoms (genus *Aulacoseira*) increased dramatically, suggesting a change in environmental conditions from predominantly marine to mixed marine/brackish/fresh. This hypothesis is supported by isotopic evidence:
   a) Comparison of the oxygen isotope record of *Globigerinoides ruber* (pink) from Site 1077 with another record from a pelagic area in the equatorial Atlantic (GeoB 1041), revealed persistent deviations of the "global" $\delta^{18}O$ signal since Termination II (during warm Stages 5.5, 5.3, 5.1, 3 and 1) at the Congo site.

b) An artificial $\delta^{18}O$ (equilibrium $\delta^{18}O_{calcite}$) curve was constructed to estimate salinity and temperature effects on the observed differences between Site 1077 and GeoB 1041, for present times and for the past 200,000 years. This showed that freshwater inputs have caused negative deviations in the $\delta^{18}O$ signal at the Congo site.

c) Using the oxygen isotope difference between both locations ($\Delta\delta^{18}O$) as a proxy for freshwater input, a general trend in the $\Delta\delta^{18}O$ record was observed, with sustained negative values since Termination II. These negative pulses in $\Delta\delta^{18}O$ coincide with Northern Hemisphere summer insolation maxima, and are attributed to increased Congo River freshwater discharge due to enhanced precipitation on land.

7. We suggest that the apparent change to a less saline environment at Site 1077 since Termination II is a consequence of a sustained equatorward displacement of the Angola-Benguela Front. This migration was responsible for a northward deflection of the Congo River plume moving plume waters further north than normal and over Site 1077. The sedimentary imprint of this shift is an assemblage that shows increments in oceanic temperate diatoms in combination with *Dictyocha speculum* (cold water silicoflagellate), and freshwater diatoms.